Approved for public release; distribution is unlimited.

Analysis of Monterey Bay CODAR-Derived Surface Currents, March to May 1992

by

Thomas Craig Neal
Lieutenant , United States Navy
B.A., Miami University, 1984

Submitted in partial fulfillment of the requirements for
the degree of

MASTER OF SCIENCE IN PHYSICAL OCEANOGRAPHY

from the

NAVAL POSTGRADUATE SCHOOL
September 1992

REPORT DOCUMENTATION PAGE

REPORT SECURITY CLASSIFICATION Unclassified	1b. RESTRICTIVE MARKINGS N/A
SECURITY CLASSIFICATION AUTHORITY N/A	3. DISTRIBUTION/ AVAILABILITY OF REPORT Approved for public release; distribution is unlimited.
DCLASSIFICATION/DOWNGRADING SCHEDULE	
PERFORMING ORGANIZATION REPORT NUMBER(S)	5. MONITORING ORGANIZATION REPORT NUMBER(S)
NAME OF PERFORMING ORGANIZATION Naval Postgraduate School 6b. OFFICE SYMBOL *(If Applicable)* 35	7a. NAME OF MONITORING ORGANIZATION Naval Postgraduate School
ADDRESS *(city, state, and ZIP code)* Monterey, CA 93943-5000	7b. ADDRESS *(city, state, and ZIP code)* Monterey, CA 93943-5000
NAME OF FUNDING/SPONSORING ORGANIZATION 8b. OFFICE SYMBOL *(If Applicable)*	9. PROCUREMENT INSTRUMENT IDENTIFICATION NUMBER
ADDRESS *(city, state, and ZIP code)*	10. SOURCE OF FUNDING NUMBERS PROGRAM ELEMENT NO. / PROJECT NO. / TASK NO. / WORK UNIT ACCESSION NO.

TITLE *(Include Security Classification)*
ANALYSIS OF MONTEREY BAY CODAR-DERIVED SURFACE CURRENTS, MARCH TO MAY 1992

PERSONAL AUTHOR(S)
Neal, Thomas Craig

TYPE OF REPORT	13b. TIME COVERED FROM TO	14. DATE OF REPORT *(year, month,day)*	15. PAGE COUNT
Master's Thesis		September 1992	103

SUPPLEMENTARY NOTATION
The views expressed in this thesis are those of the author and do not reflect the official policy or position of the Department of Defense or the U.S. Government.

COSATI CODES			18. SUBJECT TERMS *(continue on reverse if necessary and identify by block number)*
FIELD	GROUP	SUBGROUP	CODAR, HF Surface Current Radar, Monterey Bay Circulation OASIS buoy, Surface currents

ABSTRACT *(Continue on reverse if necessary and identify by block number)*
HF surface current radar (CODAR) data from two shore-based radar sites were collected and combined to form vector estimates of the near-ace currents in Monterey Bay from March to May 1992. CODAR-derived currents are measures of the flow in the upper 1 m of the water mn. The springtime mean flow pattern in the Bay and its variability based on a maximum of 760 three-hourly observations at a nominal n spatial resolution are presented. Results for each month and the canonical day are also shown. The mean patterns show strong hward flowing onshore currents (≈20 $cm \cdot s^{-1}$) in the outer bay and near zero mean flow nearshore and northwest of Moss Landing. The ability is, however, large with standard deviations typically twice the mean. The canonical day shows strong (≈40 $cm \cdot s^{-1}$) onshore flow the entire Bay in the late afternoon giving way to a weaker reverse flow near and northwest of Moss Landing in the nighttime period. se flow patterns combine to produce the observed mean flow. CODAR data show energy at semi-diurnal tidal periods (12.3 and 11.9 s), diurnal period (24 hours) and a longer period (17 days). CODAR data is compared to data from a moored buoy. Low-passed time series well correlated. Unfiltered time series have higher correlations at diurnal and semidiurnal tidal frequencies. CODAR-derived surface ents and the winds are highly correlated at near-diurnal frequencies corresponding to the daily sea breeze forcing.

DISTRIBUTION/AVAILABILITY OF ABSTRACT UNCLASSIFIED/UNLIMITED ☐ SAME AS ☐ DTIC USERS	21. ABSTRACT SECURITY CLASSIFICATION Unclassified
NAME OF RESPONSIBLE INDIVIDUAL Jeffrey D. Paduan	22b. TELEPHONE (Include Area Code)(408) 646-3350 22c. OFFICE SYMBOL OC/Pd

FORM 1473, 84 MAR 83 APR edition may be used until exhausted
All other editions are obsolete

SECURITY CLASSIFICATION OF THIS PAGE
Unclassified

ABSTRACT

HF surface current radar (CODAR) data from two shore-based radar sites were collected and combined to form vector estimates of the near-surface currents in Monterey Bay from March to May 1992. CODAR-derived currents are measures of the flow in the upper 1 m of the water column. The springtime mean flow pattern in the Bay and its variability based on a maximum of 760 three-hourly observations at a nominal 2 km spatial resolution are presented. Results for each month and the canonical day are also shown. The mean patterns show strong southward flowing onshore currents ($\approx$20 cm$\cdot$s^{-1}) in the outer bay and near zero mean flow nearshore and northwest of Moss Landing. The variability is, however, large with standard deviations typically twice the mean. The canonical day shows strong ($\approx$40 cm$\cdot$s^{-1}) onshore flow over the entire Bay in the late afternoon giving way to a weaker reverse flow near and northwest of Moss Landing in the nighttime period. These flow patterns combine to produce the observed mean flow. CODAR data show energy at semi-diurnal tidal periods (12.3 and 11.9 hours), diurnal period (24 hours) and a longer period (17 days). CODAR data is compared to data from a moored buoy. Low-passed time series are well correlated. Unfiltered time series have higher correlations at diurnal and semidiurnal tidal frequencies. CODAR-derived surface currents and the winds are highly correlated at near-diurnal frequencies corresponding to the daily sea breeze forcing.

TABLE OF CONTENTS

ACKNOWLEDGMENT

Most sincere gratitude is offered to my thesis advisor Dr. Jeffrey D. Paduan for his patience and guidance. It was rich learning experience for both of us. Thanks to the following people who made this thesis possible: Dr. Jeffrey A. Nystuen for his insight and timely guidance. Dr. Leslie Rosenfeld, MBARI for supplying time series data from the OASIS mooring. Dr. Gary Sharp and Mr. William Schramm of NOAA/COAP, Monterey, California for providing the local support for the CODAR data. Dr. Steve Clifford of NOAA/WAP, Boulder, Colorado for supporting the installation and operation of the CODAR units in Monterey Bay. Dr. Donald Barrick and CODAR Ocean Sensors, LTD., Mountain View, California for day-to-day operation of the CODAR unit. Mr. Mike Cook, Mr. Pedro Tsai and Mr. Tarry Rago provided technical support and answered my endless questions on how to use computers. Ms. Lelaine Bushey provided word processing and moral support. Finally, I would like to thank Katherine Muhlbach my wife for her wonderful and enduring love, support and encouragement.

I. INTRODUCTION

The Coastal Ocean Dynamics Applications Radar (CODAR) system provides a remote method to sense the nearshore ocean, covering a large area with frequent observations at low cost. The remote sensing data can be related to the velocity of the upper 1 m of the water column. The purpose of this project is to explore the viability and use of CODAR for long-term oceanographic studies. In this thesis I investigate CODAR-derived surface current data in the Monterey Bay using three months of near-continuous observations from 1 March to 31 May 1992. This includes exploring the spatial and temporal coverage of the data and analyzing time series. CODAR data is compared with concurrent Acoustic Doppler Current Profiler (ADCP) and wind data measured from the Monterey Bay Aquarium Research Institute (MBARI) mooring.

A. POSSIBLE USES OF CODAR

Surface current maps from CODAR-derived velocities can be used to track and predict the movement of floating objects and suspended materials. This monitoring capability has potential applications in oil spill tracking and containment, surface drifter studies and modeling biologic material transportation. The surface current maps show the location of eddies and convergence and divergence areas. The mapping of these phenomena could be used to plan biological studies, rescue missions, fishing activities, and to asses the effects of surface pollutants in Monterey Bay.

As the Navy's interest shifts to littoral warfare, coastal oceanography and meteorology are becoming areas of intense research. CODAR could be used in mine and amphibious warfare operations. Drifting mines could be tracked and mine hazard areas predicted. Real-time knowledge of the surface currents could be used to safely conduct precise navigation and piloting of mine-hunting and salvage vessels. In amphibious operations,

CODAR could be used as a planning tool for landing craft operations, swimmer defense, SEAL team insertion/recovery and pilot rescue operations. CODAR and CODAR-derived current information could enhance real-world and real-time nearshore operations.

For scientific purposes, CODAR could be used in coastal oceanography research. Fine-scale coastal circulation and air-sea interaction models could be developed and verified using CODAR. CODAR systems can provide information over a large ocean area to help understand the dynamic and complex air-sea interactions along the coast.

B. BACKGROUND

1. HF Radar Current Measurements

Crombie (1955) discovered that decimeter wavelength (HF) radar signals backscatter off ocean surface waves (surface gravity waves). The dominant returning signals (echoes) are backscattered from ocean waves moving directly toward or away from the radar. The wavelength of the ocean wave backscattering the radar signal is one-half the radar's wavelength, λ. This type of scattering is known as Bragg scattering (Barrick et al., 1977). Spectral analysis of the returning signals reveals two dominant peaks in the frequency spectrum surrounded by a continuum of higher order scatters and noise. The frequencies of the dominant peaks are at the Doppler shift associated with the phase velocities of the ocean waves responsible for the backscattering, the "Bragg waves", divided by their wavelength, L. Surface gravity waves travel at constant phase speed, V_{ph} , determined by their wavelength. The phase velocity of a surface gravity wave is given by $V_{ph} = (gL/2\pi)^{1/2}$, where g is the gravitational constant. The Doppler shift, f_d, seen by the radar is shown in equation (1).

$$\pm f_d = 2V_{ph}/\lambda = 2(gL/2\pi)^{1/2}/\lambda = (g/\lambda\pi)^{1/2} \quad (1)$$

Slight changes from the expected Doppler shift have been detected and attributed to surface currents advecting the ocean wave field (Crombie 1972). These small shifts are used to measure the surface current radial velocity. The change in Doppler is $\Delta f = 2V_{cr}/\lambda$ where V_{cr} is the radial velocity of the current (Figure 1). Stewart and others (1974) qualitatively demonstrated the accuracy of deriving the surface current radial velocities from HF radar returns. They noted that by changing the radar frequency varying depths of surface currents are measured. The depth of the surface current measured is directly proportional to the radar wavelength. The average depth sensed by the radar is approximately the radar wavelength divided by 8 π (Stewart and Joy, 1974).

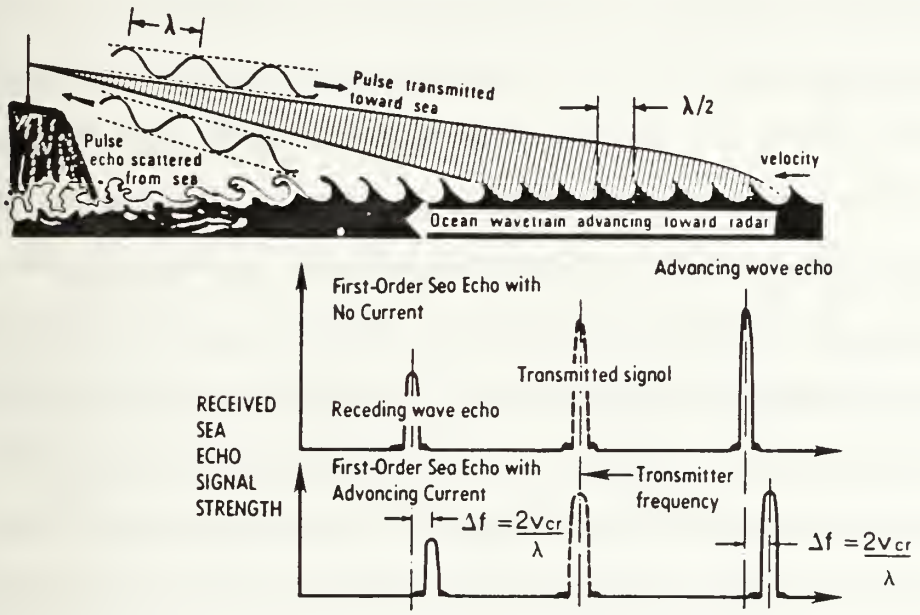

Figure 1. **Bragg Scattering from the Ocean Surface**: (from Barrick, 1977) This sketch shows the principles of first-order HF Bragg scatter from the sea, and resulting signal echo spectra without and with an underlying current.

2. CODAR

During the early 1980s, the National Oceanic and Atmospheric Administration (NOAA) Wave Propagation Laboratory developed a particular HF surface current radar,

CODAR. Like any HF radar system, each CODAR site is capable of measuring currents along radials emanating from each site. With two CODAR sites, vector currents can be computed within ocean areas observed by both radar units.

Although the theory for remote sensing of ocean surface currents using HF radar has been available for many years, actual field verification of this technique has been limited. Experiments conducted off the Florida coast compared CODAR-derived surface currents to a small number of drifter trajectories with fair agreement (Barrick et al., 1977). In 1979, the Marine Remote Sensing (MARSEN) Experiment compared CODAR and various other HF surface current radar systems to in situ measurements. During MARSEN, CODAR was compared to a moored current meter. The depth at the mooring was 15 m and the current meter was set at a 7 m depth. A month long time series of the current meter and CODAR were compared. CODAR transmissions were at four hour intervals and a splined interpolation scheme was used to calculate interpolated currents every 15 minutes to compare to the current meter measurements. The experiment did not result in close agreement of CODAR and the current meter arrays. Janopaul and others (1982) stated the differences between the CODAR-derived currents and the measured values of the current meters were probably due to the differences in the sampling intervals, the presence of vertical shear and the errors inherent in HF surface current radar systems.

Innovative antenna designs and advanced data extraction techniques have improved CODAR's performance. Lipa and Barrick (1983) developed a small crossed-loop/monopole antenna system and a least squares method of data extraction to increase the accuracy of surface current vectors. Additional field experiments conducted on Delaware Bay compared CODAR-derived surface currents to Remote Acoustic Doppler System (RADS). Results were consistent between the two methods, allowing for the different spatial scales and depths measured by the two techniques (Barrick et al., 1985).

CODAR development has continued, but problems have been reported in the derived surface current data. These problems include poor spatial coverage, difficulty in ground truthing, limited data sets and a preponderance of inaccurate CODAR-derived current vectors. A recent study on CODAR in the Straits of Florida describes many problems and weaknesses existing in the CODAR system (McLeish and Maul, 1991). McLeish and Maul state probable causes of the problems include unreliable equipment, ship interference, excessive data filtering and electromagnetic noise sources. NOAA's intended use of CODAR was to provide information to the public concerning ocean currents and waves offshore of the coast of Florida. The CODAR-derived surface current maps were deemed to be unreliable, sparse and deficient for the intended purpose. Despite these problems, with careful processing of the data, McLeish and Maul believe CODAR has potential as a tool for ocean research.

3. Comparison of CODAR and OSCR

During the 1980s, Rutherford Appleton Laboratories, United Kingdom, developed a competing HF surface current radar system, the Ocean Surface Current Radar (OSCR). The OSCR system uses a long linear array receive antenna system to execute beam forming and to determine signal direction; CODAR uses a crossed loop/monopole receive antenna system. Field tests conducted on the Swansea Bay in southwest England showed OSCR-derived surface currents to be within 5% to 10% of speed and 10 in direction of surface-floating current meters (Hammond et al., 1987).

We do not analyze data from any OSCR systems in this study but it is instructive to compare CODAR and OSCR to show what parts of the processing steps are shared by all HF systems and what parts are unique to CODAR. Both CODAR and the OSCR derive range distance based upon range gating the time of arrival of the returning signal. The

systems differ in the method of deriving direction. CODAR uses a system based on direction finding (DF) methods. Three antennas are used, two crossed-loop and one monopole. The monopole antenna has an omni-directional beam pattern. The crossed-loop antennas have cosine beam patterns set perpendicular to each other. The same returning signal will have different amplitudes for each antenna depending upon angle of arrival. The direction of the signal is determined by comparing differences in amplitude (Figure 2). Angular accuracy varies from 2.5° to 12° depending on the signal-to-noise ratio (Lipa and Barrick, 1983).

The OSCR system requires a large area of undisturbed coastline, precise antenna placement and on-site calibration. 1/4 wavelength monopole antenna illuminates the ocean surface. Sixteen evenly spaced elements create an array 85 m long that comprises the receiving antenna system and provides a beam width of 6°. The receive antenna direction can be pointed in 16 different directions within a 90° sector. Range bins are 1.2 km wide with a maximum of 32 bins. OSCR scans one cell of the 32x16 area at a time. Scanning is preprogrammed and computer controlled. Computer processing derives the radial component of the surface current. The OSCR method of angle determination is intrinsically simpler than that of CODAR but is has the obvious disadvantage of requiring 85 m of straight beach front property for its installation. Modern CODAR units can, by contrast, be placed in the trunk of a car and easily installed on a small piece of waterfront beach or headland. This practical advantage of CODAR places a premium on verifying that the system works, despite its more complicated direction finding techniques.

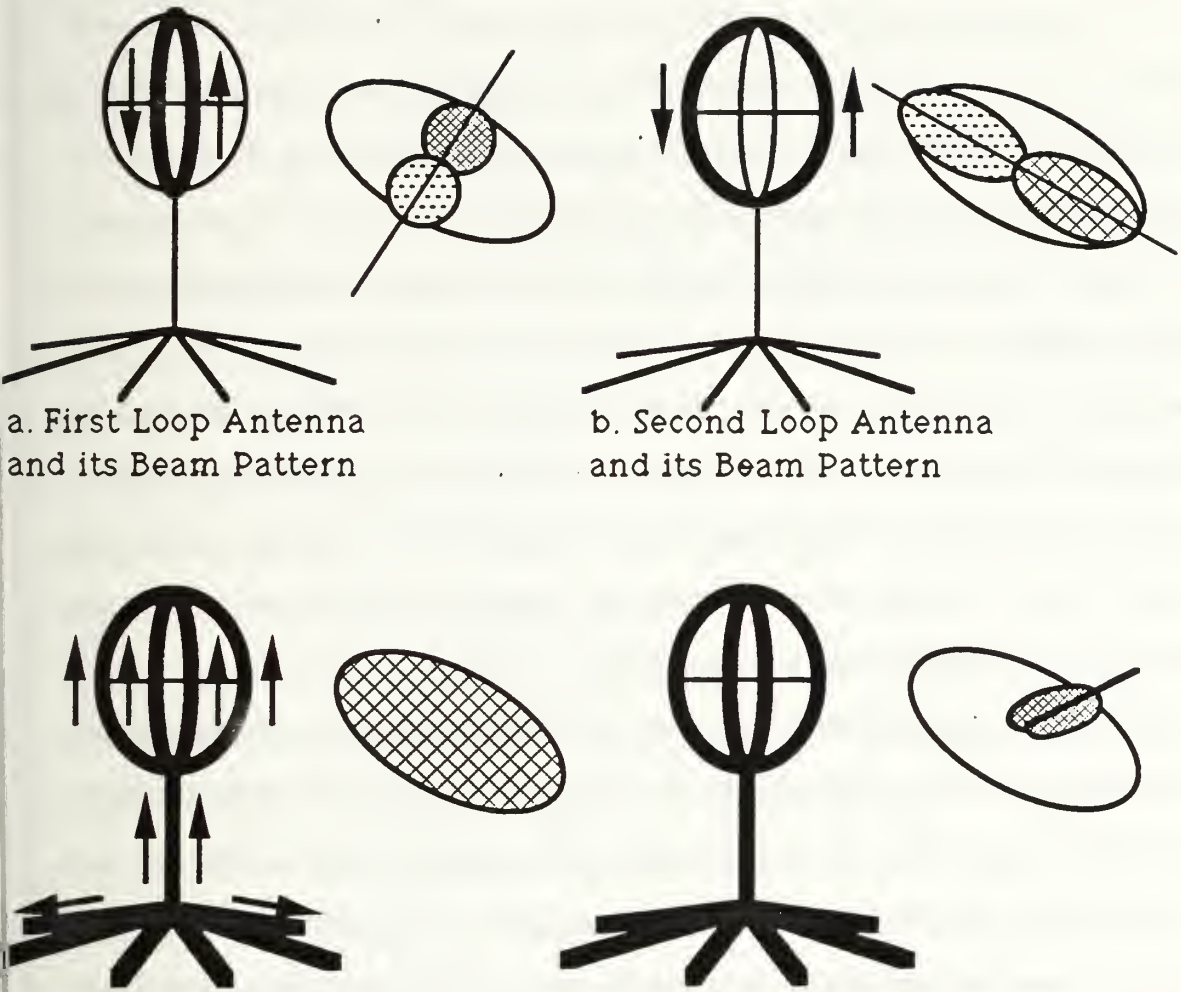

a. First Loop Antenna and its Beam Pattern

b. Second Loop Antenna and its Beam Pattern

c. Monopole Antenna and its Beam Pattern

d. Synthesis of Crossed Loop/Monopole Antenna and its Effective Beam Pattern

Figure 2. **CODAR Signal Direction Finding:**

II. PROCEDURES

A. PRESENT SYSTEM

NOAA presently operates two CODAR sites alongside Monterey Bay, one at Moss Landing and the other at Hopkins Marine Laboratory at Pacific Grove; both sites operate at 25.4 MHz (λ=12 m) and provide useful coverage out to approximately 22 km offshore based on the results of this study. The average depth observed, based on the radar wavelength, is 1/2 m. The maximum range of CODAR is variable and depends on sea state, atmospheric conditions and the presence of electromagnetic noise sources. Range resolution is two km. Each CODAR grid point represents the center of a 2 km by 2 km box. CODAR gridpoints on Monterey Bay are shown in Figure 3. CODAR measurements are taken every three hours. Radar pulses are transmitted for 26 minutes and the collection of echoes is stored. Surface current information is extracted, after post processing, using the least squared method detailed by Lipa and Barrick (1983).

The geometry of the CODAR sites at the baseline between the two stations presents unique problems. The alongshore velocity component of the current can be accurately measured by both sites; however, the onshore velocity component cannot be detected. The CODAR programmed software assumes that the onshore velocity component is zero at the coastline. The software artificially determines the onshore current velocities on and inshore of the baseline by interpolation of velocities further offshore. The onshore velocities are linearly reduced to zero at the coast. This assumption is not inherent to the CODAR system and if the radial velocity files are used this software baseline assumption can be bypassed. The software also computes the surface current velocity uncertainties at all gridpoints. If the velocity uncertainty is greater than 10 $cm \cdot s^{-1}$ at any gridpoint, the data for the point is discarded. Barrick and others (1983) list the average surface current velocity uncertainties

as ±2-3 $cm \cdot s^{-1}$ rms errors and the bearing uncertainties as ±2.5° rms. Both CODAR sites independently gather the radial current vectors then a central site uses both sets of radial current vectors to resolve the total current vectors. Detailed specifications of CODAR's design and operation are discussed in the *Coastal Ocean Dynamics Applications Radar-A User's Guide* (Georges, 1984).

B. CODAR DATA ANALYSIS

The CODAR data consists of total current and radial current vector files. Time series were created for each CODAR gridpoint from the collection of total current vector files. From the time series files, mean velocity and standard deviation plots were produced. The number of missing records in the time series varied at each gridpoint . The number of gaps increased with range. The percentage of coverage at each gridpoint was calculated by dividing the actual number of records by the possible number of CODAR measurements during the time period. When required for spectral analysis, these missing records or gaps in the time series were filled using linear interpolation.

The CODAR data was compared to ADCP and wind measurements obtained from a mooring in Monterey Bay located at 36°44.9'N, 122°02.3' W (see Figure 4) and operated by MBARI. ADCP and wind measurements concurrent with the CODAR data set were processed and compared with nearby CODAR gridpoints. Details and precautions of the data processing and comparison procedures are discussed in the following paragraphs.

The CODAR sites transmitted every three hours for 26 minutes; eight transmissions were completed daily. The transmission times started at midnight Pacific Daylight Time (PDT) and followed every three hours. Each CODAR site derived radial surface current vectors from the 26-minute collection of echoes. This process took one to two hours. A central site collected the radial surface current vectors from both sites and resolved them into total current vectors, storing the radial and total current vectors in separate data files.

The central site sent the data files to the Naval Postgraduate School (NPS) via modem and a dedicated Macintosh computer at NPS, provided by NOAA, stored the CODAR data files. Only total current vector files are used in this study. A total current vector file consists of header information containing the date and time of the CODAR transmission and data lines containing the location and U and V velocity components. The locations are referenced by km east and north from the midpoint between the operating sites at Moss Landing and Pacific Grove (36°42.78' N, 121°51.01' W). The locations correspond to fixed gridpoints shown in Figure 3. An example of a complete and reasonable CODAR total current vector map is shown in Figure 5. The map shows a large area of coverage out to 26 km and most vectors are consistent with the general current pattern. It is important to note that not all CODAR gridpoints have surface current vectors in this map. Many CODAR gridpoints were out of range of one or both operating sites. Lack of vectors could have been caused by interference from shipping, electromagnetic noise sources and/or poor atmospheric conditions.

Time series were created for each CODAR gridpoint from the collection of total current vector files. These were used to produce mean velocity vectors and standard deviations for each CODAR gridpoint. Means were calculated for the weekly, monthly and total three-month time periods. Next, the canonical mean vectors were calculated at each of the eight daily transmission times (midnight, 03:00, 06:00, etc.) to form a view of a typical day during this springtime period. All mean vector fields were plotted with their standard deviation fields. Percentage of coverage was then contoured and plotted. For each mean surface current map a contour plot of the accompanying percentage of coverage was drawn.

Finally, CODAR time series were spectrally analyzed. CODAR transmitted every three hours; the minimum resolvable period was six hours. To conduct spectra analyses, complete time series were required; therefore, the interpolated time series were used. The interpolated time series consisted of 762 data points from which the rotary power spectra

were calculated. The rotary power spectra split the energy of the currents into clockwise and counterclockwise directional frequencies.

C. MOORING DATA ANALYSIS

MBARI operates an OASIS mooring to obtain weather and oceanic data in the Monterey Bay. Details of MBARI's OASIS mooring can be found in the article *The MBARI Program for Obtaining Real-time Measurements in Monterey Bay* (Chavez et al., 1991). On the mooring, ADCP measures the ocean currents in 8 m depth bins. The second depth bin is the shallowest reliable bin and was used to compare with CODAR. It measured currents in the depth range of 12 to 20 m. The ADCP sampled every 15 minutes, 110 pings per sample, at one second intervals. Every second sample was transmitted to shore every 30 minutes. Occasionally the telemetry system failed and automatically reset itself. This resulted in a 15 minute shift in the time of data transmission. These shifts produced gaps in the time series that were flagged. ADCP data was received in Greenwich Mean Time (GMT) and referenced to magnetic north. Wind and SST data were measured roughly every 10 minutes.

The mooring data for this study period was processed to compare with the CODAR data. The mooring data times were converted to PDT and the data directions were corrected for magnetic variation where required. The mooring data was riddled with gaps and the longest continuous time series were typically five days. These gaps hindered the comparison to CODAR and future analysis should attempt to compare complete time series. Once the ADCP and wind data sets were corrected, U-V velocity components, speeds, directions, correlations and rotary power spectra were computed and examined. When continuous time series were required, gaps were linearly interpolated.

D. COMPARISON OF CODAR AND MOORING DATA

The ADCP and CODAR data were matched in time and the speed and directional differences were calculated. To view low frequency events, the high frequency

components of the CODAR and mooring time series were removed from the interpolated data using a 24-hour, running-mean, boxcar filter. The half-power point of this filter was 50 hours. The filtered data sets were also matched in time and the speed and directional differences were calculated.

Spectral and correlation analyses were conducted to further compare the data types. First the rotary power spectra were calculated and plotted for CODAR The mooring data had several large gaps in the data. To more accurately compare the ADCP data, 120-hour continuous segments of the time series were identified and the rotary power spectra were calculated. The correlation coefficients were then calculated between CODAR and the wind and CODAR and ADCP. Both filtered and unfiltered time series correlation coefficients were calculated.

E. PRECAUTIONS

1. CODAR's Baseline Assumption

Near the baseline the CODAR software processing system makes questionable assumptions. At the baseline offshore velocity components cannot be accurately derived. To produce a total vector at or inshore of the baseline, the CODAR software uses the offshore component derived from the gridpoint next to the baseline (2 km from baseline). The offshore component was linearly interpolated from this value to the coastline after setting onshore flow at the coastline to zero. All vectors at the baseline and in toward the shore should be viewed cautiously or ignored. These vectors are plotted as dotted arrows in the surface current maps.

2. Erratic Total Current Vectors

Another precaution involves the occurrence of erratic total current vectors. These erratic vectors were noted when the size and/or direction of a vector was incompatible with the neighboring general flow. McLeish and Maul (1991) also reported the presence of erratic vectors. Figure 6 is an example of a current map with poor spatial coverage and

numerous erratic vectors. Erratic vectors appear most often at the fringes of CODAR coverage. Vectors on the limits of CODAR coverage are therefore suspicious and should be disregarded. Vectors that were unusually large and/or pointing in incompatible directions are also suspicious. Specific examples of erratic vectors are marked in Figure 6. The presence of erratic vectors reduces the effectiveness of CODAR for real-time applications.

3. Spatial and Depth Differences of CODAR and Mooring Data

The mooring data contain problems that might affect comparison to CODAR. The wind, CODAR and ADCP measurements were at different depths and on different spatial and temporal scales. CODAR measures within the top meter of the ocean, covers a footprint of 4 square km and averages a 26-minute period of transmission. The ADCP measured the currents 12 to 20 m below the surface. The position of the mooring is not fixed, but is within the range of it's swing circle. ADCP's footprint was directly below the mooring and samples were averaged over two minutes. Due to these differences the measurements were not expected to match precisely, a common mismatch-of-scale problem when trying to verify unique remote sensing techniques.

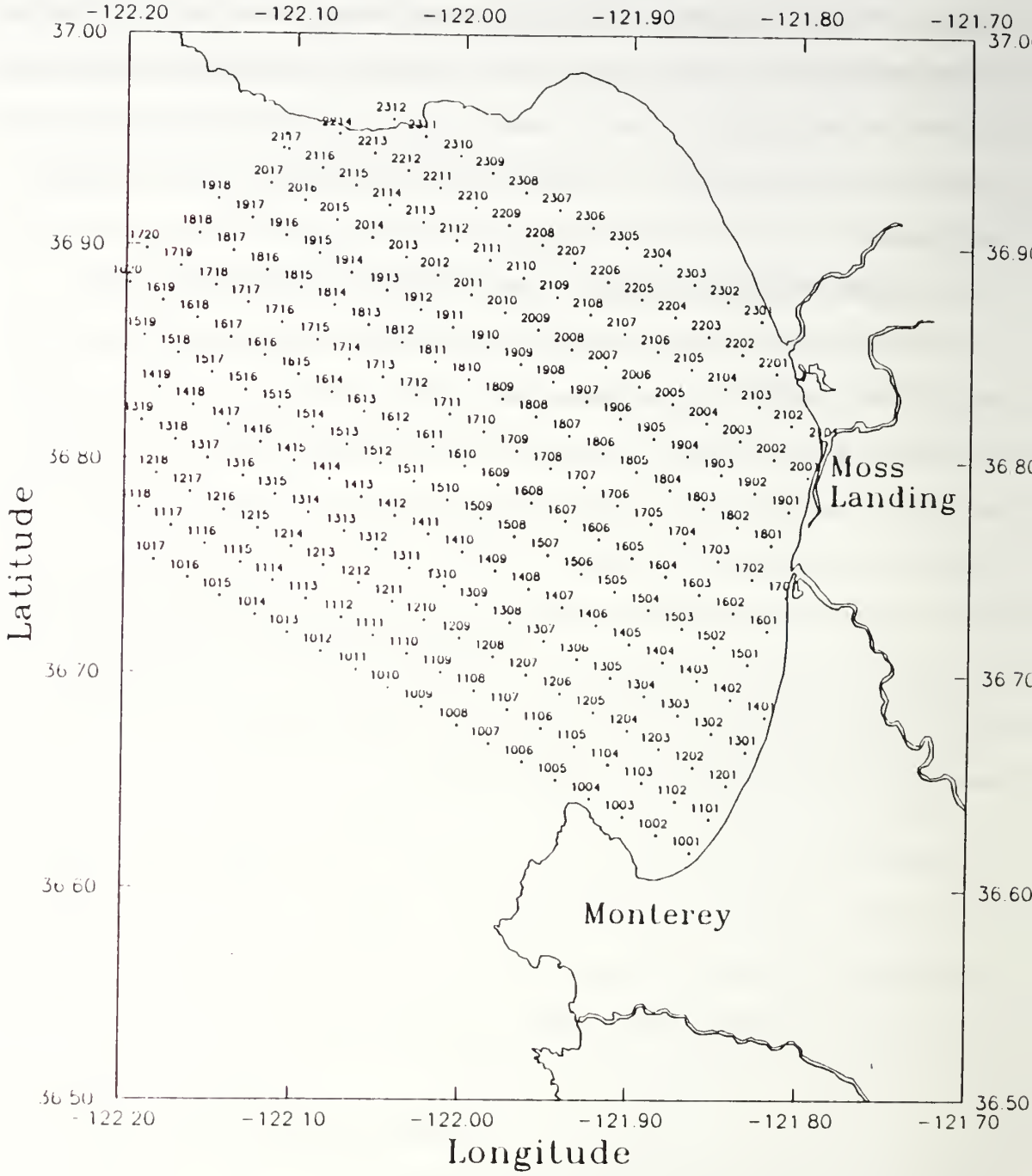

Figure 3. **CODAR Gridpoint Locations in Monterey Bay:** The number designates locations relative to a grid oriented with the baseline between Monterey and Moss Landing. The first two digits denote the row number, beginning with 10 in the south. The second two digits give the column number, beginning at the shoreline.

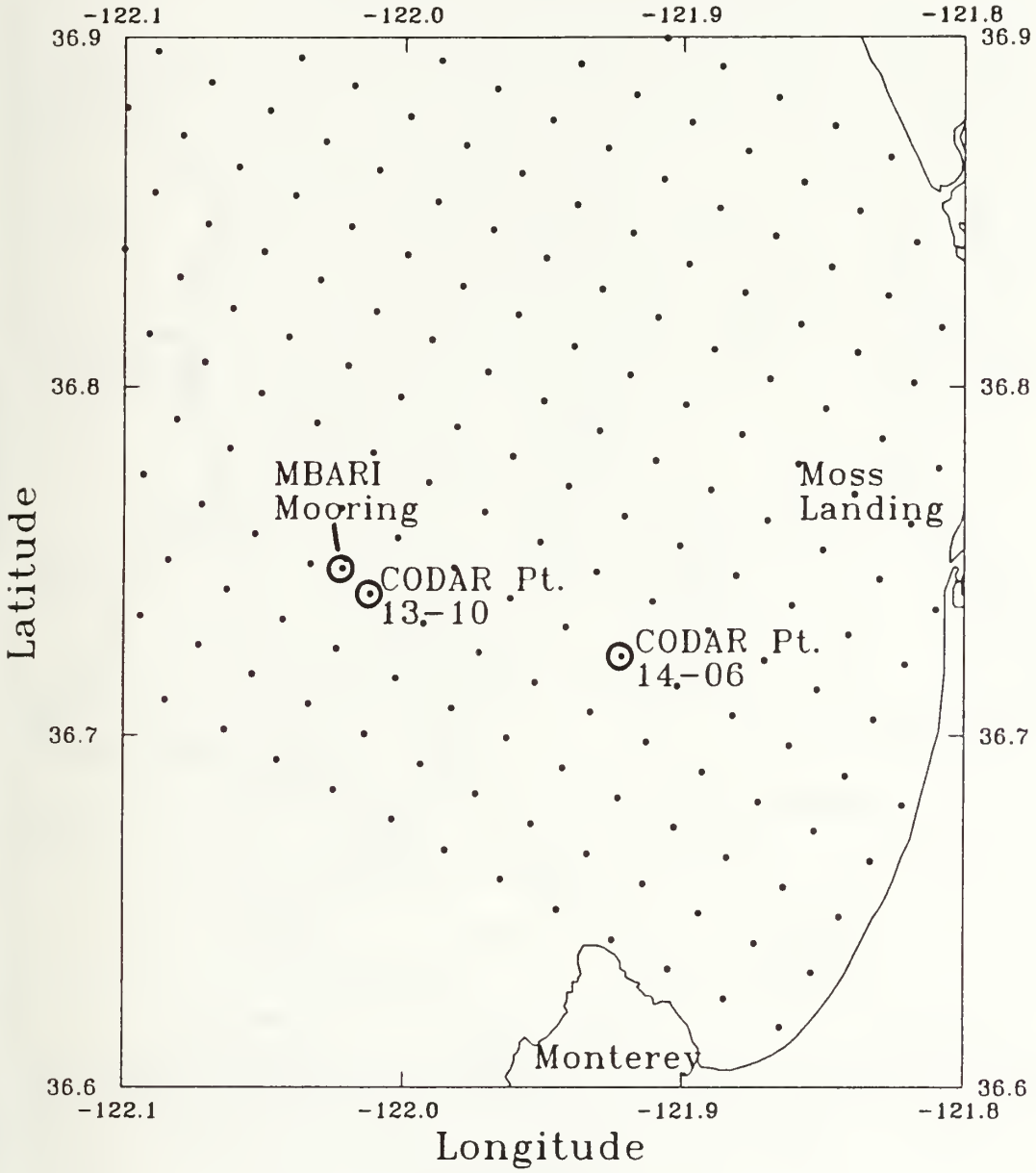

Figure 4. **MBARI'S OASIS Mooring Location Monterey Bay:** The location of the OASIS mooring is indicated and CODAR Pt. 1310, which is 1.6 km away, and CODAR Pt. 1406, which is 7.0 km away.

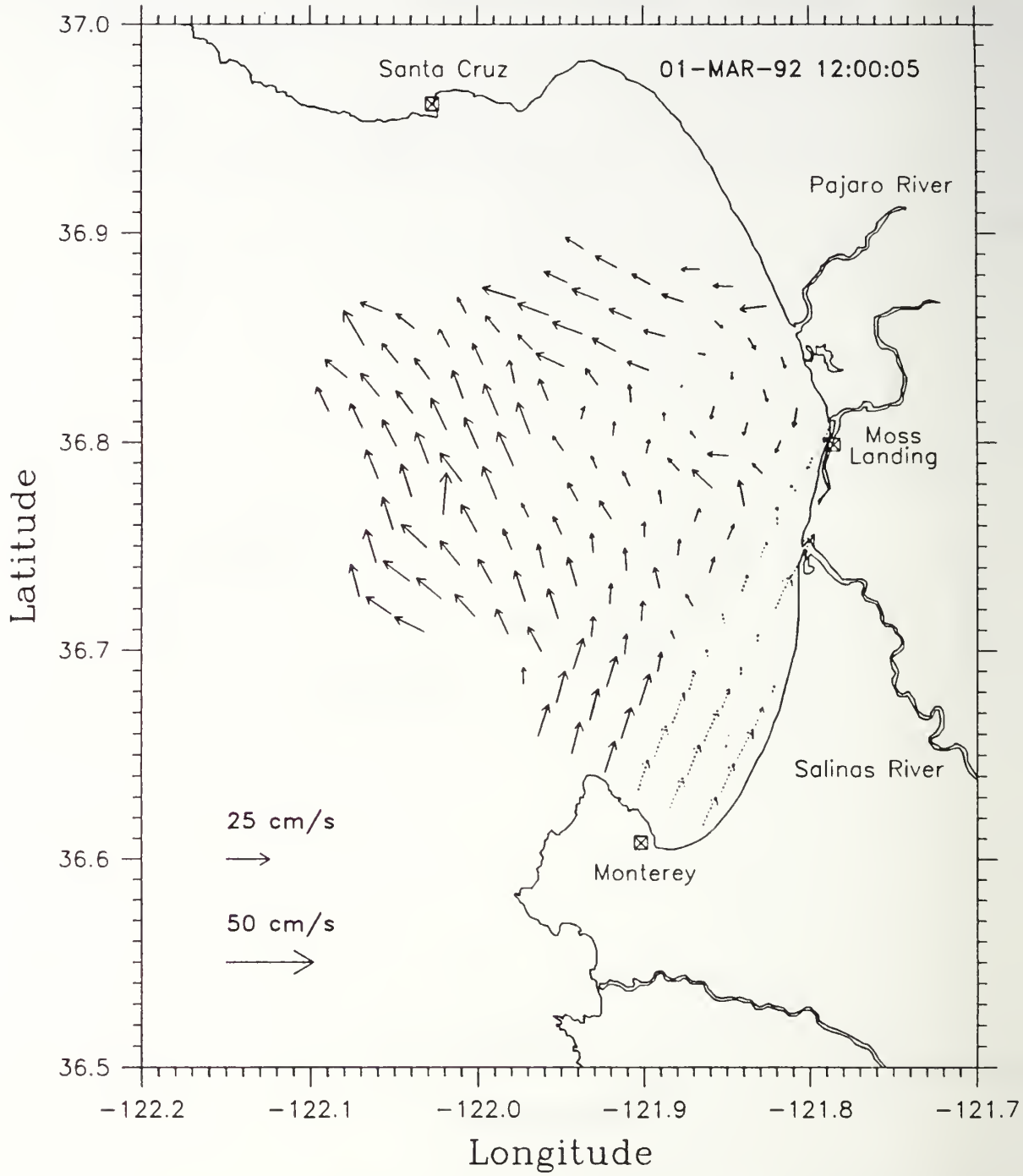

Figure 5. **Good Example of a CODAR-derived Surface Current Map:** This map shows a complete, reasonable and high coverage current map. Maps of this type are useful for real-time applications. Dotted vectors were derived with the baseline assumption and are questionable.

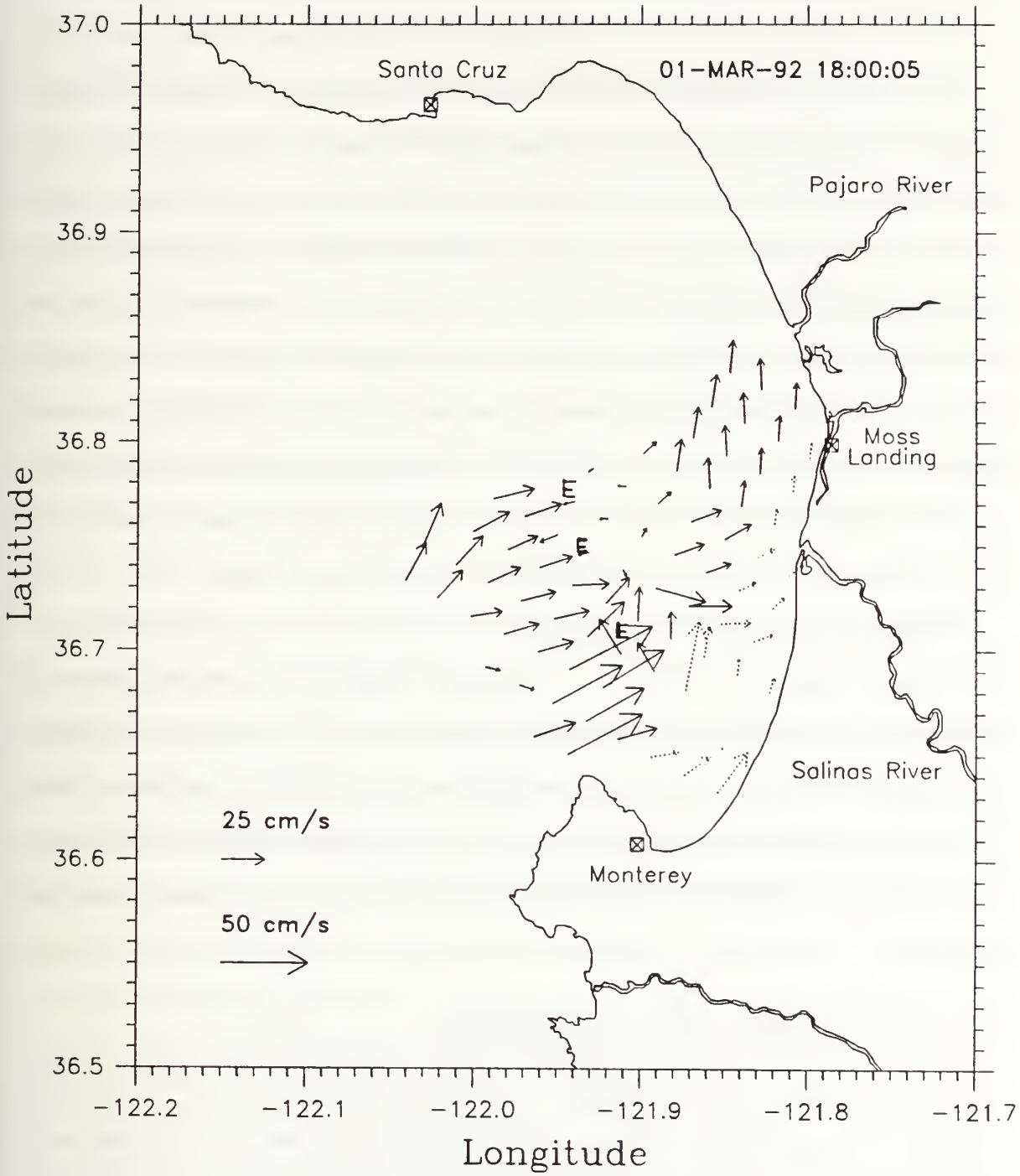

Figure 6. **Poor Example of a CODAR-derived Surface Current Map:** This map shows a reduced area of coverage, missing and erratic vectors. Some erratic vectors are marked with an "E" and are thought to be inaccurate. This current map could not be used for real-time applications without extensive verification.

III. MEAN CODAR-DERIVED SURFACE CURRENTS

The mean CODAR-derived surface currents are presented in the following subsections. These maps show the general surface circulation patterns in Monterey Bay. Also shown are the contoured CODAR coverage maps, which are plotted on the same scale as the mean current maps. These plots show the spatial and temporal coverage of CODAR at each gridpoint. Gridpoints with less than 10% coverage should be viewed with caution due to low number of actual vectors from which the mean is calculated. Large mean current vectors in the less than 10% coverage areas represent few actual vectors from which the mean is calculated (i.e., less than 76 out of 762 possible data points for the three-month mean) and should be disregarded. The 10% coverage contour lines were drawn on the mean current and standard deviation maps to denote these dubious vectors.

Standard deviation plots indicate the variability of the currents over the time period. The standard deviation of the U and V velocity components are calculated for each gridpoint and plotted as a vector. Standard deviation vectors pointing at a 45° angle indicate equal variability in the U and V velocity components. Vectors pointing at other angles indicate higher variability in the U or V velocity component. In the area of less than 10% coverage the standard deviation vectors were often smaller than in the areas of higher coverage.

A. THREE-MONTH MEAN CURRENTS

The mean CODAR-derived surface currents from 1 March to 31 May 1992 are shown in Figure 7. The general flow is a semi-counterclockwise gyre centered 10 km northwest of Moss Landing. The map reveals the lack of conservation of surface mass as shown by the areas of convergence near the baseline and a few kilometers north of the Monterey

Peninsula. The currents are stronger in the outer bay and flow onshore to the Southeast. The currents weaken nearshore and turn alongshore. The mean currents turn offshore north of Moss Landing and flow to the west. Typical mean speeds are 15 $cm \cdot sec^{-1}$ in the outer bay and 6 $cm \cdot sec^{-1}$ in the southeast inner bay and near zero mean flow northwest of Moss Landing. The interpretation of these and other current maps is subject to the variable amount of data available at each gridpoint. The data and the resulting means are most reliable in regions that routinely return data. McLeish and Maul (1991) made similar statements when describing the CODAR data off Miami, Florida. Figure 8 shows the percentage of CODAR coverage for the three-month period. An area of 496 km^2 has greater than 50% coverage. An area of 194 km^2 has greater than 90% coverage. The outer edge of the coverage maps returned less than 10% of the possible data and interpretations for these areas are inconclusive.

The interpretation of the mean currents is also influenced by the observed variability. The standard deviations of CODAR-derived current are presented in Figure 9 for the March through April period. The standard deviation field differs greatly from that of the mean current maps. The map shows the vectors to be uniform and aligned, predominately, along 45° angles in the outer bay, which means that the variability was equal in both component directions. In the outer bay, the magnitudes of the standard deviation are typically 30 $cm \cdot sec^{-1}$ and are comparable to the mean current magnitudes. In the inner bay, the vectors point more horizontally indicating greater east-west variability. The magnitude of the standard deviation vectors in the inner bay are typically 25 $cm \cdot sec^{-1}$ which is some 2 to 5 times larger than those of the mean current vectors. The 10% coverage line is drawn on the map and indicates the area in which interpretation of the data is inconclusive. It is clear that the three-month mean CODAR-derived currents result from stronger flows at higher frequencies. They are not representative of the typical flow conditions but rather the

outcome of averaging widely varying currents. We shall see below that the dominant variability comes from the daily cycle.

B. MONTHLY MEAN CURRENTS

1. March Mean Currents

The mean CODAR-derived surface currents for March 1992 are shown in Figure 10. Mean currents during March are weaker than the three-month mean currents. The mean current minimum is present, centered 8 km west of Moss Landing and a clockwise gyre is present centered 16 km northwest of Monterey near the 10% coverage area. Between the two features, the current flows south and onshore to the south-southeast. Figure 11 shows the percentage of CODAR coverage for March. An area of 556 km^2 has greater than 50% coverage. No gridpoints have greater than 90% coverage for March. The March standard deviation plot is similar to the three-month standard deviation and is shown in Figure 12.

2. April Mean Currents

The mean CODAR-derived surface currents for April 1992 are shown in Figure 13. The mean currents in April are stronger than those for March. An area of minimum mean flow is centered 8 km west of Moss Landing. The currents are much stronger in the outer bay and flow is onshore to the southeast. Nearshore the currents weaken and turn alongshore. The mean currents turn offshore north of Moss Landing and flow to the west. Two convergence areas are seen one 4 km northwest of the Monterey Peninsula and the other along the baseline. Figure 14 shows the percentage of CODAR coverage for April. An area of 574 km^2 has greater than 50% coverage. An area of 370 km^2 has greater than 90% coverage. The April standard deviation plot is similar to the three-month standard deviation and is shown in Figure 15.

3. May Mean Currents

The mean CODAR-derived surface currents for May 1992 are shown in Figure 16. The strong southeasterly currents in the outer bay are weaker but the currents elsewhere are stronger. The general surface current flow pattern has a counterclockwise gyre centered 12 km west of Moss Landing and large convergence areas northwest of the Monterey Peninsula and along the baseline. Figure 17 shows the percentage of CODAR coverage for May. An area of 521 km^2 has greater than 50% coverage. An area of 205 km^2 has greater than 90% coverage. The May standard deviation plot has uniform vectors indicating greater east-west variability in the outer and inner bay and is shown in Figure 18.

4. Comparison of the Monthly Mean Currents

The monthly mean currents show the development of the summertime upwelling-favorable regime. In March, the outer bay currents are weak and flow to the south. April shows strong currents in the outer bay and the convergence areas at the baseline and to the northwest of Monterey Peninsula. By May, the currents north of Moss Landing show an offshore and northward flow and a gyre has developed centered northwest of Moss Landing. The convergence areas are similar for April and May.

The variability in all three months was uniformly high and exceeds the mean fields. The exception to this is in the outer bay during April where the magnitudes of the mean currents and standard deviation are nearly the same. The pattern of the standard deviation fields bears no similarity to the mean fields and indicates that the variability is associated with large-scale forcing mechanisms, including diurnal winds and tides. The diurnal wind and tidal effects are discussed in the following sections.

C. WEEKLY MEAN CURRENTS

The weekly mean CODAR surface currents are shown in Figures 19 to 31. The sequence of weekly mean current maps show interesting features that are not seen in the

monthly mean maps. A synopsis of the weekly mean surface currents follows. The standard deviation and coverage plots, however, are similar to the longer-time mean plots and are not shown.

The current pattern during the first week of March is vastly different from any other weekly current pattern. It shows northward flowing currents sweeping through the entire bay. An area of minimum or no flow is centered 16 km west of Moss Landing. A convergence area 10 km south of Santa Cruz is found between the northward currents of the outer bay and the westward offshore currents north of Moss Landing. This week is probably influenced by the northward-flowing Davidson current and is indicative of the winter time regime. During the week of 8 March, the currents reverse, flow to the southeast and increase in velocity. The previous convergence and no-flow areas disappear. New convergence areas form off the coast at Moss Landing and 8 km northwest of the Monterey Peninsula. During the week of 15 March, the currents weaken in the outer bay and two areas of no flow develop, one centered 8 km west of Moss Landing the other northwest of the Monterey Peninsula. Strong offshore flow north of Moss Landing returns. During the week of 22 March an interesting current pattern emerges. Strong northward flowing currents develop in the outer bay while nearshore the currents flow to the southeast. Two no-flow areas are centered 6 km and 20 km west of Moss Landing and for the first time strong convergence is noted near the baseline. The strong northward flow suggests an oceanic current from the south and is also recorded in the ADCP data discussed in the next chapter.

The weekly mean currents of April are dominated by strong southeastward flow in the outer bay. During the first week of April the currents shift back to a strong southeastward flow throughout the bay. No offshore flow is evident north of Moss Landing and a strong convergent area with possible downwelling is centered 8 km northwest of the Monterey Peninsula. During the week of 5 April currents in the outer bay weaken and a large no-

flow area exists over most of the inner bay west of Moss Landing. Immediately north of Moss Landing and very nearshore the flow is south, west of Pajaro River the flow is offshore. The currents increase slightly and shift more onshore during the week of 12 April. Convergence areas develop west of Moss Landing and near the baseline. During the week of 19 April the currents in the outer bay increase dramatically. The week of 26 April is similar to the previous week.

The weekly mean currents of May show the development of a counterclockwise gyre centered west of Moss Landing. The first week of May the currents in the outer bay weaken and the counterclockwise gyre develops. There is no mean flow in the area 8 km northwest of the Monterey Peninsula. This weekly pattern is similar to the three-month mean. From the week of 10 May the pattern is similar but with lower current velocities. The gyre erodes and southward flow results over most of the bay during the week of 17 May. The last week in May shows a strengthening counterclockwise gyre with higher velocities.

D. CANONICAL DAY CURRENTS

The CODAR-derived currents for a canonical day are obtained by calculating the mean currents for each of the eight transmission times over the three-month period. This is done to determine if any daily patterns exist. The standard deviation and coverage plots are essentially the same as the three-month plots so only mean plots are shown here. All times referenced are in PDT. The canonical current maps significantly help in the interpretation of the previous mean current maps.

The 00:00 to 09:00 canonical currents consist of strong currents flowing offshore north of Moss Landing and weaker currents flowing onshore south of Moss Landing (see Figures 32 to 35). In the outer bay, currents range from southwestward to southeastward during these times. At 00:00 the southeast portion of the bay has little or no mean flow. At

03:00 the currents in the outer bay weaken and nearshore currents in the southeast portion of the bay flow alongshore to the north. At 06:00 the currents in the outer bay remain low or show basically no flow. North of the Monterey coast the currents flow offshore to the northwest. At 09:00 the currents in the outer bay increase but there is a large no-flow area centered 18 km west of Moss Landing.

The 12:00 to 21:00 canonical currents are dominated by onshore southeasterly flow as shown in Figures 36 to 39. The currents north of Moss Landing have reversed and flow onshore to the southeast. Strong convergence areas develop along the baseline. By 15:00 all surface currents are flowing strongly onshore. At 18:00 the currents shift to the south-southwest. The onshore currents near Moss landing weaken. By 21:00 the currents north of Moss Landing reverse and slowly flow offshore to the northwest.

The canonical currents show interesting features and variability. The dominant features of the canonical currents are the intense daily shifts in current speed and direction. During the afternoon all the currents flow onshore and are associated with the daily sea breeze. After the sea breeze diminishes, the strong onshore currents in the outer bay relax and north of Moss Landing offshore currents flow to the west. The offshore flow north of Moss Landing is perhaps due to the effects of a nightly land breeze. This pattern of weak currents and offshore flow continues from midnight until 09:00.

The effect of the canonical currents is reflected in the mean currents upon close inspection. The near zero flow in the three-month mean north of Moss Landing is a result of averaging the westward nighttime flow with the eastward daytime flow. The sea breeze effects are canceled by the nightly land breeze effects. In the outer bay the large south-southeastward flow is almost entirely an afternoon sea breeze effect. During the morning hours there is near zero flow. The three-month mean current map only reflects this afternoon effect in the outer bay. The convergence near the coast around the baseline is also an effect of the afternoon breeze. At this time the currents are driven onto the beach.

Overall the canonical currents indicate that the mean current field is dominated by the daily effects of the sea breeze.

E. DISCUSSION

The mean CODAR-derived surface currents provide a useful tool in the study and visualization of the current structure of Monterey Bay. The mean CODAR-derived surface currents show the general flow patterns associated with the daily sea-breeze effect. By using the canonical currents, a clearer picture of the flow patterns can be seen. The effect of the erratic vectors is reduced with mean currents, indicating the errors are random; however, it would be better to remove the erratic vectors from the individual maps so the data could be used in real time.

The CODAR system provides remote observations covering approximately 550 km^2 of the sea surface 50% of the time. This coverage extends 26 km out from the Monterey site, and 22 km from the Moss Landing site. The reduced ranges from the Moss Landing site are likely due to antenna corrosion. In July 1992 the antenna from the Moss Landing site was found to be corroded and was replaced. Ranges from the Moss Landing site improved after the antenna replacement.

Inspection of the mean currents shows that the largest current velocities occur at the edges of CODAR coverage. These outer edges have only a few actual vectors from which the mean is derived. If the CODAR currents are accurate, two possibilities exist: the maximum range of CODAR is dependent on the current velocity (a selection process that is not understood) and/or sub-sampling the field a very small number of times permits the high, variable current to be depicted rather than the low mean. To counter this possible error in the mean currents, only gridpoints with greater than 10% coverage should be expected to be accurate.

The weekly mean currents can be a tool to study oceanic events that affect the bay's circulation. The mean CODAR-derived currents from the first week of March show a weak northward flow over the majority of the bay. The second week the currents shift to the southeast. This pattern continues during the third week of March. During the week of 22-29 March, strong northward currents develop in the southwest section of the outer bay. ADCP, SST and wind records verify this northward current event and are shown in the next chapter. This northward flow corresponds to a warming of the sea surface. In the first week in April, strong southeastward currents sweep the bay and correspond to the SST dropping almost 2°C (see Figure 47). During the following three weeks of April the currents weaken and correspond to the SST gradually increasing. Another week of large southeastward currents occur the last week of April. The SST quickly drops over 3°C in response to the stronger wind mixing and possible cold water advection from the north. This cycle of gradually rising SST associated with lower current speeds followed by strong currents associated with a quick reduction of the SST is repeated two more times.

The daily canonical surface currents reveal the typical diurnal surface current patterns. From 09:00 to 21:00 PDT the currents increase in speed and flow onshore as expected from the daily sea breeze. During the day the winds increase and blow onshore and surface currents respond. As the winds decrease the onshore currents relax. From 24:00 to 06:00 PDT the currents in the outer bay weaken and the currents north of Moss Landing flow offshore to the northwest. This is probably a result of the fading sea breeze and possible onset of the evening land breeze.

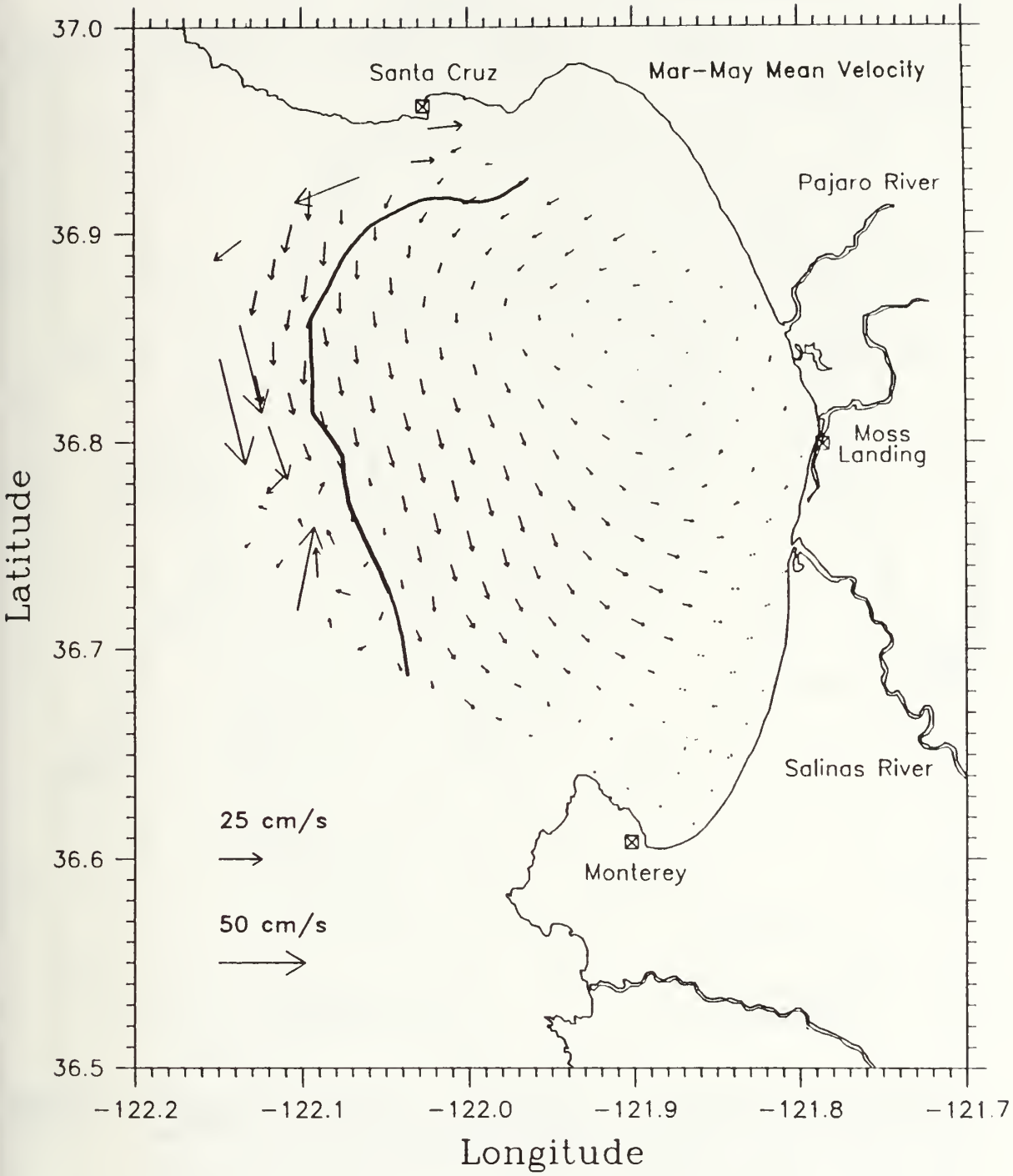

Figure 7. **Mean CODAR-derived Surface Currents March to May, 1992:** The main features of the currents are stronger currents in the outer bay and near zero flow north of Moss Landing. The dark line represents the 10% coverage line and is the limit of reasonable data. Dotted arrows represent current vectors made with the baseline assumption.

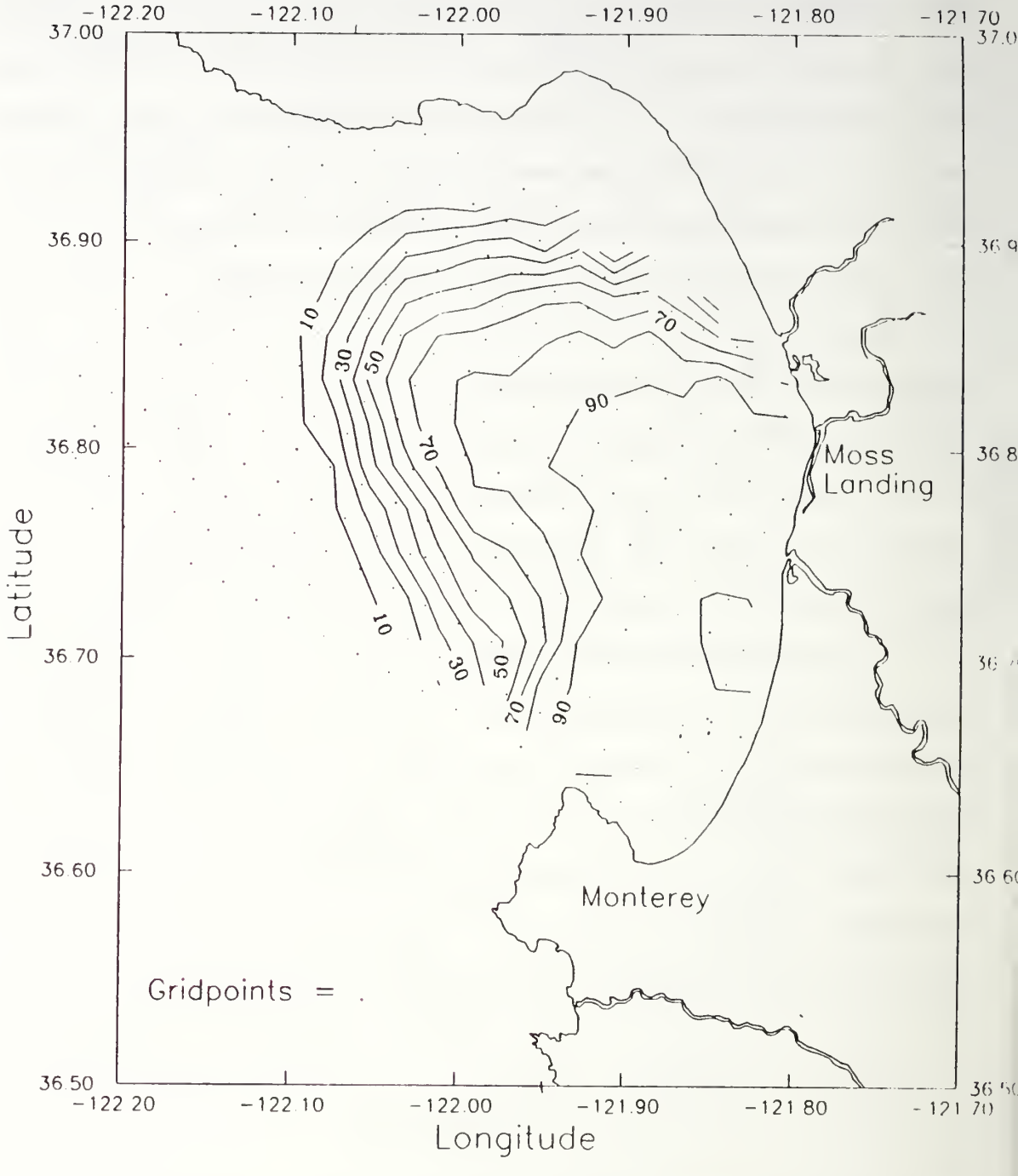

Figure 8. **CODAR Coverage March to May, 1992:** Contours indicate percentage of time the CODAR system produced total current vectors for each gridpoint. Coverage was calculated at each gridpoint by dividing the number of actual measurements derived by the possible number of measurements (762 in this case).

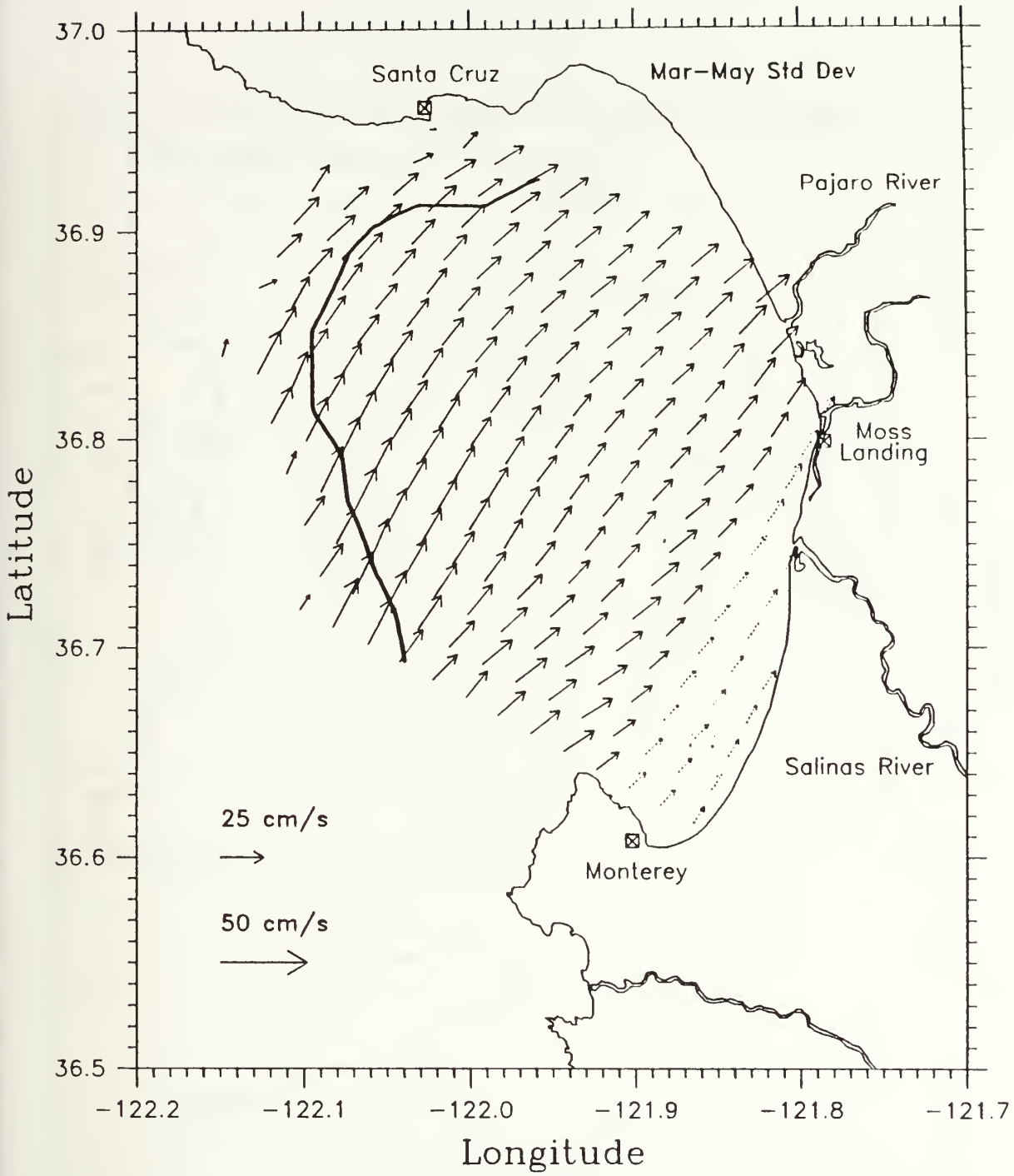

Figure 9. **Standard Deviation of CODAR-derived Surface Currents March to May, 1992:** Standard deviation values are represented by a vector formed from the U and V component standard deviations. Vectors pointing 45° indicate equal amounts of variability in each component. The standard deviation vectors are larger than the mean vectors in the inner bay and comparable to the mean in the outer bay and indicate highly variable currents. The dark line represents the 10% coverage line and is the limit of reasonable data. Dotted arrows represent current vectors made with the baseline assumption.

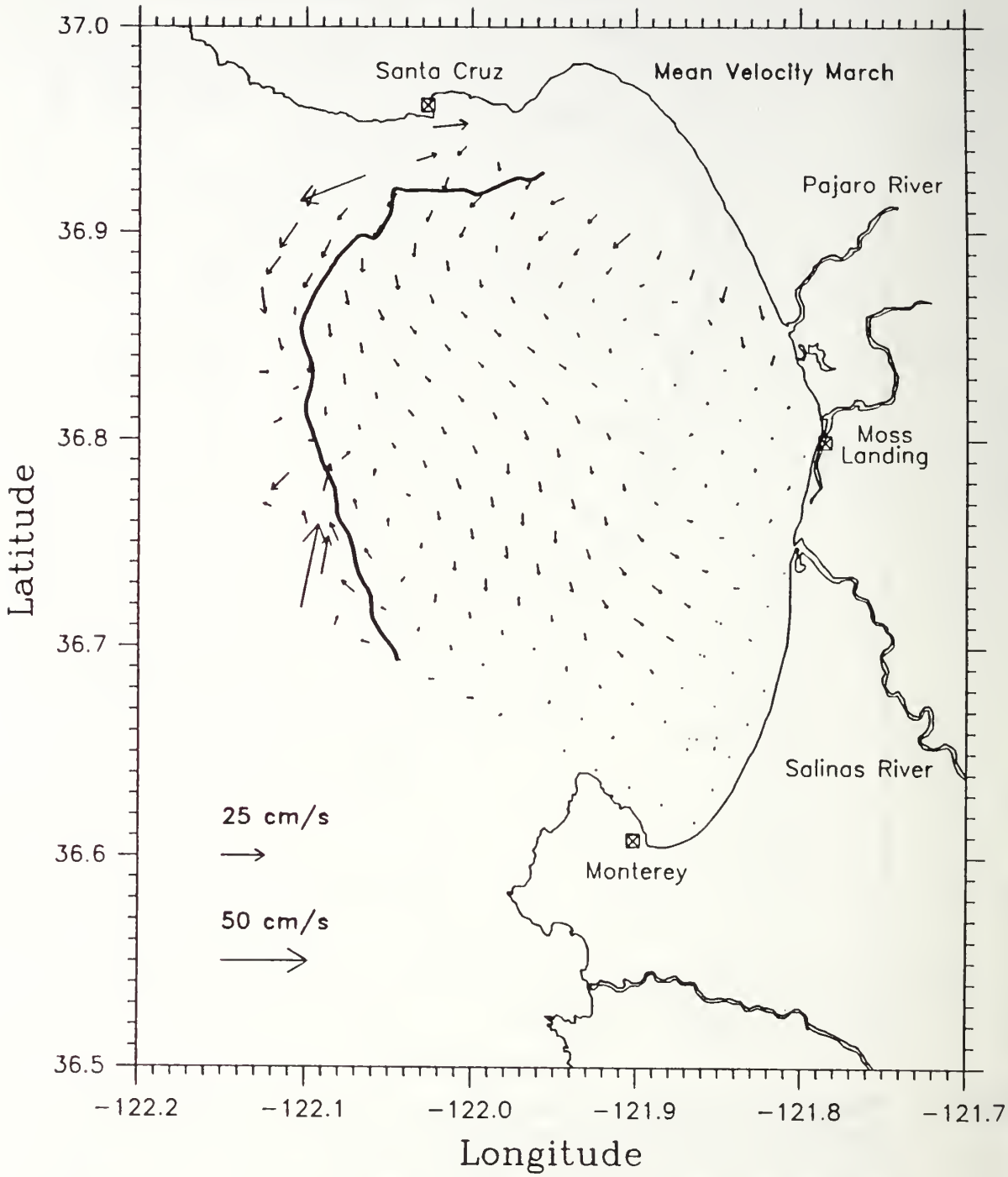

Figure 10. **Mean CODAR-derived Surface Currents March 1992:** The March mean currents are smaller than the three-month mean. The dark line represents the 10% coverage line and is the limit of reasonable data. Dotted arrows represent current vectors made with the baseline assumption.

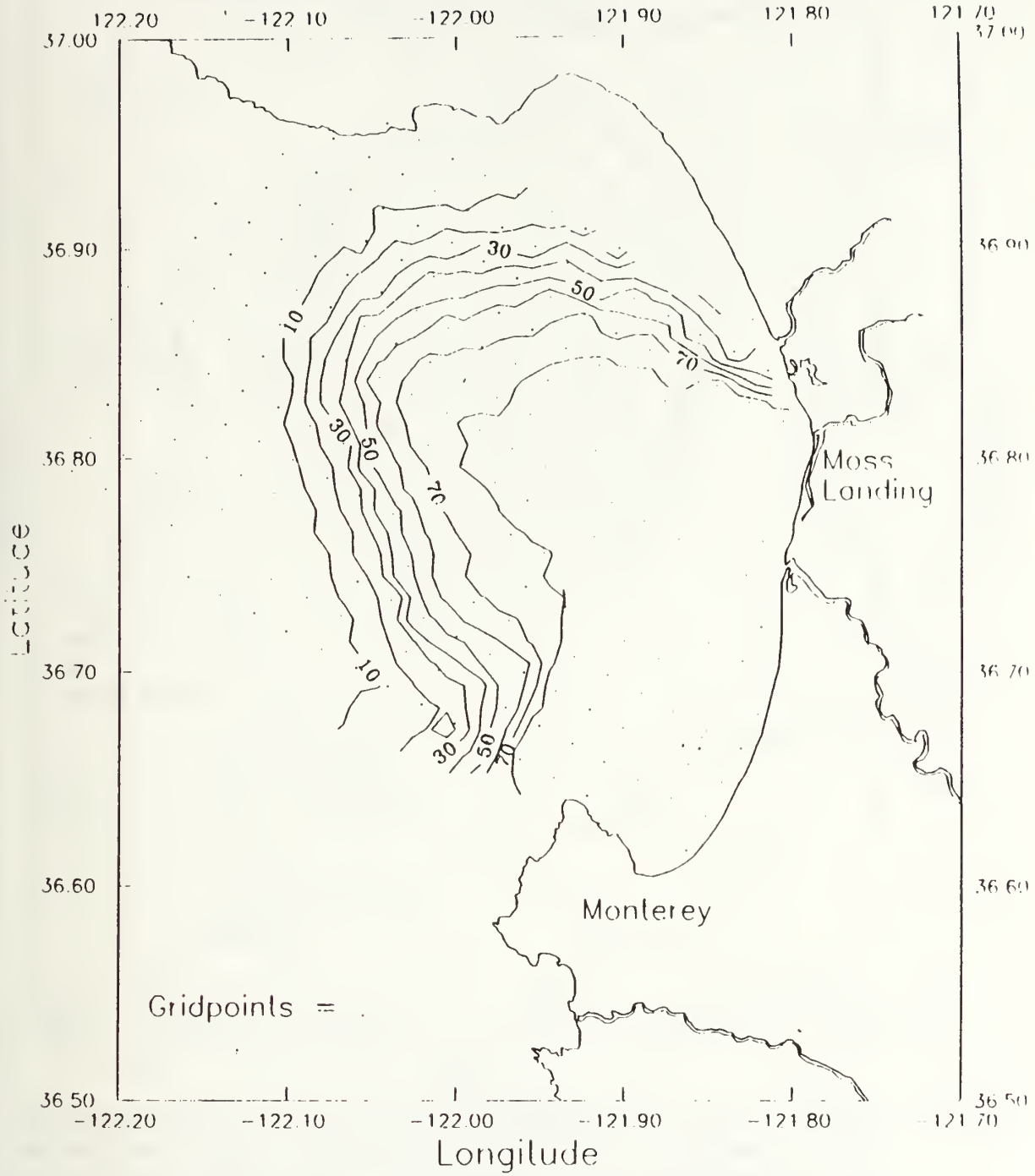

Figure 11. **CODAR Coverage March, 1992:** Contours indicate percentage of time the CODAR system produced total current vectors for each gridpoint. Coverage was calculated at each gridpoint by dividing the number of actual measurements derived by the possible number of measurements (248 in this case).

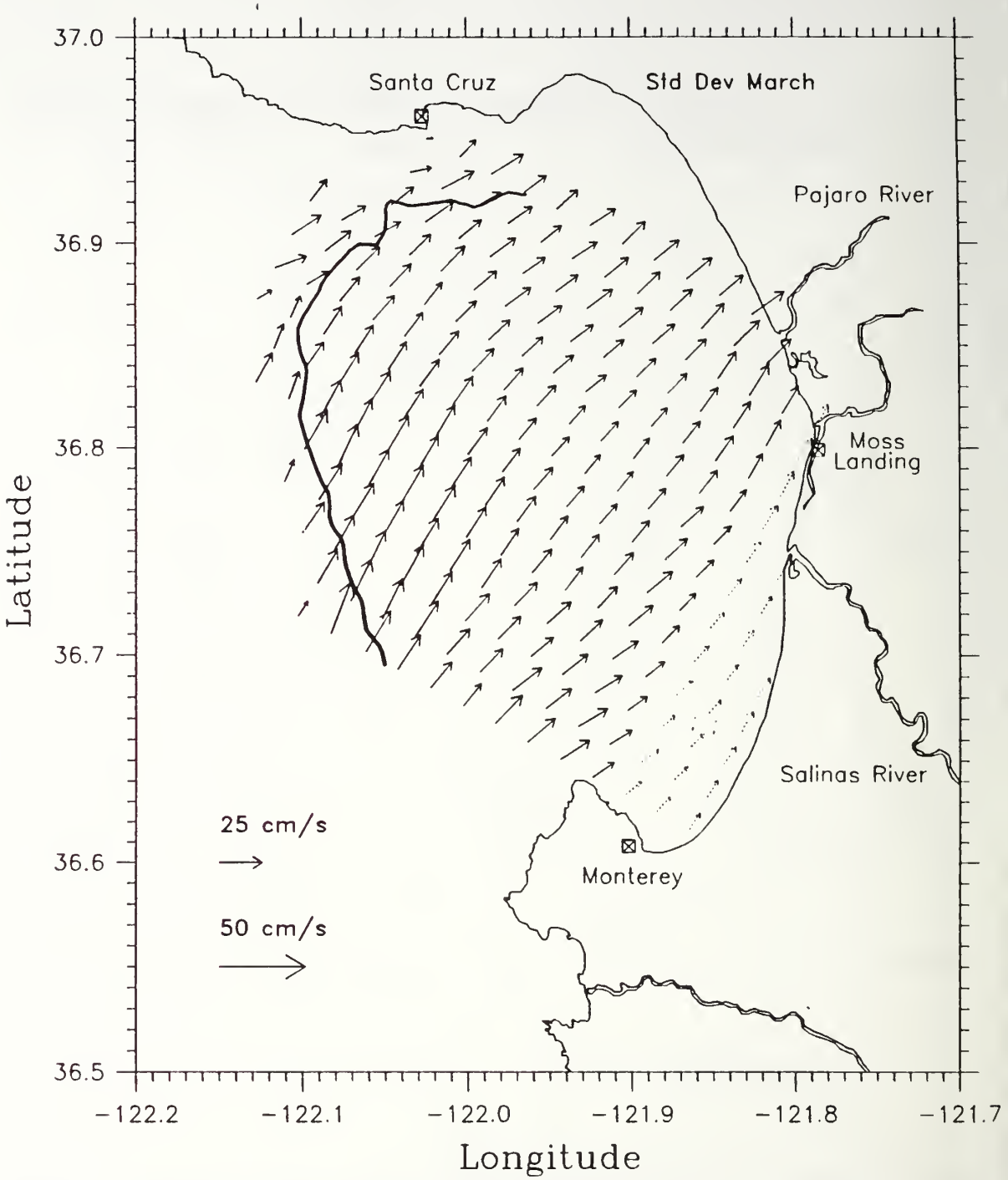

Figure 12. **Standard Deviation of CODAR-derived Surface Currents March, 1992:** Standard deviation values are represented by a vector formed from the U and V component standard deviations. Vector pointing at a 45° angle indicate equal amount of variability for each component. The standard deviation vectors are larger than the mean vectors indicating highly variable currents. The dark line represents the 10% coverage line and is the limit of reasonable data.

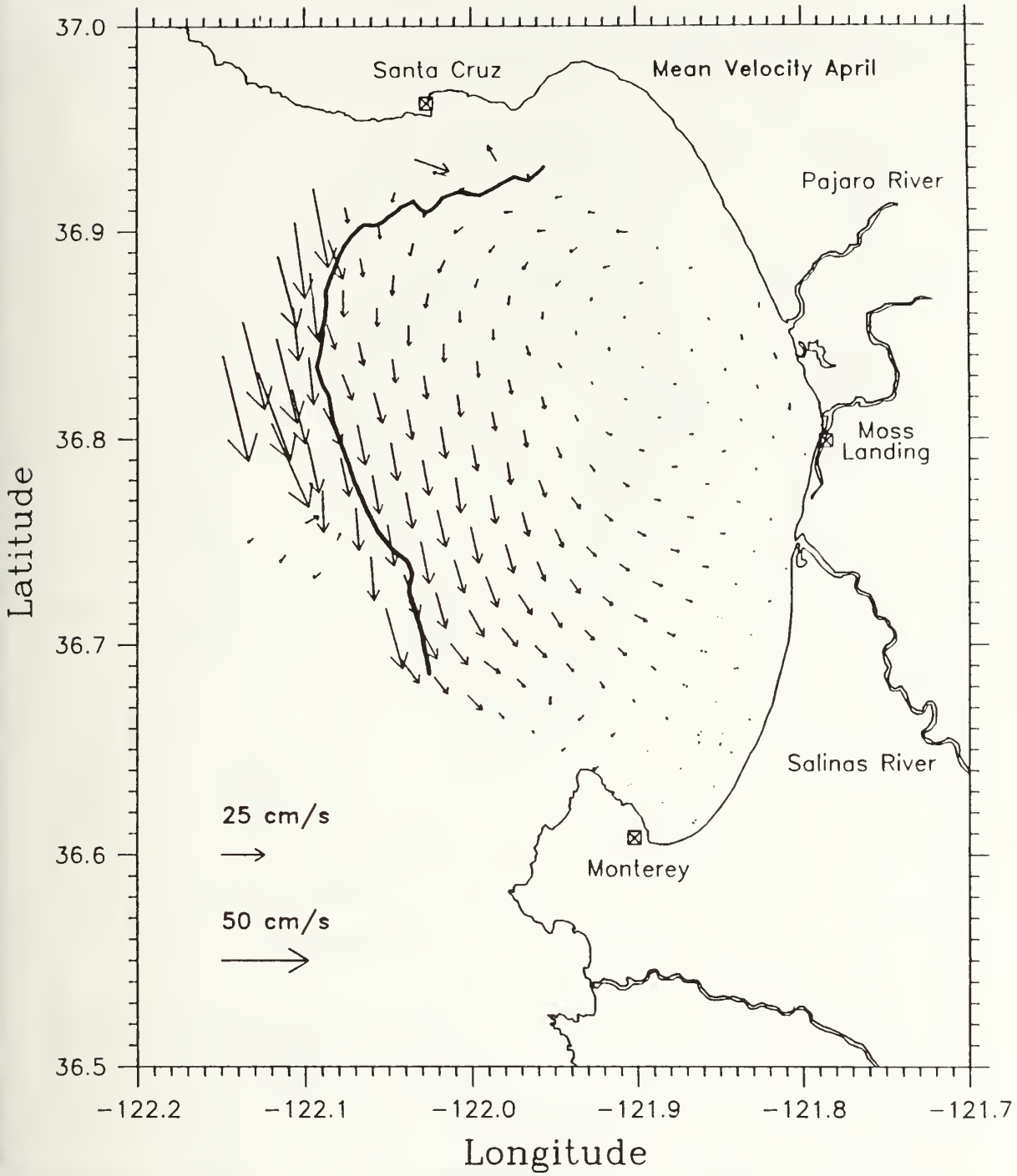

Figure 13. **Mean CODAR-derived Surface Currents April 1992:** The April means currents were the strongest of the three-month mean. The dark line represents the 10% coverage line and is the limit of reasonable data. Dotted arrows represent current vectors made with the baseline assumption.

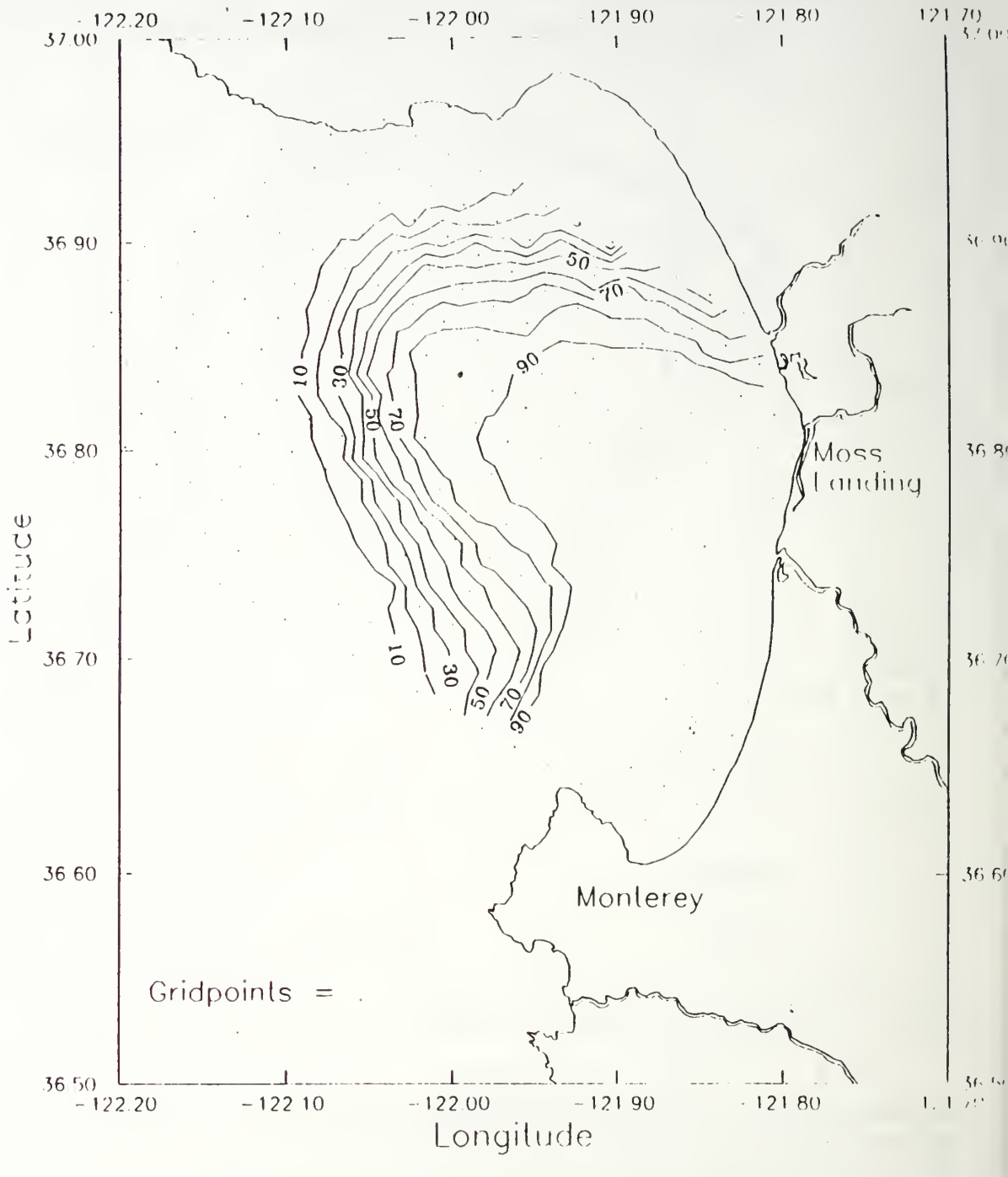

Figure 14. **CODAR Coverage April, 1992:** Contours indicate percentage of time the CODAR system produced total current vectors for each gridpoint. Coverage was calculated at each gridpoint by dividing the number of actual measurements derived by the possible number of measurements (240 in this case).

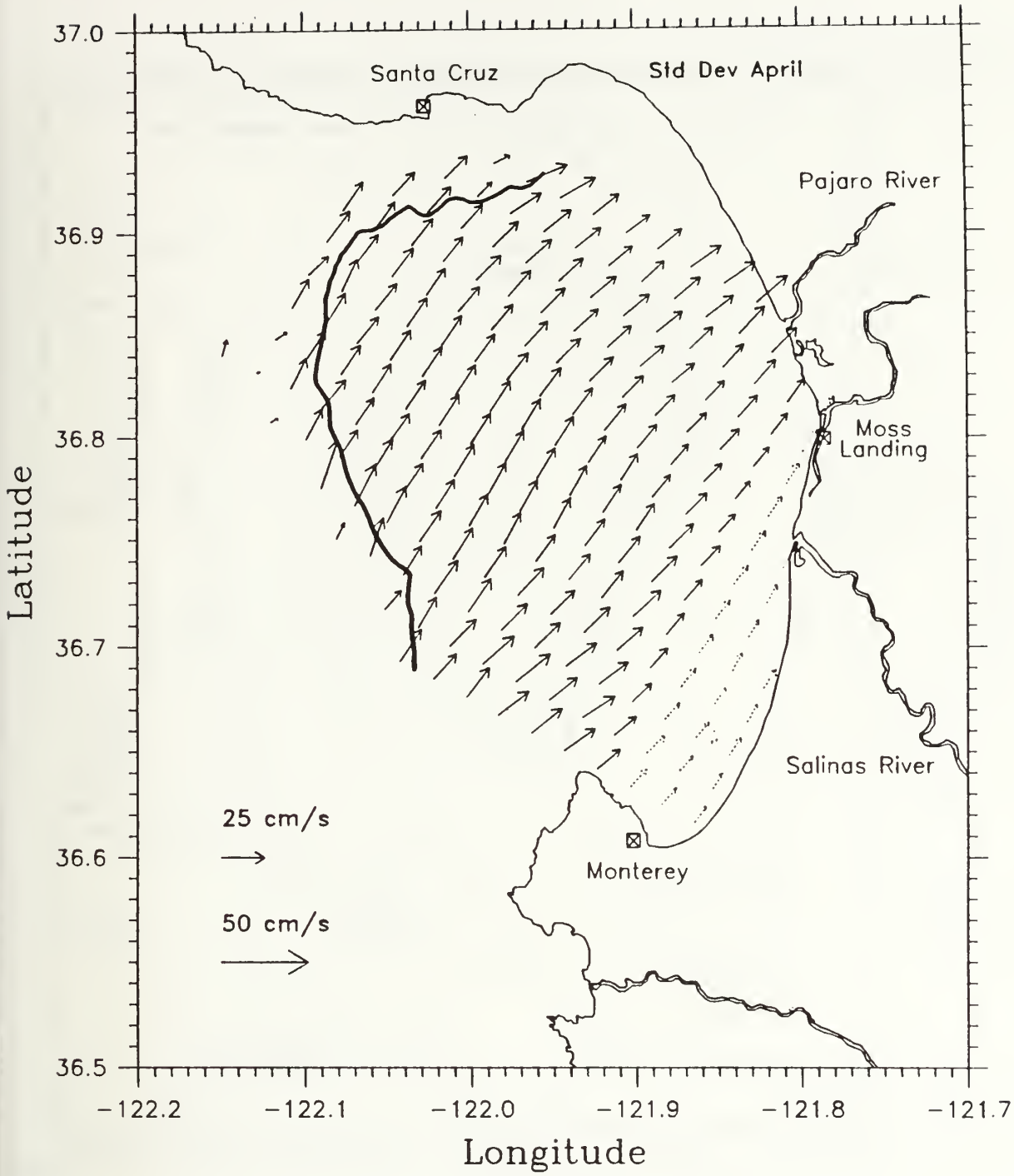

Figure 15. **Standard Deviation of CODAR-derived Surface Currents April 1992:** Standard deviation values are represented by a vector formed from the U and V component standard deviations. Vector pointing at a 45° angle indicate equal amount of variability for each component. The standard deviation vectors are larger than the mean vectors indicating highly variable currents. The dark line represents the 10% coverage line and is the limit of reasonable data.

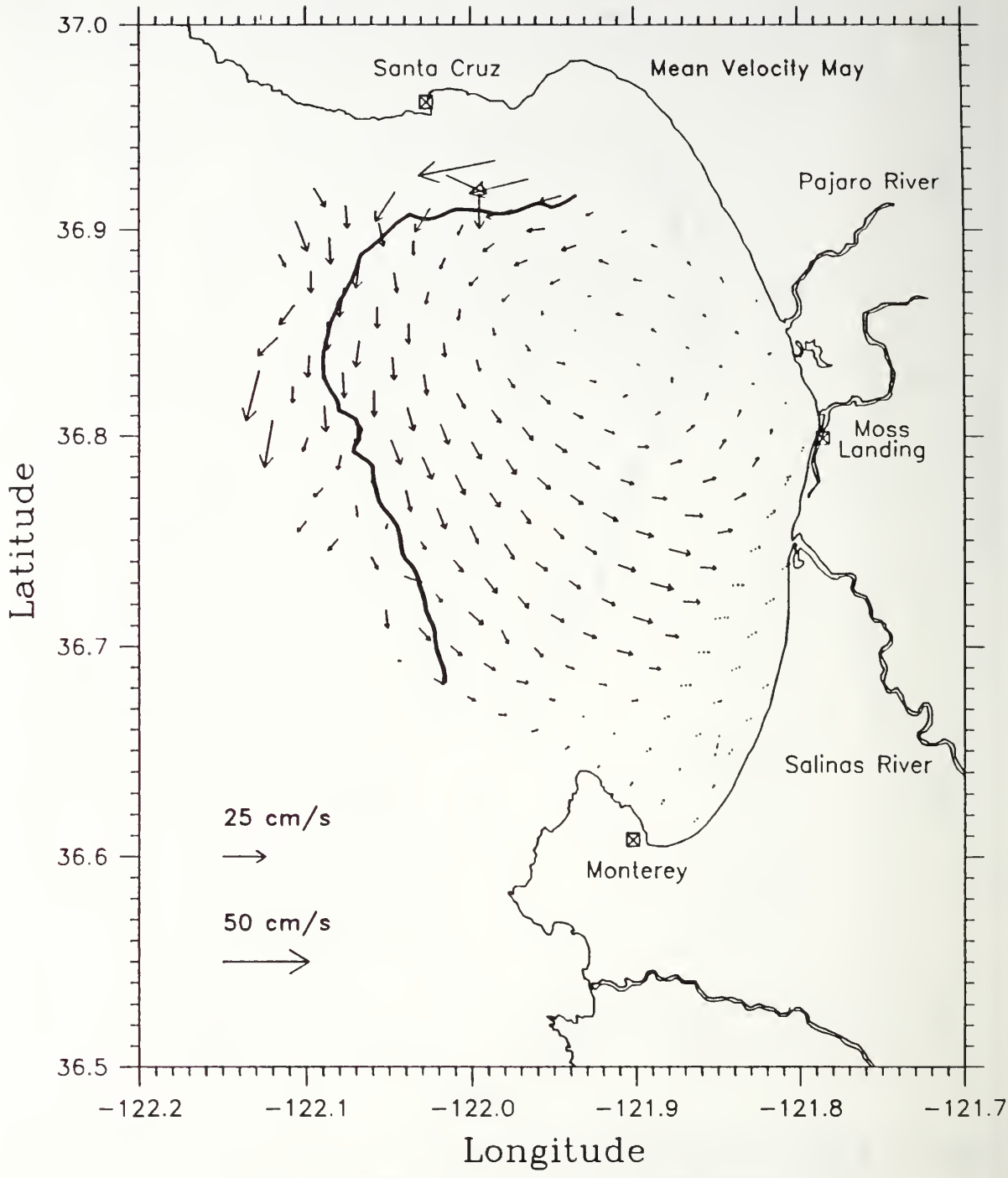

Figure 16. **Mean CODAR-derived Surface Currents May 1992:** The May mean currents show a counterclockwise gyre. The dark line represents the 10% coverage line and is the limit of reasonable data. Dotted arrows represent current vectors made with the baseline assumption.

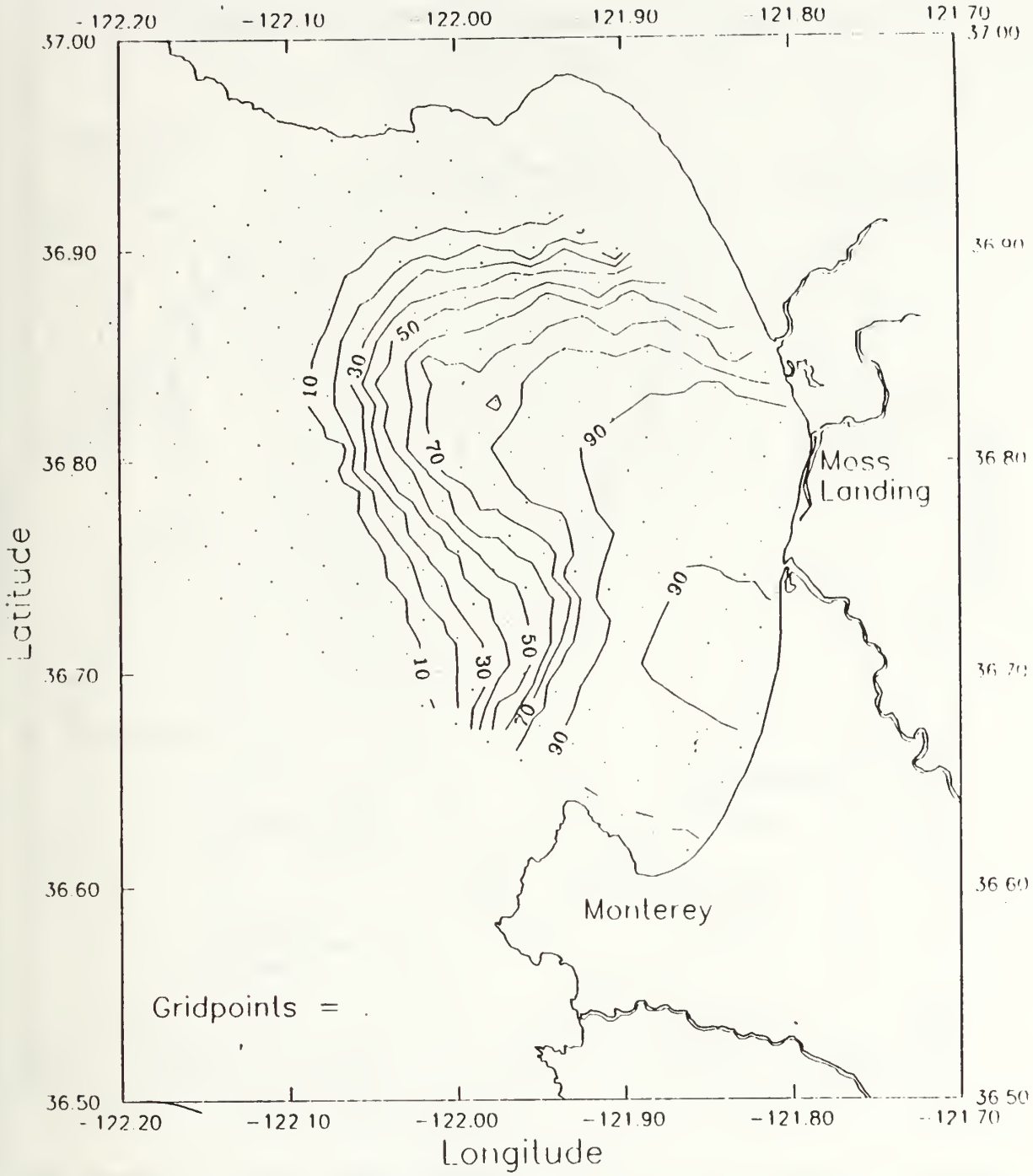

Figure 17. **CODAR Coverage May 1992:** Contours indicate percentage of time the CODAR system produced total current vectors for each gridpoint. Coverage was calculated at each gridpoint by dividing the number of actual measurements derived by the possible number of measurements (240 in this case).

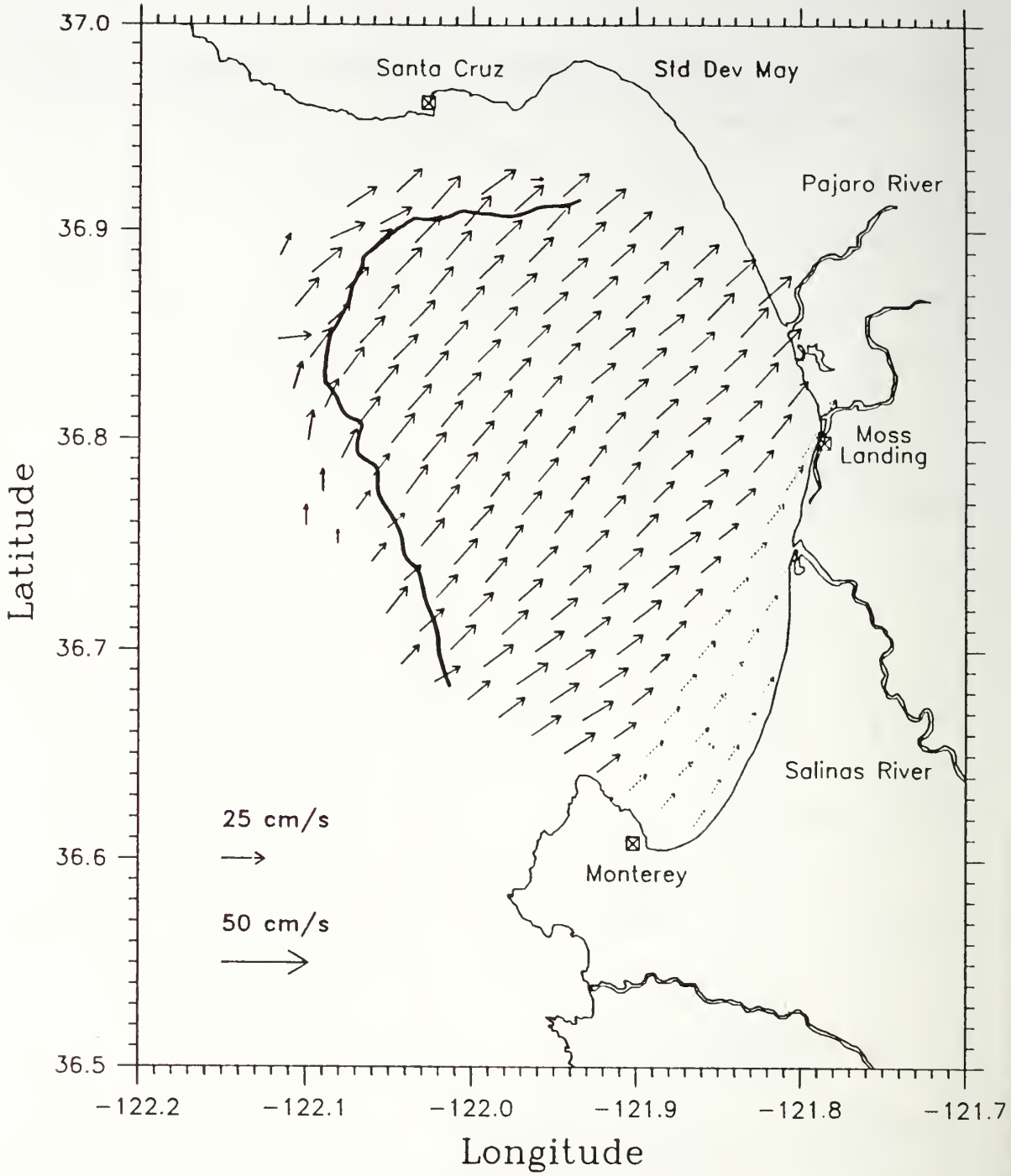

Figure 18. **Standard Deviation of CODAR-derived Surface Currents May 1992:** Standard deviation values are represented by a vector formed from the U and V component standard deviations. Vector pointing at a 45° angle indicate equal amount of variability for each component. The standard deviation vectors are larger than the mean vectors indicating highly variable currents. The dark line represents the 10% coverage line and is the limit of reasonable data.

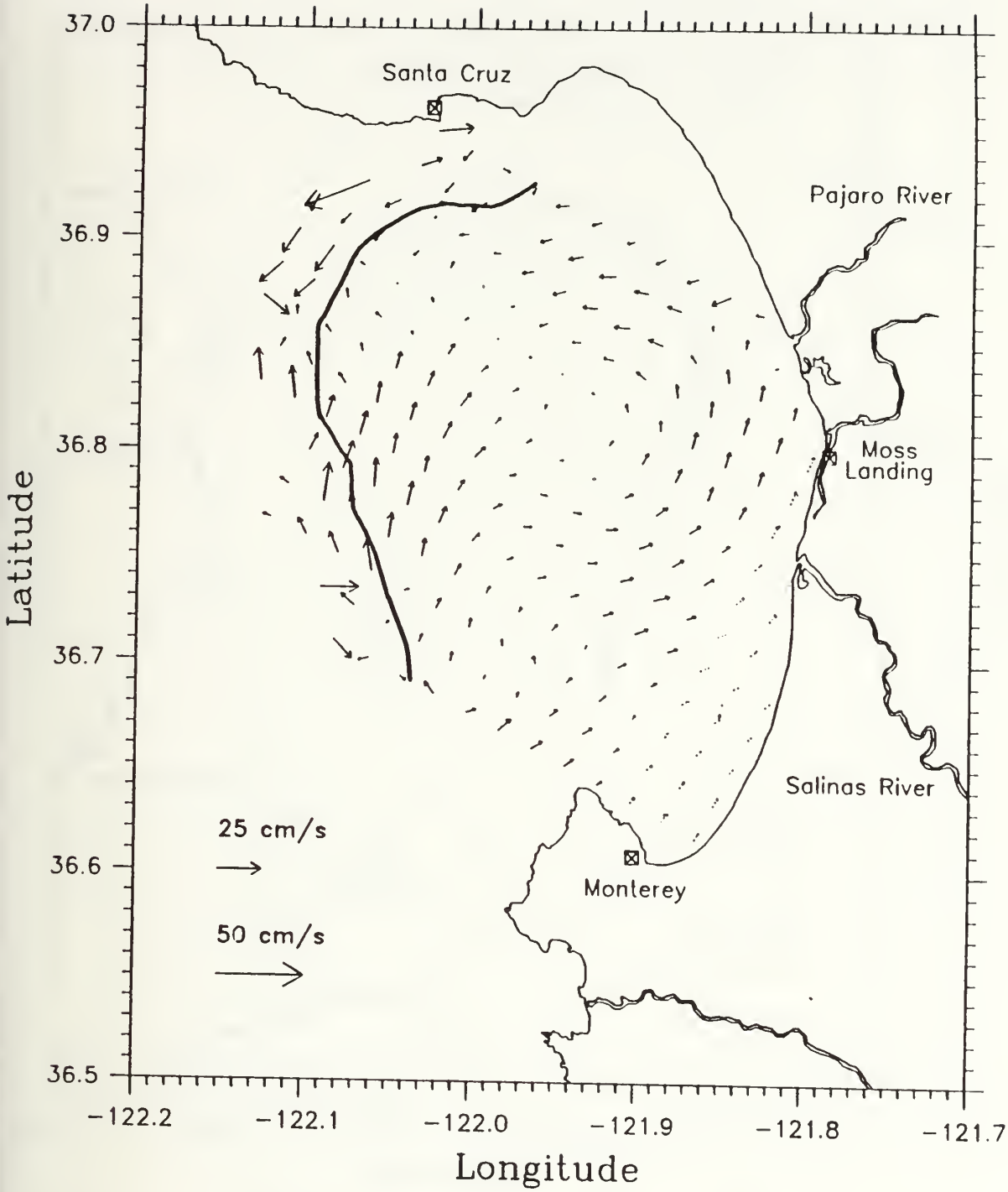

Figure 19. **Mean CODAR-derived Surface Currents March 1 to 7, 1992:** Note northerly currents in the outer bay. The dark line represents the three-month mean 10% coverage line and is the limit of reasonable data. Dotted arrows represent current vectors made with the baseline assumption.

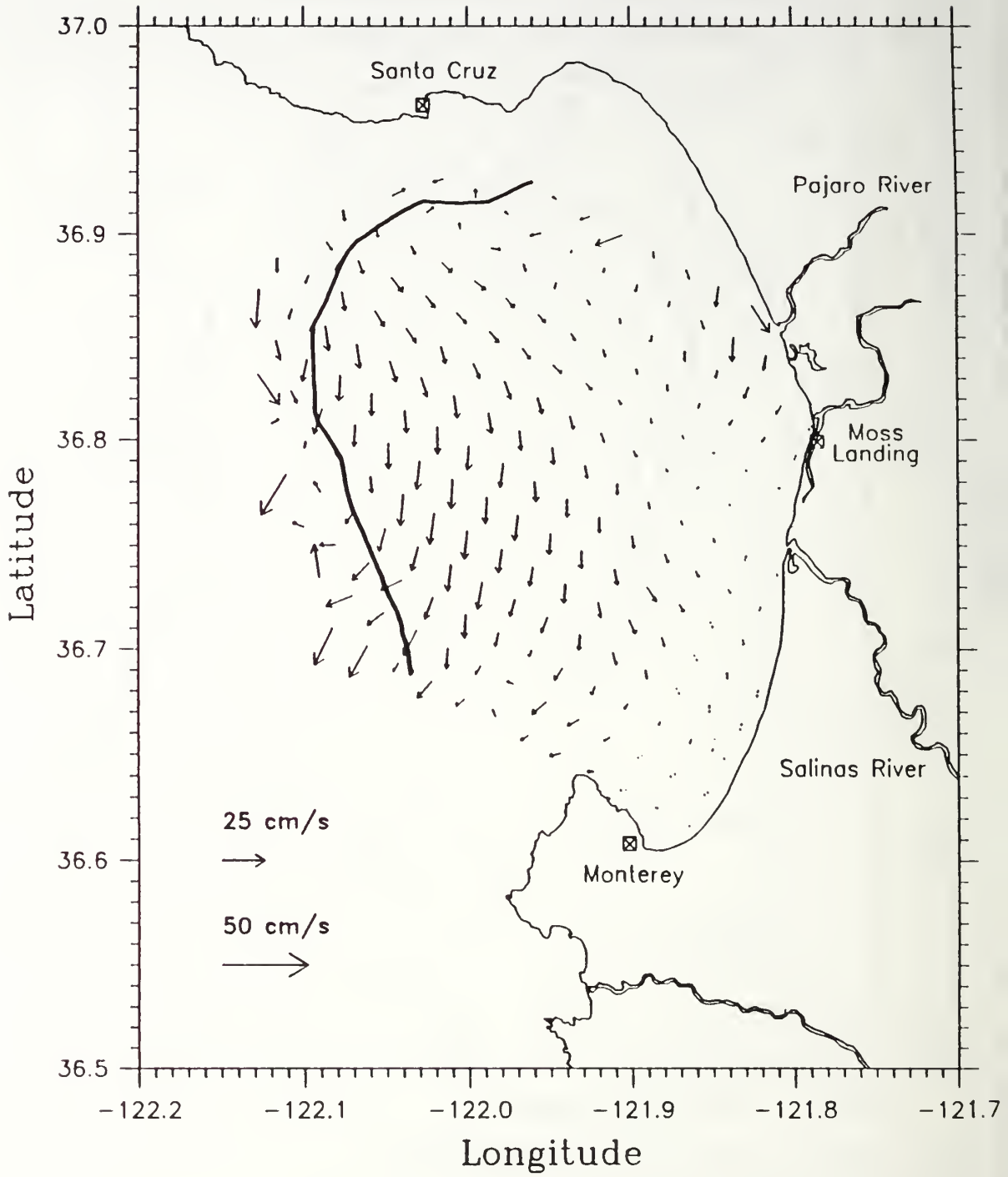

Figure 20. **Mean CODAR-derived Surface Currents March 8 to 14, 1992:** Note reversal of flow in outer bay. The dark line represents the three-month mean 10% coverage line and is the limit of reasonable data. Dotted arrows represent current vectors made with the baseline assumption.

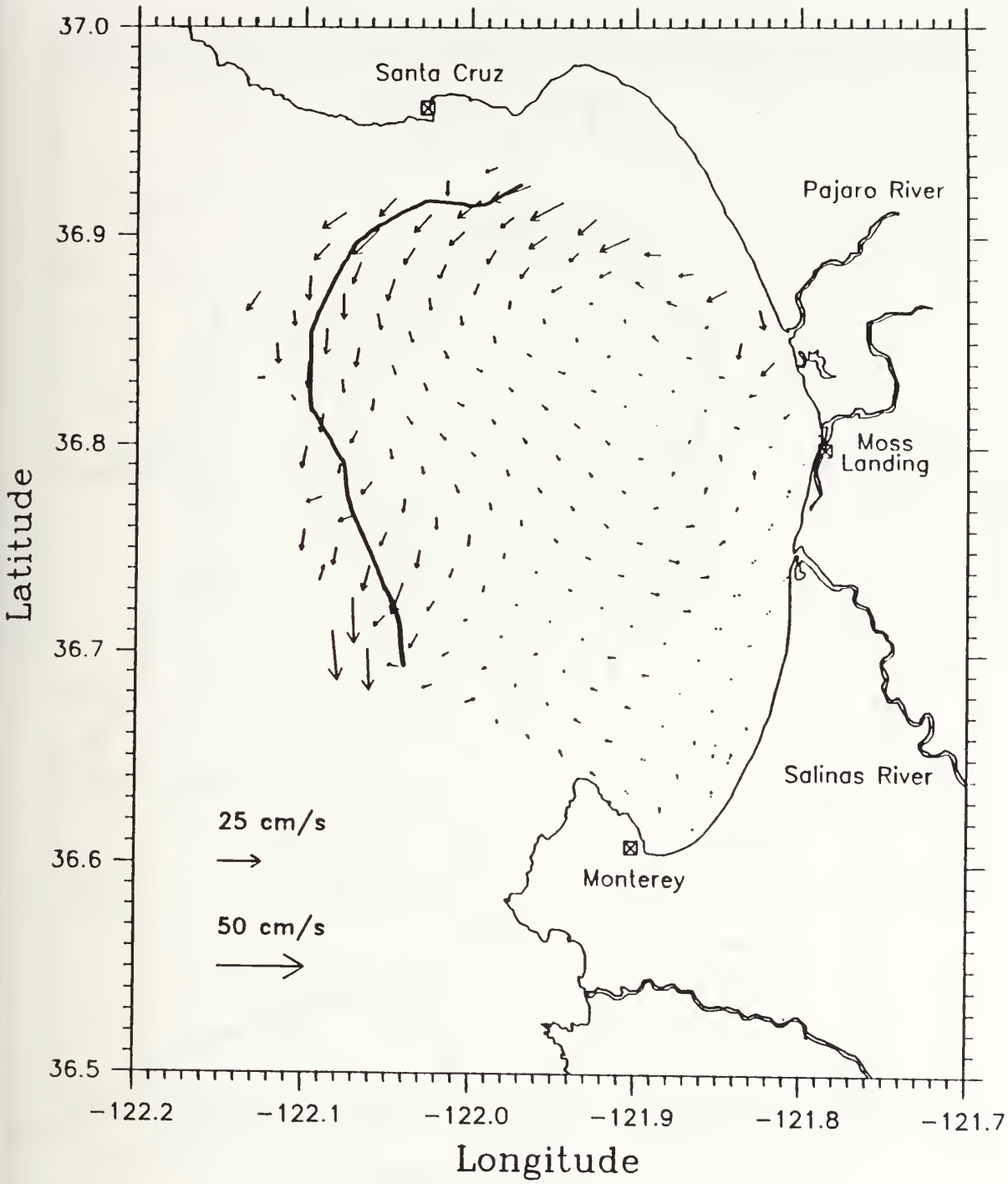

Figure 21. **Mean CODAR-derived Surface Currents March 15 to 21, 1992:** Note the low flow throughout most of the bay. The dark line represents the three-month mean 10% coverage line and is the limit of reasonable data. Dotted arrows represent current vectors made with the baseline assumption.

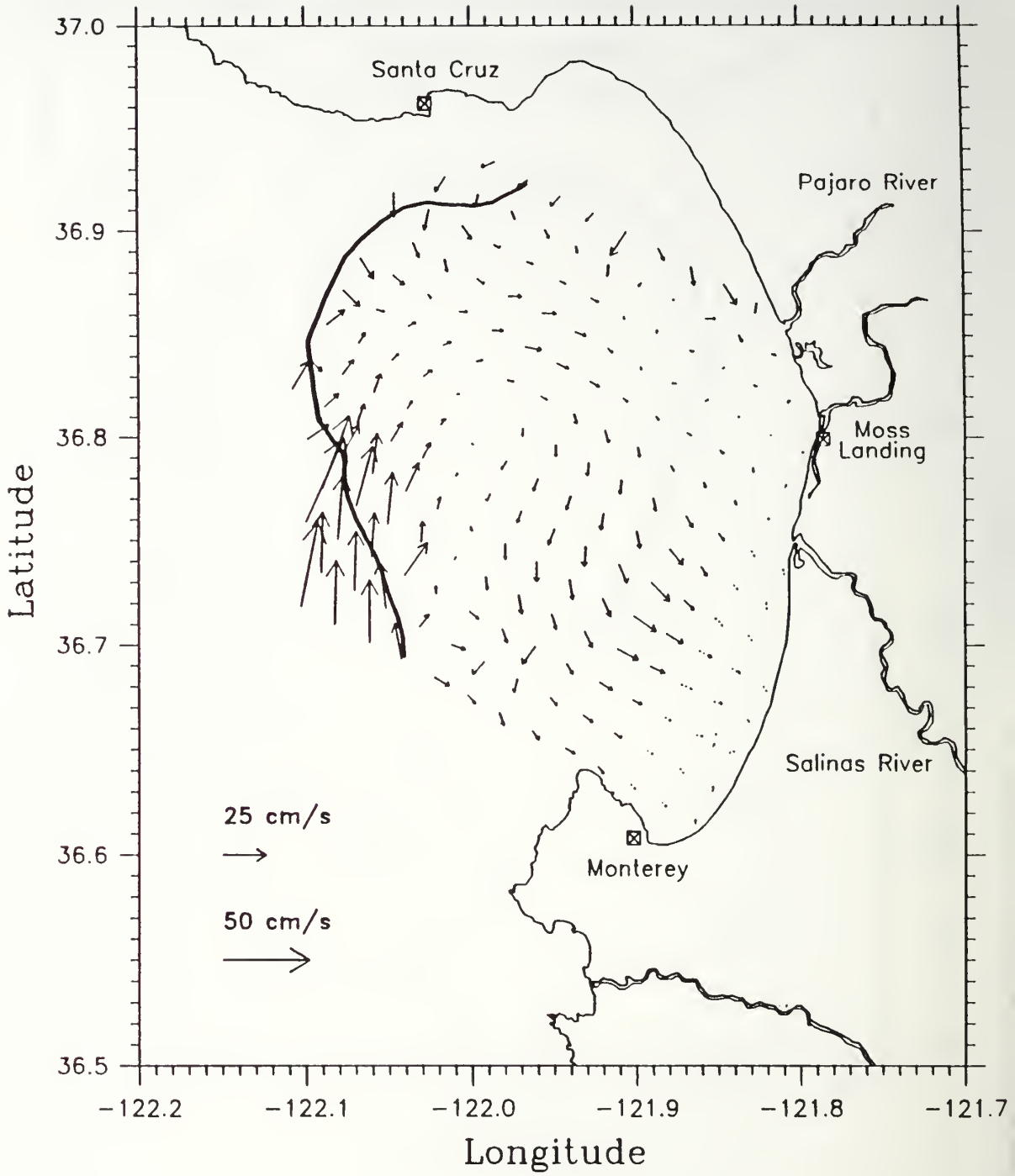

Figure 22. **Mean CODAR-derived Surface Currents March 22 to 28, 1992:** Note the strong northerly flow in outer bay. The dark line represents the three-month mean 10% coverage line and is the limit of reasonable data. Dotted arrows represent current vectors made with the baseline assumption.

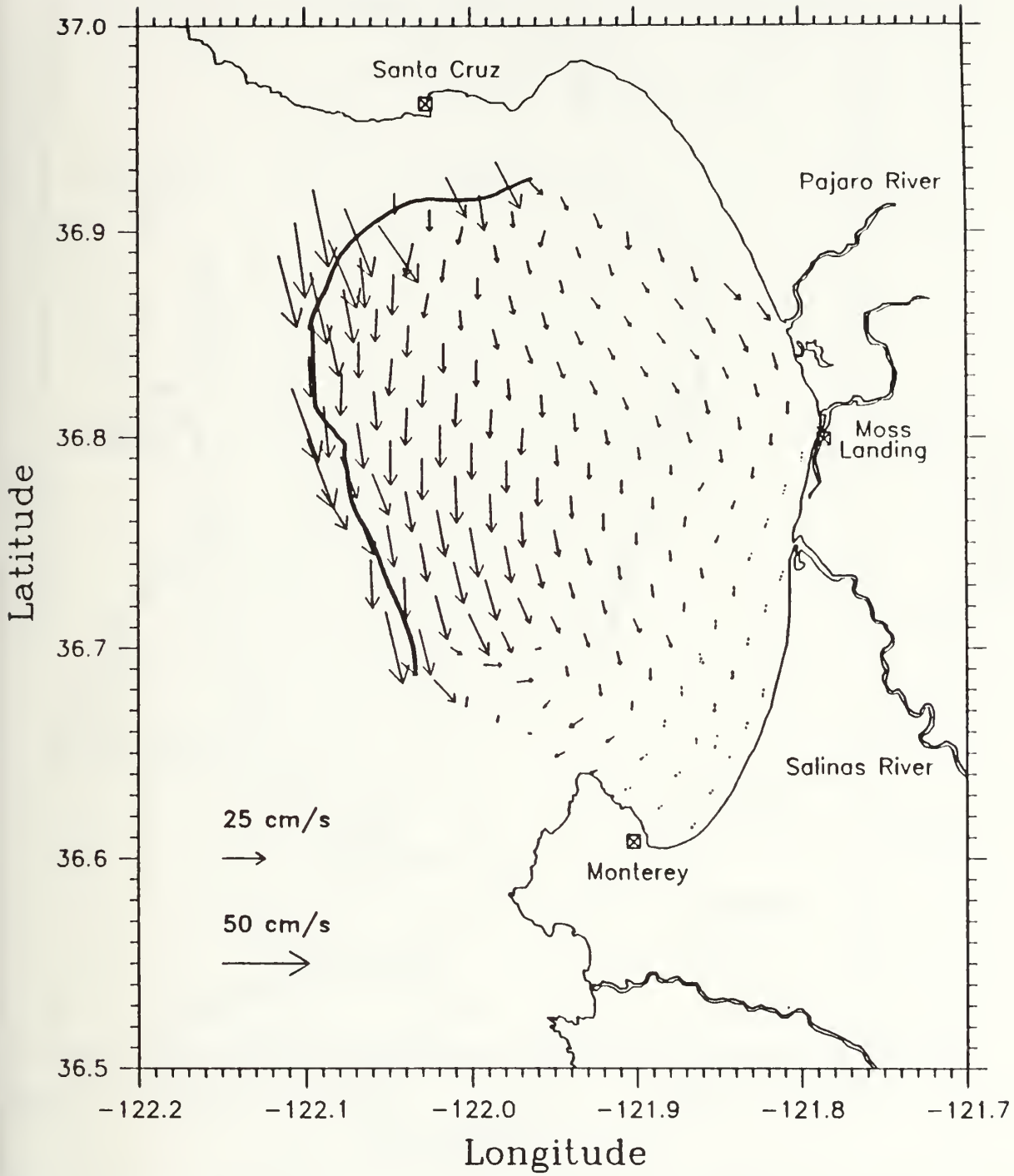

Figure 23. **Mean CODAR-derived Surface Currents March 29 to April 4, 1992:** Note the strong southerly flow. This corresponds with a drop in SST measured at the MBARI mooring. The dark line represents the three-month mean 10% coverage line and is the limit of reasonable data. Dotted arrows represent current vectors made with the baseline assumption.

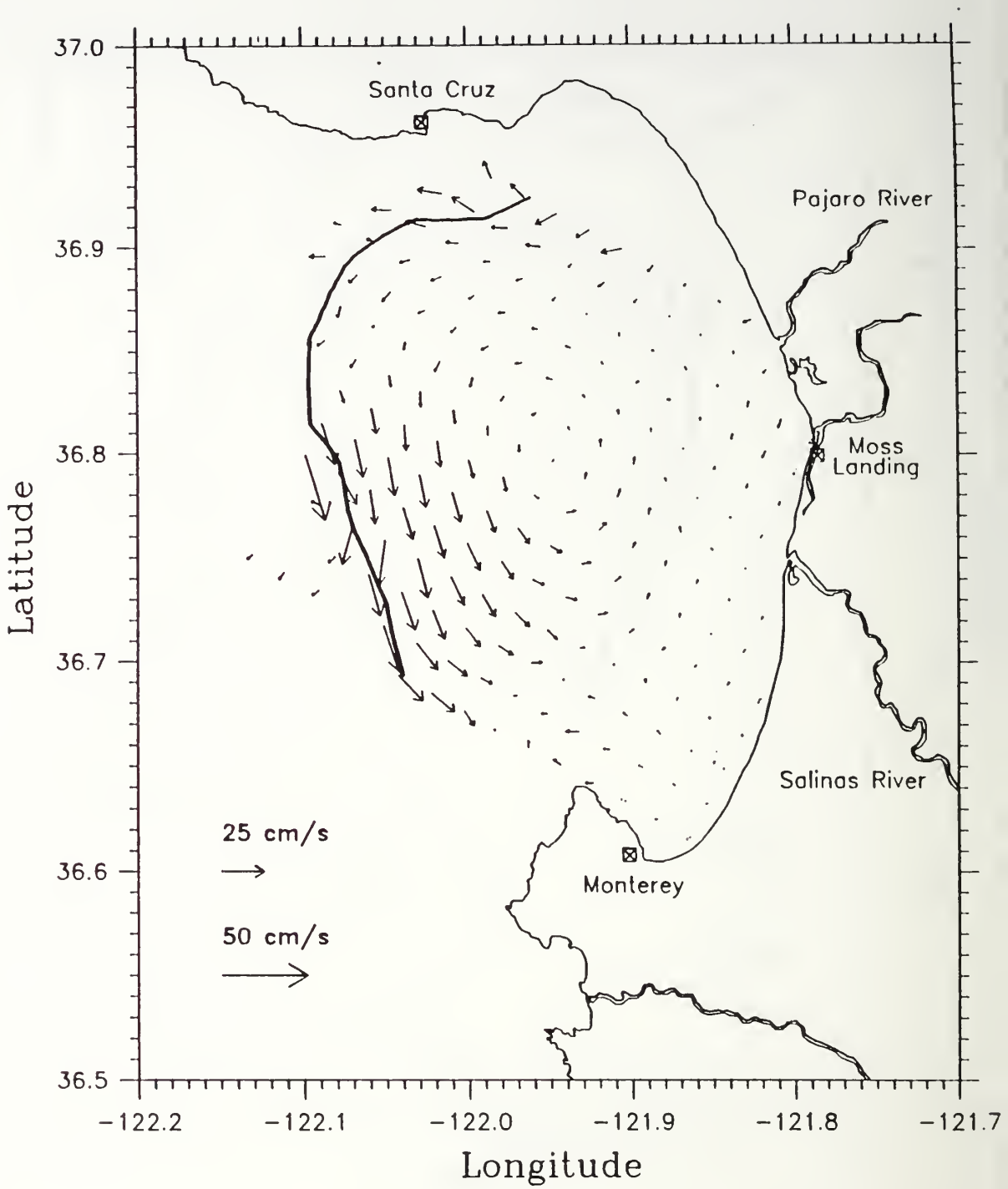

Figure 24. **Mean CODAR-derived Surface Currents April 5 to 11, 1992:** The currents have substantially decreased. The dark line represents the three-month mean 10% coverage line and is the limit of reasonable data. Dotted arrows represent current vectors made with the baseline assumption.

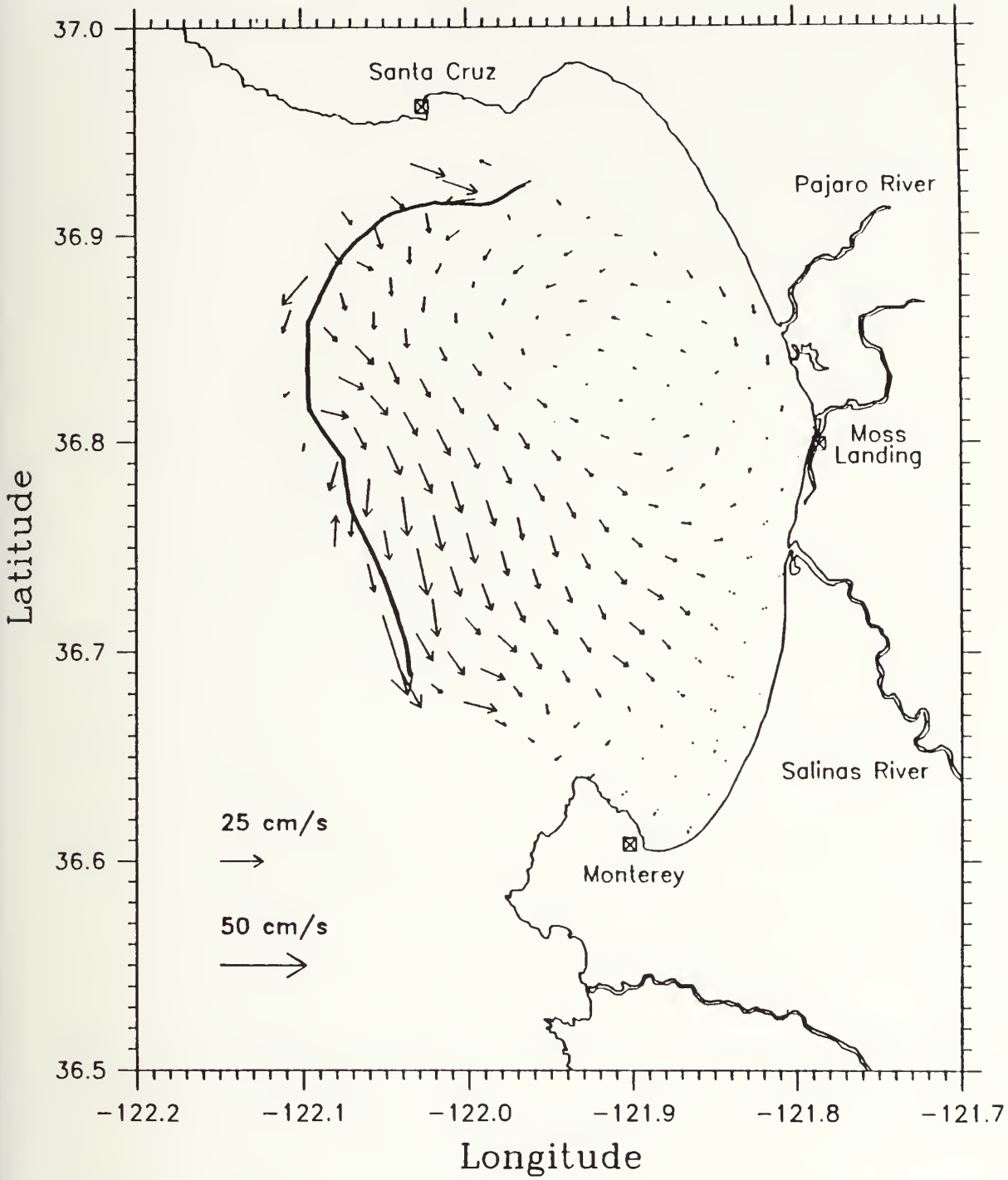

Figure 25. **Mean CODAR-derived Surface Currents April 12 to 18, 1992:** Interesting features are the area of convergence near the baseline. The dark line represents the three-month mean 10% coverage line and is the limit of reasonable data. Dotted arrows represent current vectors made with the baseline assumption.

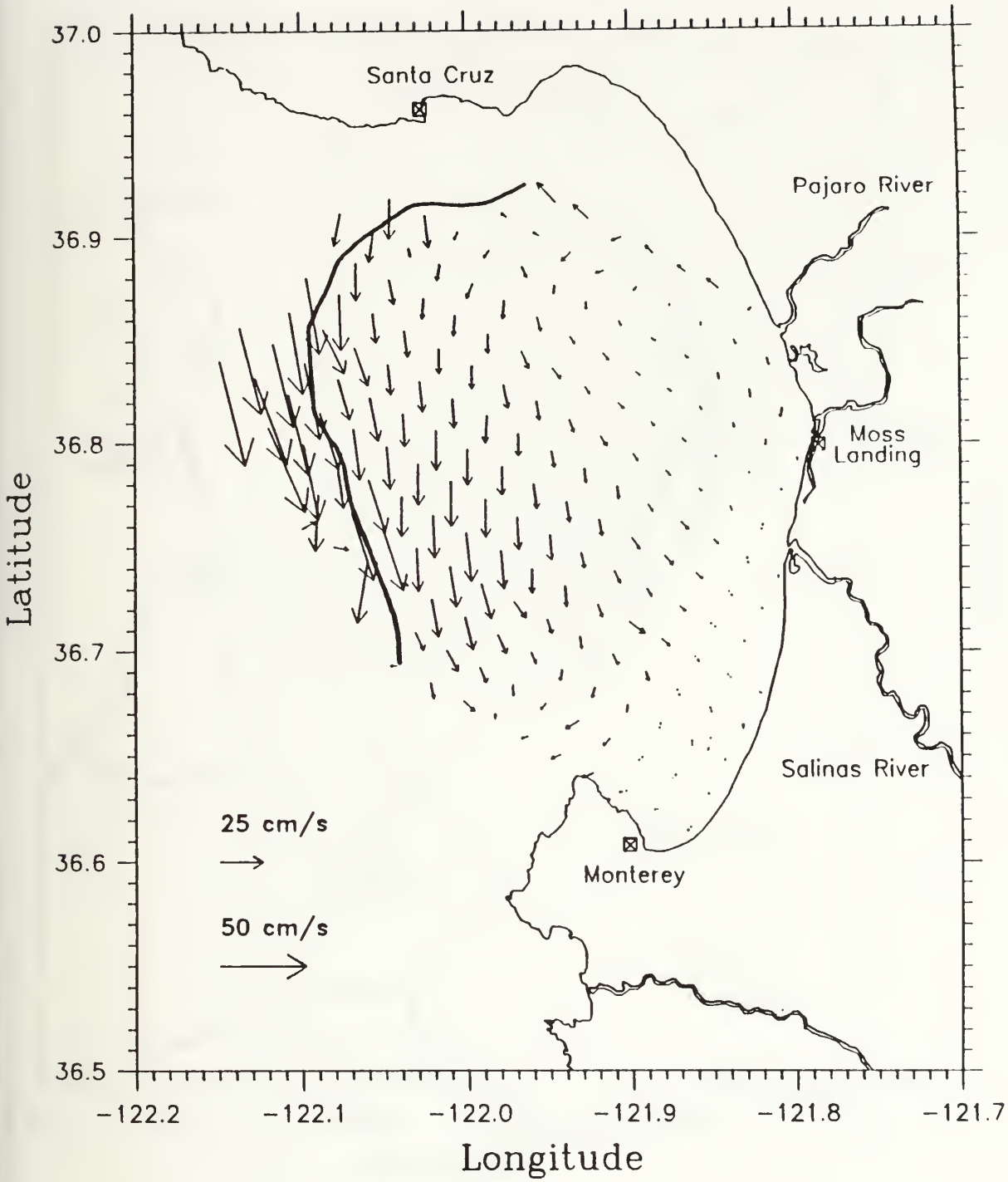

Figure 26. **Mean CODAR-derived Surface Currents April 19 to 25, 1992:** Strong southerly flow in the outer bay corresponds to a drop in the SST at the MBARI mooring. The dark line represents the three-month mean 10% coverage line and is the limit of reasonable data. Dotted arrows represent current vectors made with the baseline assumption.

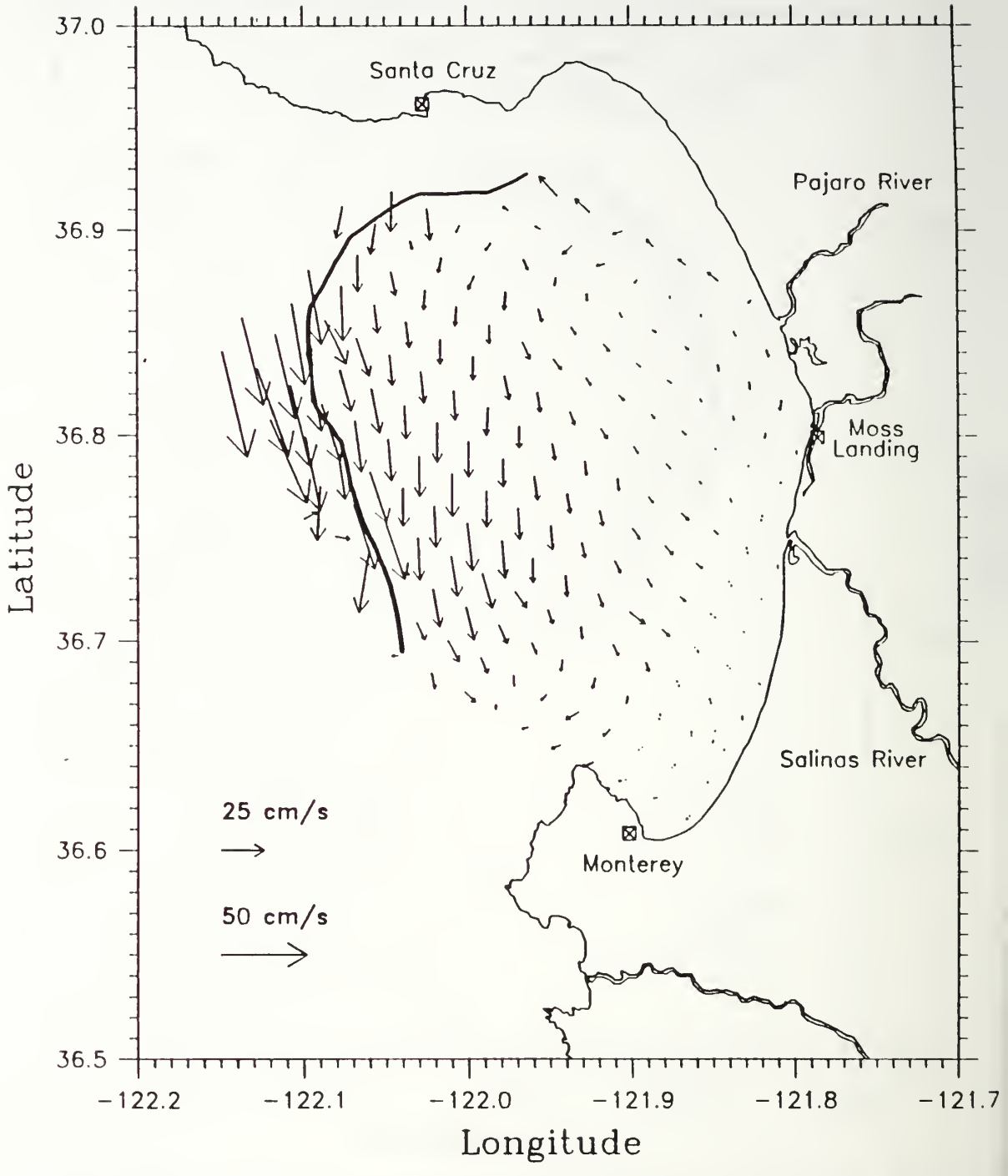

Figure 27. **Mean CODAR-derived Surface Currents April 26 to May 2, 1992:** The flow is similar to the previous week. The dark line represents the three-month mean 10% coverage line and is the limit of reasonable data. Dotted arrows represent current vectors made with the baseline assumption.

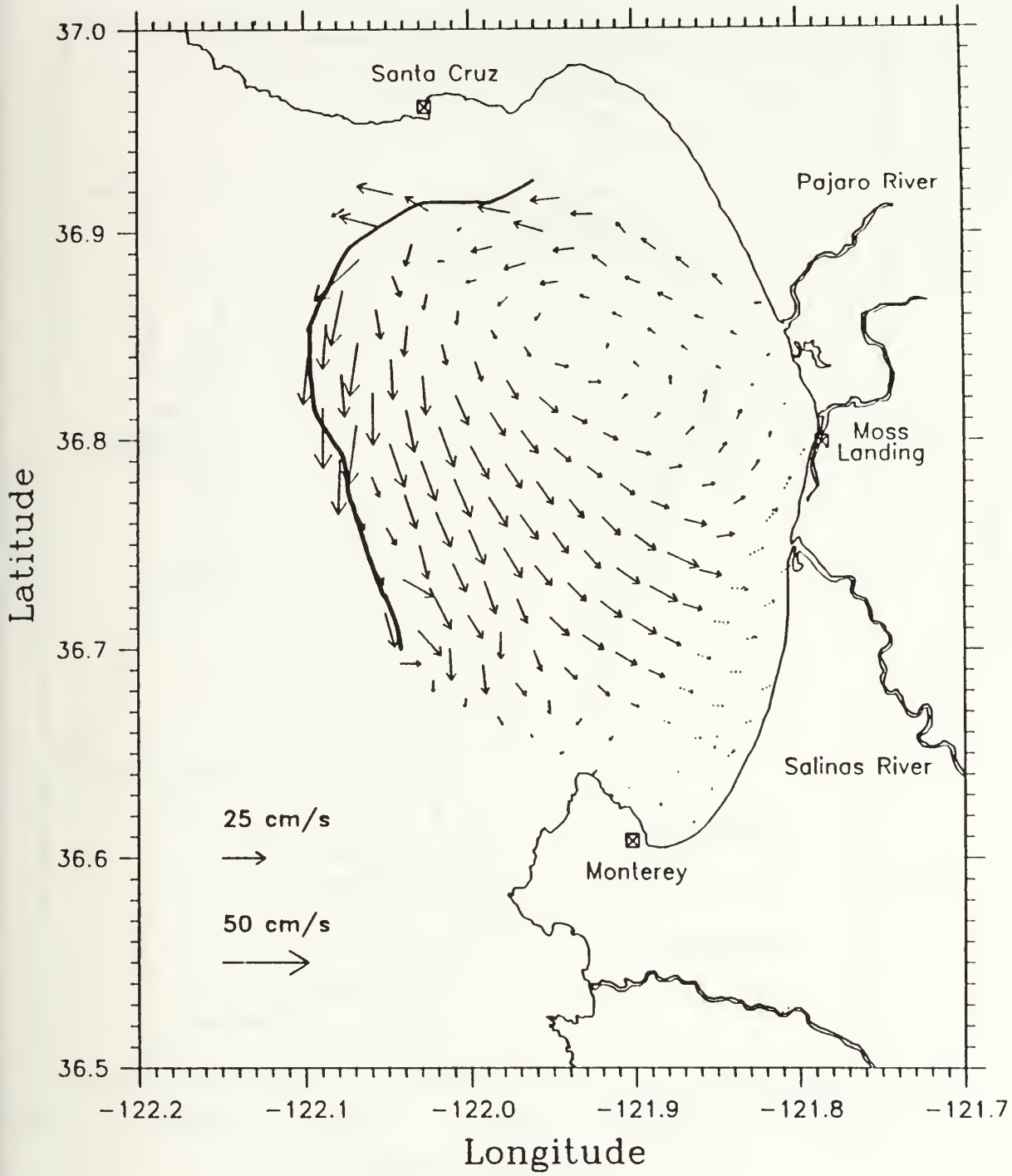

Figure 28. **Mean CODAR-derived Surface Currents May 3 to 9, 1992:** The dark line represents the three-month mean 10% coverage line and is the limit of reasonable data. Dotted arrows represent current vectors made with the baseline assumption.

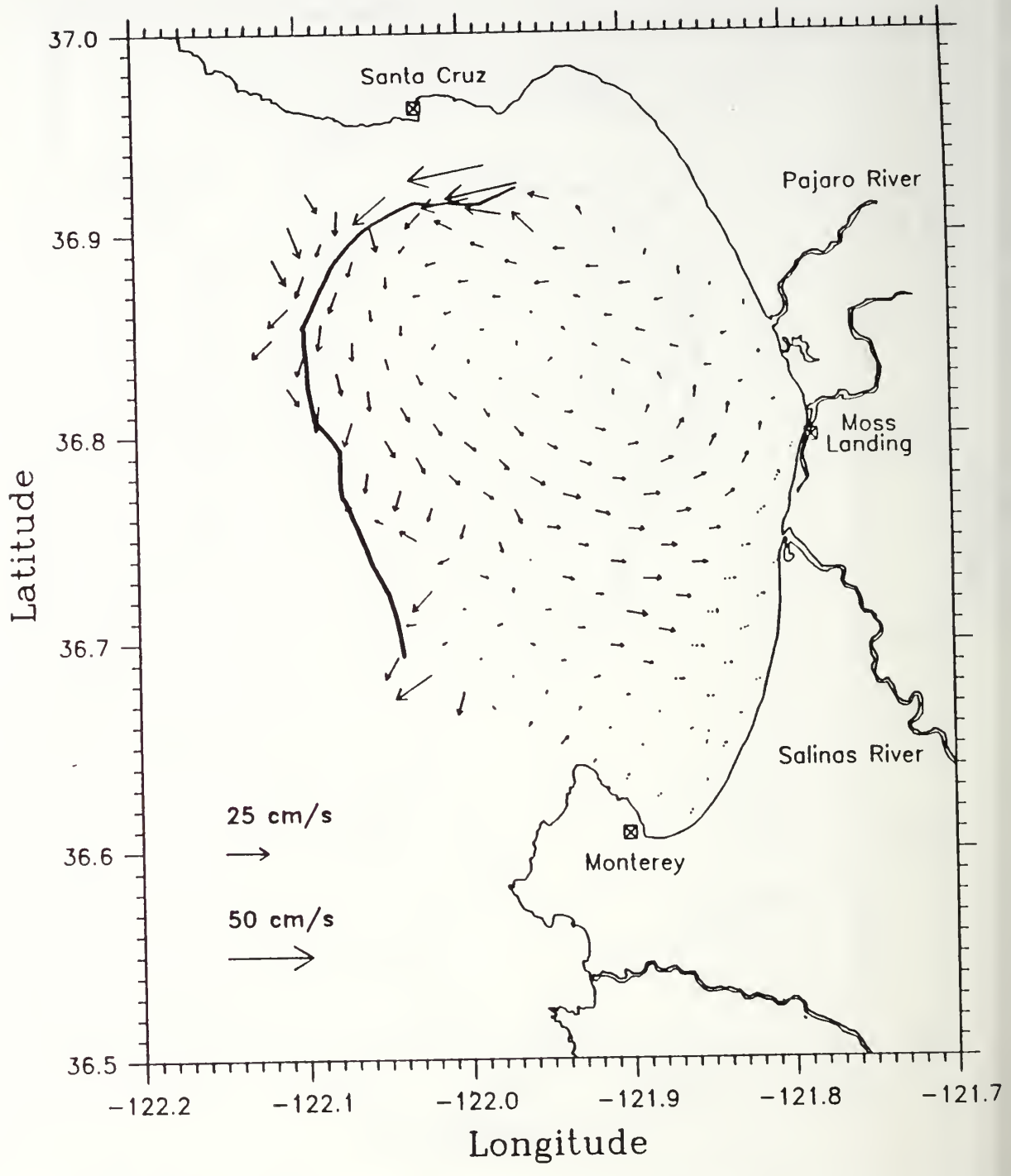

Figure 29. **Mean CODAR-derived Surface Currents May 10 to 16, 1992:** For the first time a gyre has developed centered off Moss Landing. The dark line represents the three-month mean 10% coverage line and is the limit of reasonable data. Dotted arrows represent current vectors made with the baseline assumption.

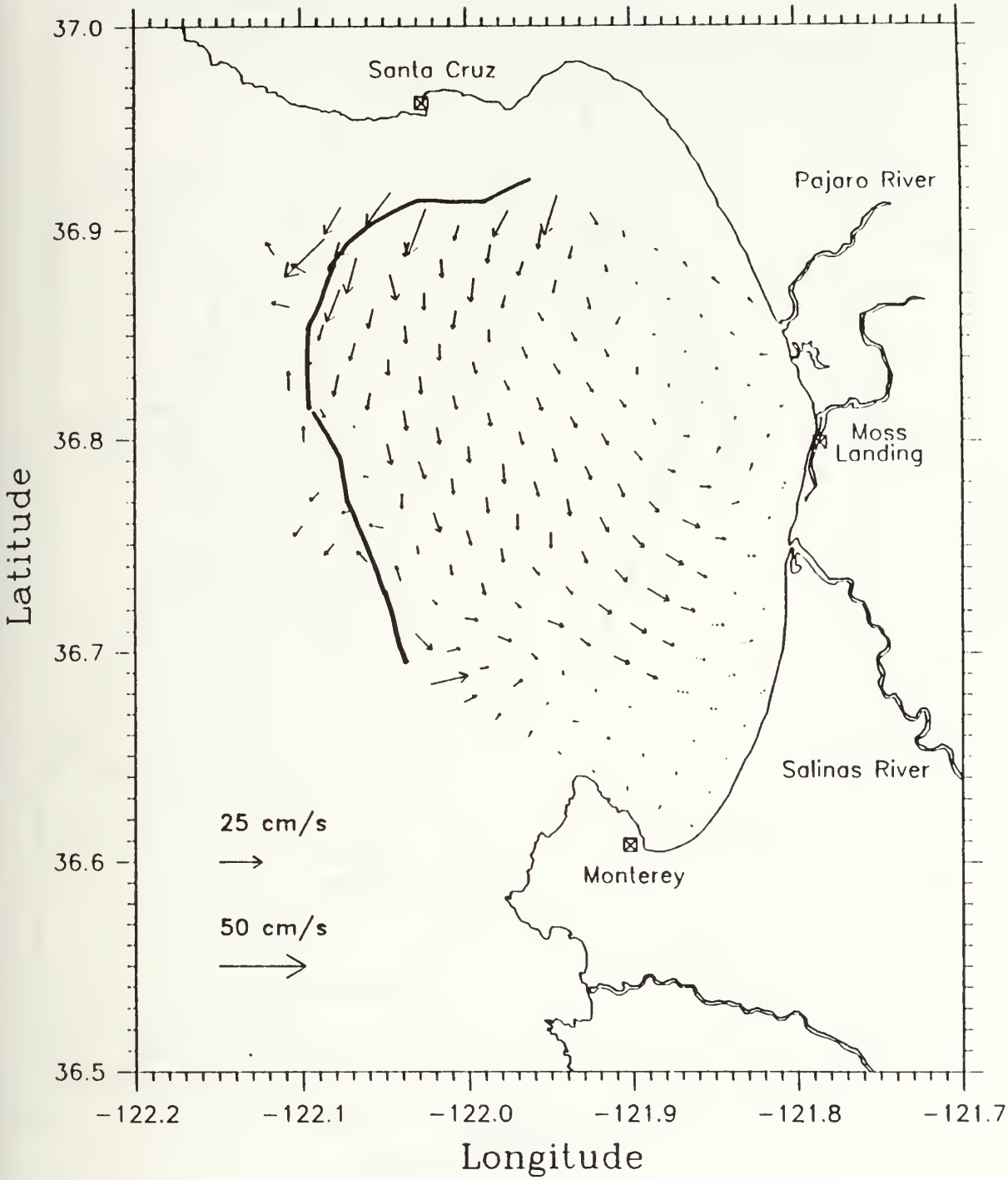

Figure 30. **Mean CODAR-derived Surface Currents May 17 to 23, 1992:** Note generally weak flow west of Moss Landing and north of the Monterey Peninsula. The dark line represents the three-month mean 10% coverage line and is the limit of reasonable data. Dotted arrows represent current vectors made with the baseline assumption.

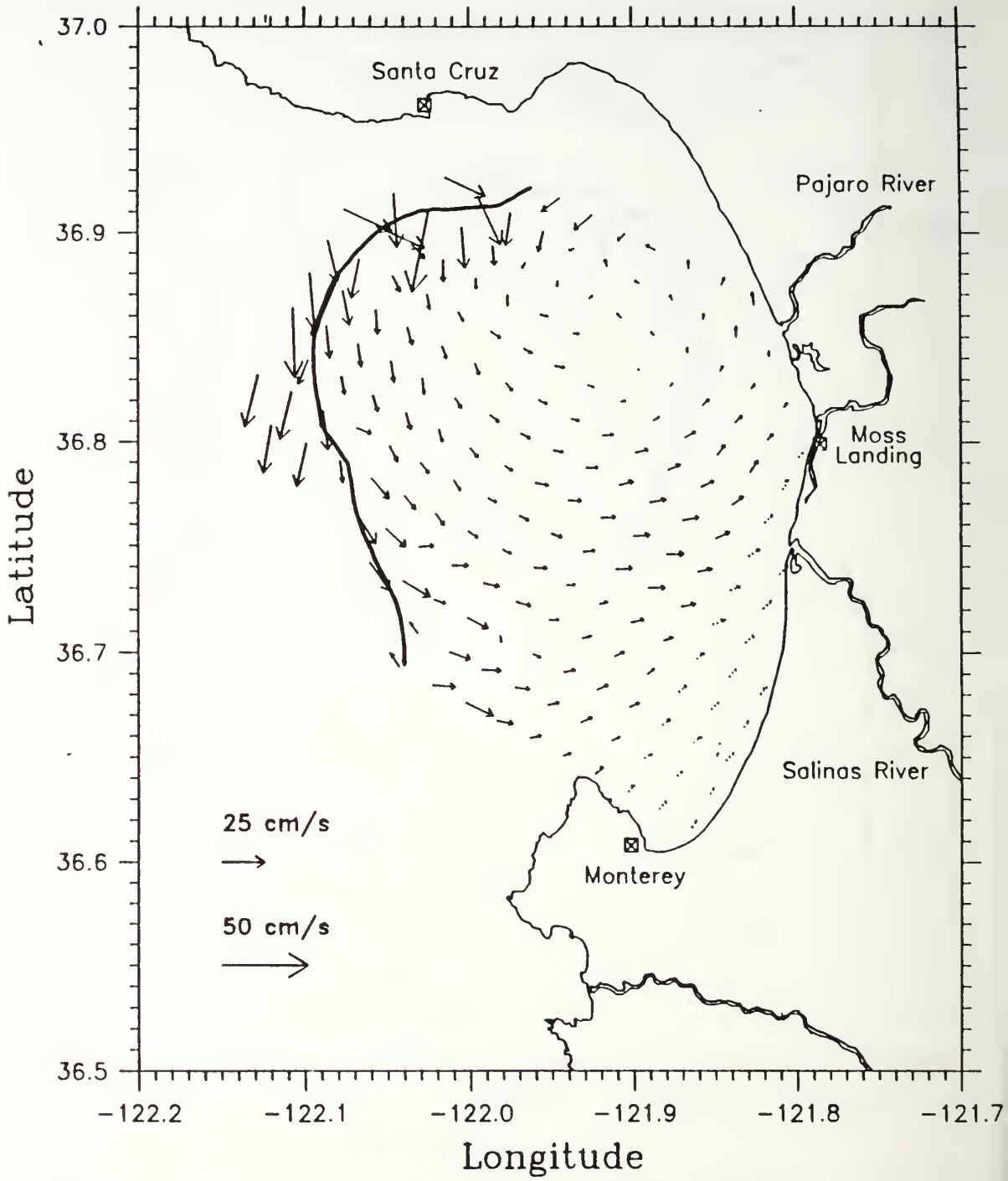

Figure 31. **Mean CODAR-derived Surface Currents May 24 to 31, 1992:** The last week of May shows the return of the gyre and a general increase in the currents. The dark line represents the three-month mean 10% coverage line and is the limit of reasonable data. Dotted arrows represent current vectors made with the baseline assumption.

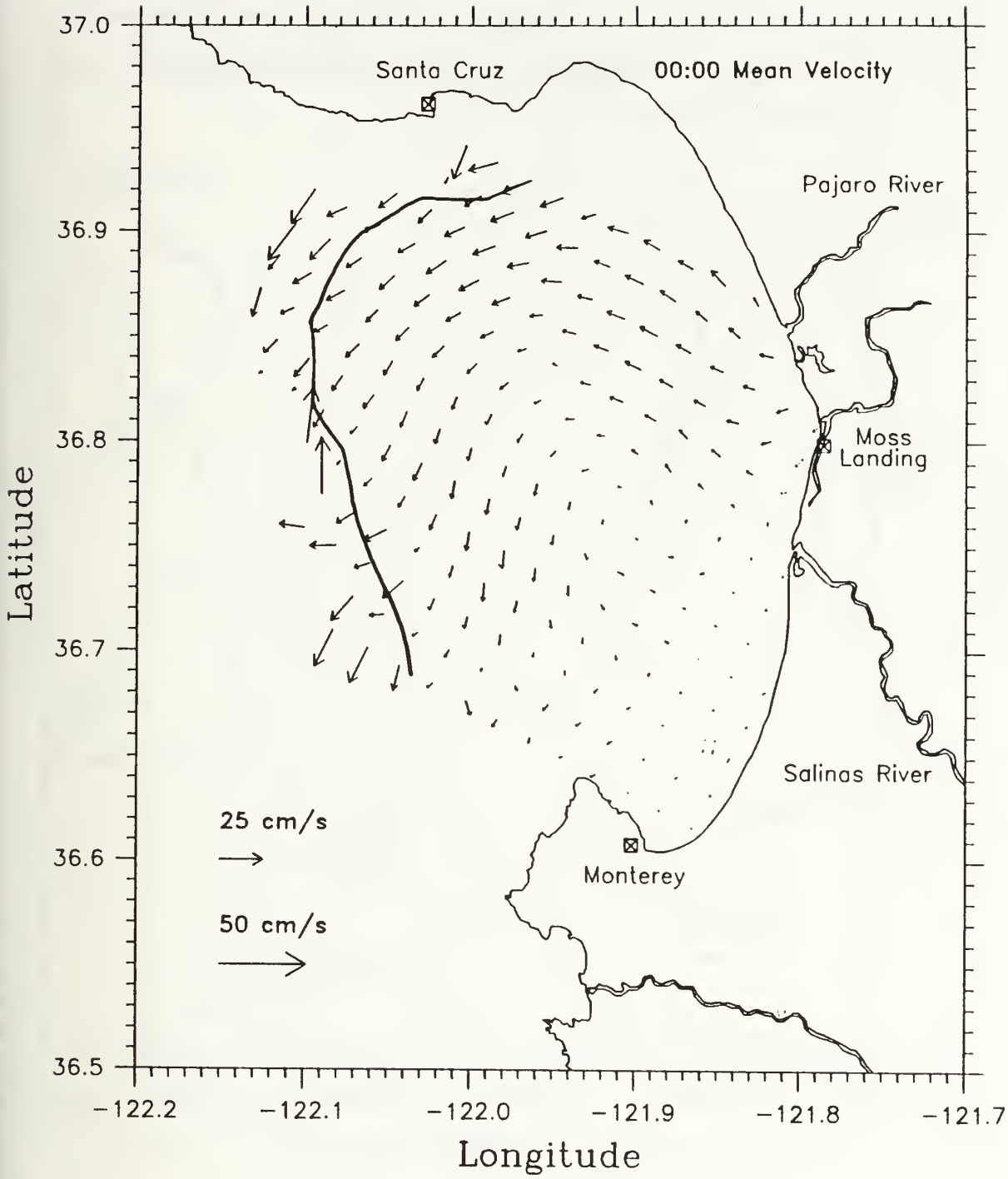

Figure 32. **00:00 PDT Canonical CODAR-derived Surface Currents:** Note the offshore currents north of Moss Landing possibly due to the land breeze. The dark line represents the three-month mean 10% coverage line and is the limit of reasonable data. Dotted arrows represent current vectors made with the baseline assumption.

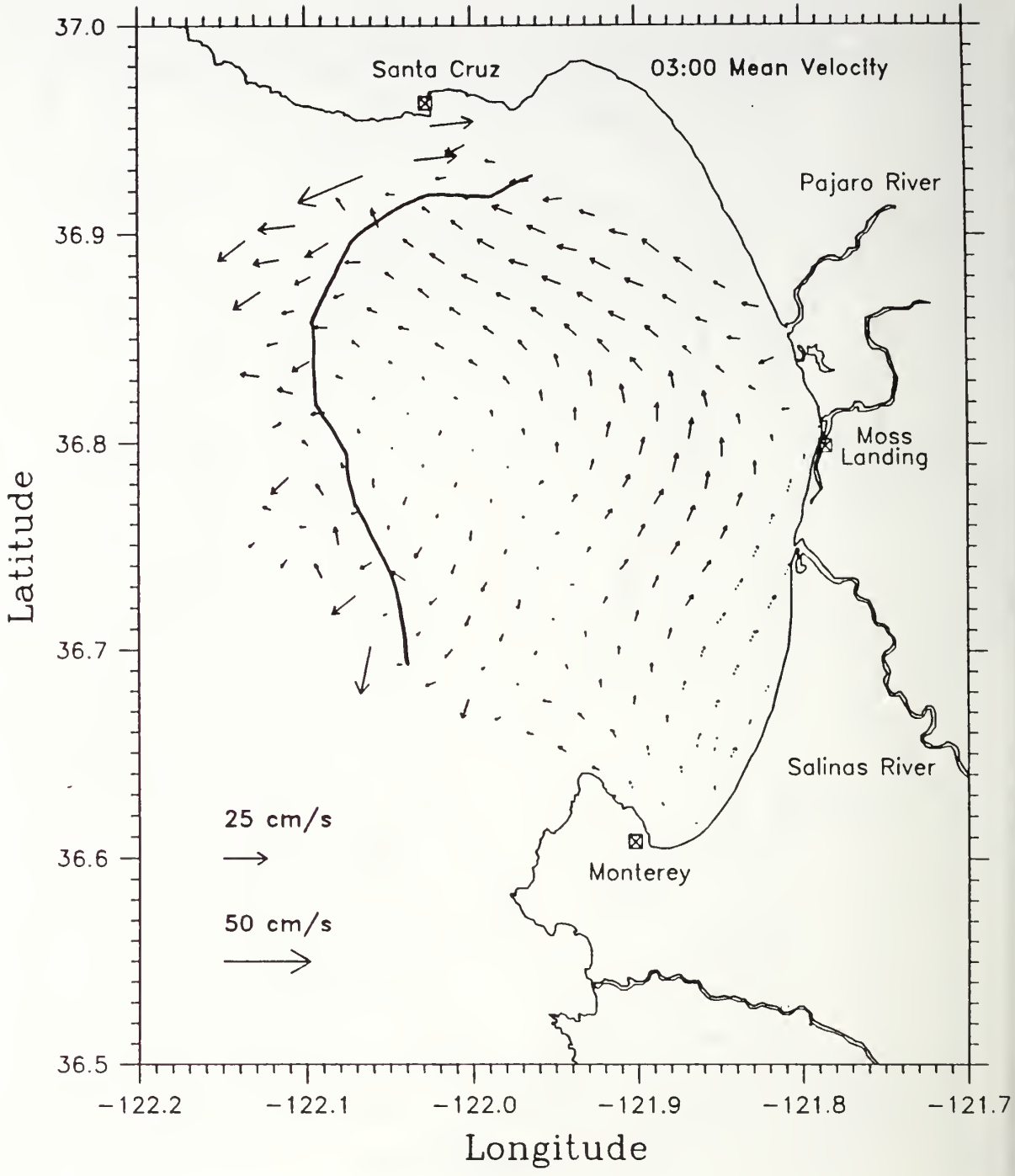

Figure 33. **03:00 PDT Canonical CODAR-derived Surface Currents:** The currents near the coast have shifted to flow to the north. The dark line represents the three-month mean 10% coverage line and is the limit of reasonable data. Dotted arrows represent current vectors made with the baseline assumption.

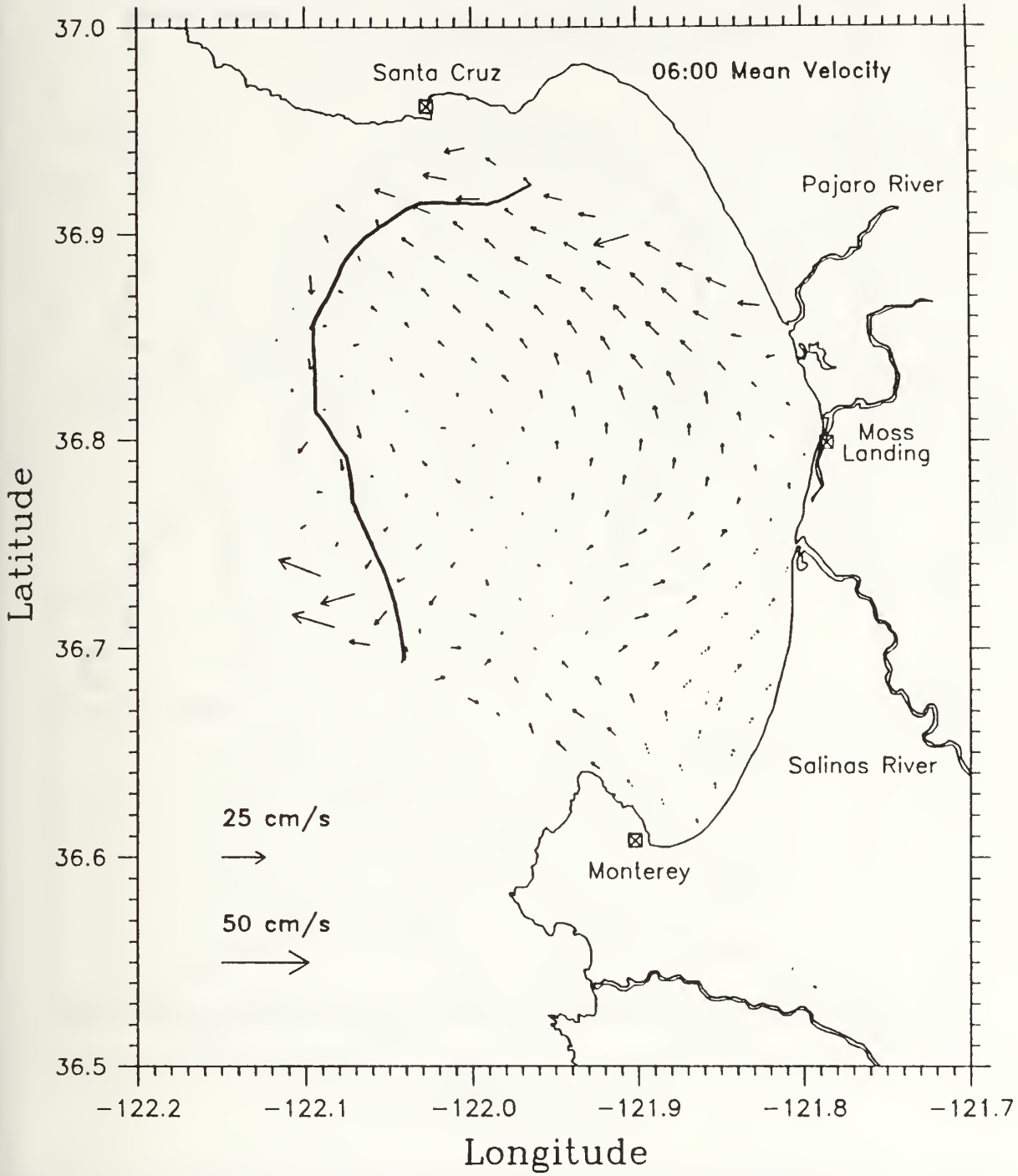

Figure 34. **06:00 PDT Canonical CODAR-derived Surface Currents:** The pattern is similar to the previous 03:00 canonical currents. The dark line represents the three-month mean 10% coverage line and is the limit of reasonable data. Dotted arrows represent current vectors made with the baseline assumption.

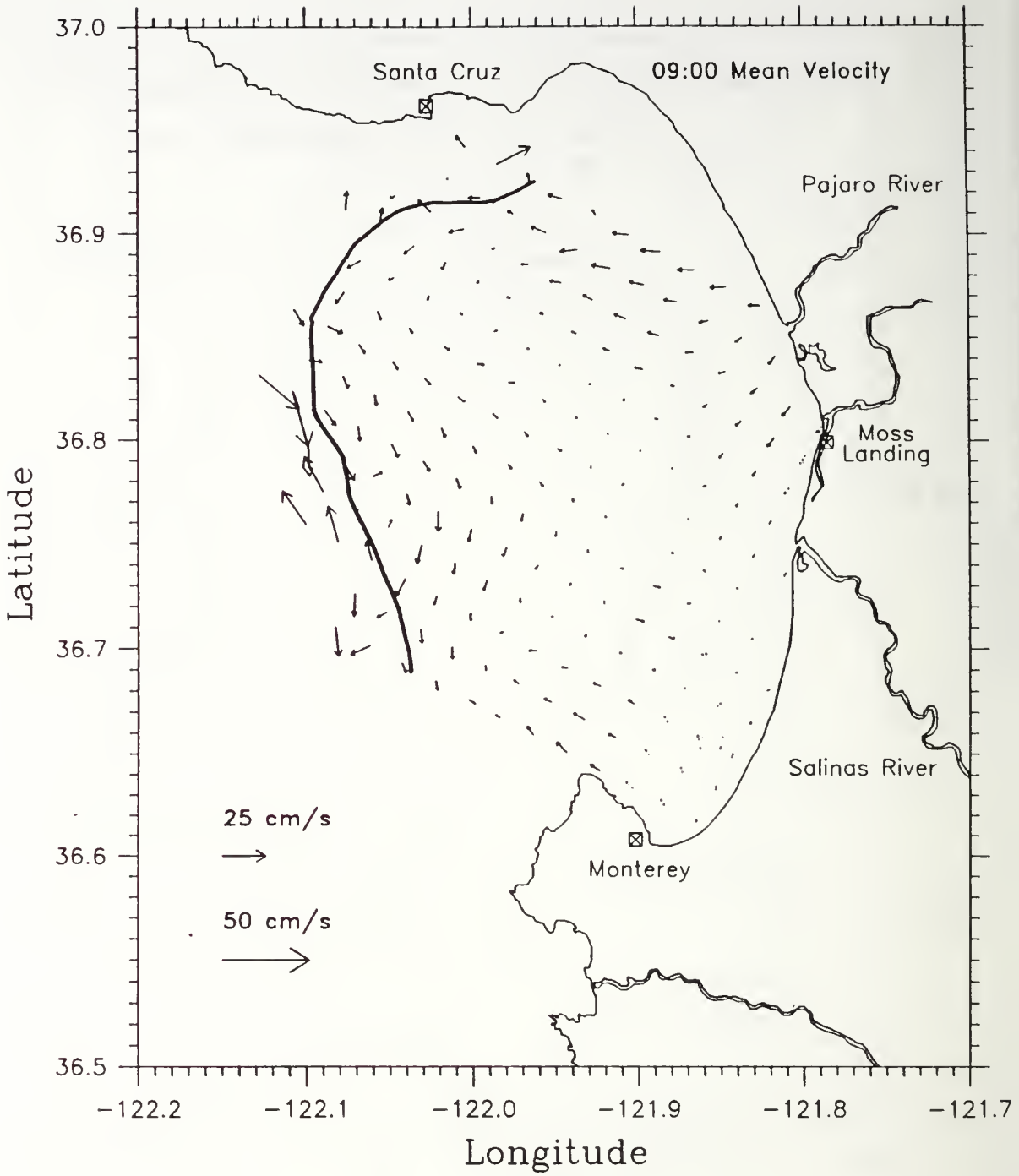

Figure 35. **09:00 PDT Canonical CODAR-derived Surface Currents:** The currents are generally weak and are a transition to the afternoon currents. The dark line represents the three-month mean 10% coverage line and is the limit of reasonable data. Dotted arrows represent current vectors made with the baseline assumption.

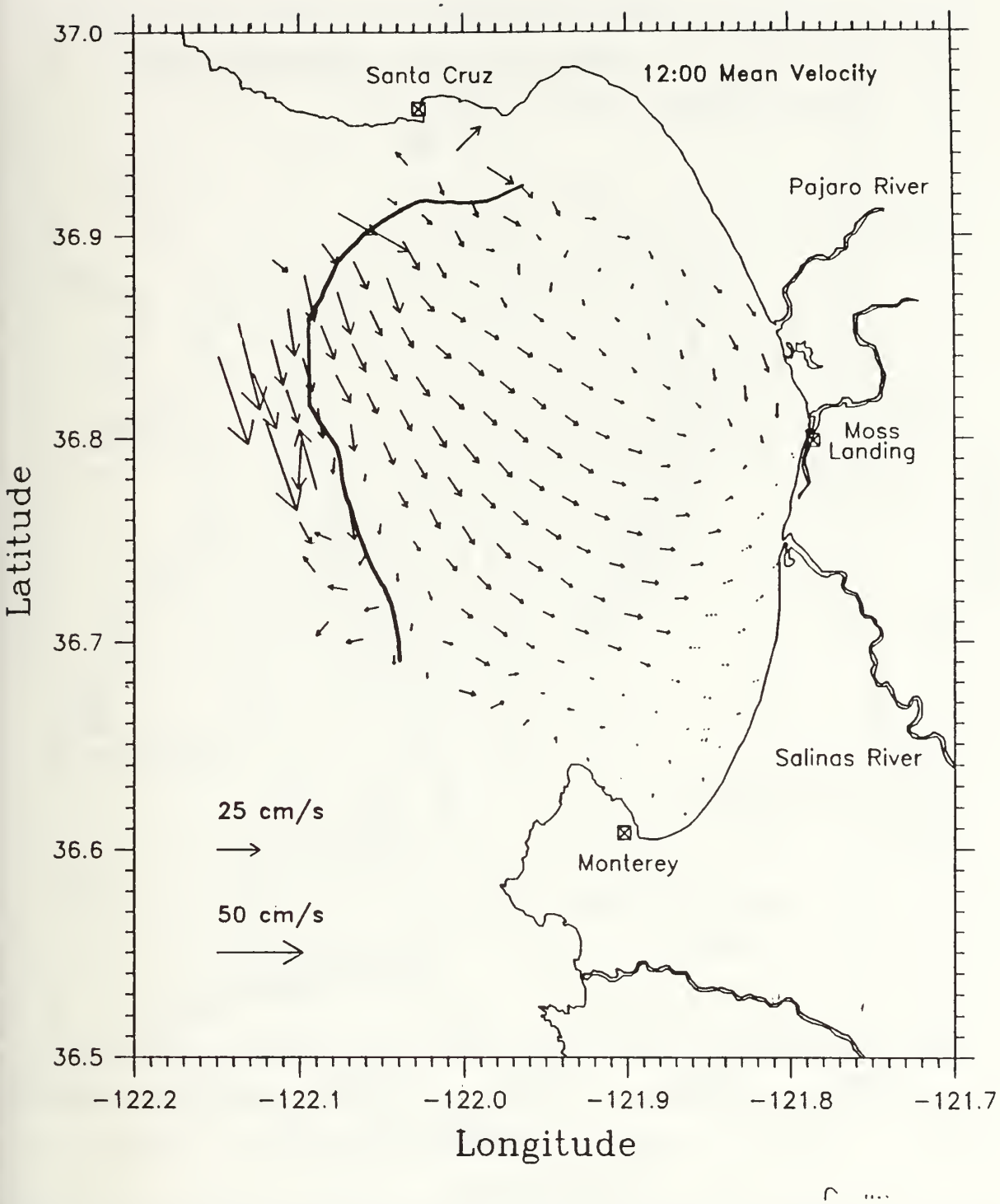

Figure 36. **12:00 PDT Canonical CODAR-derived Surface Currents:** Strong onshore currents are present throughout the bay due to the afternoon sea breeze. The dark line represents the three-month mean 10% coverage line and is the limit of reasonable data. Dotted arrows represent current vectors made with the baseline assumption.

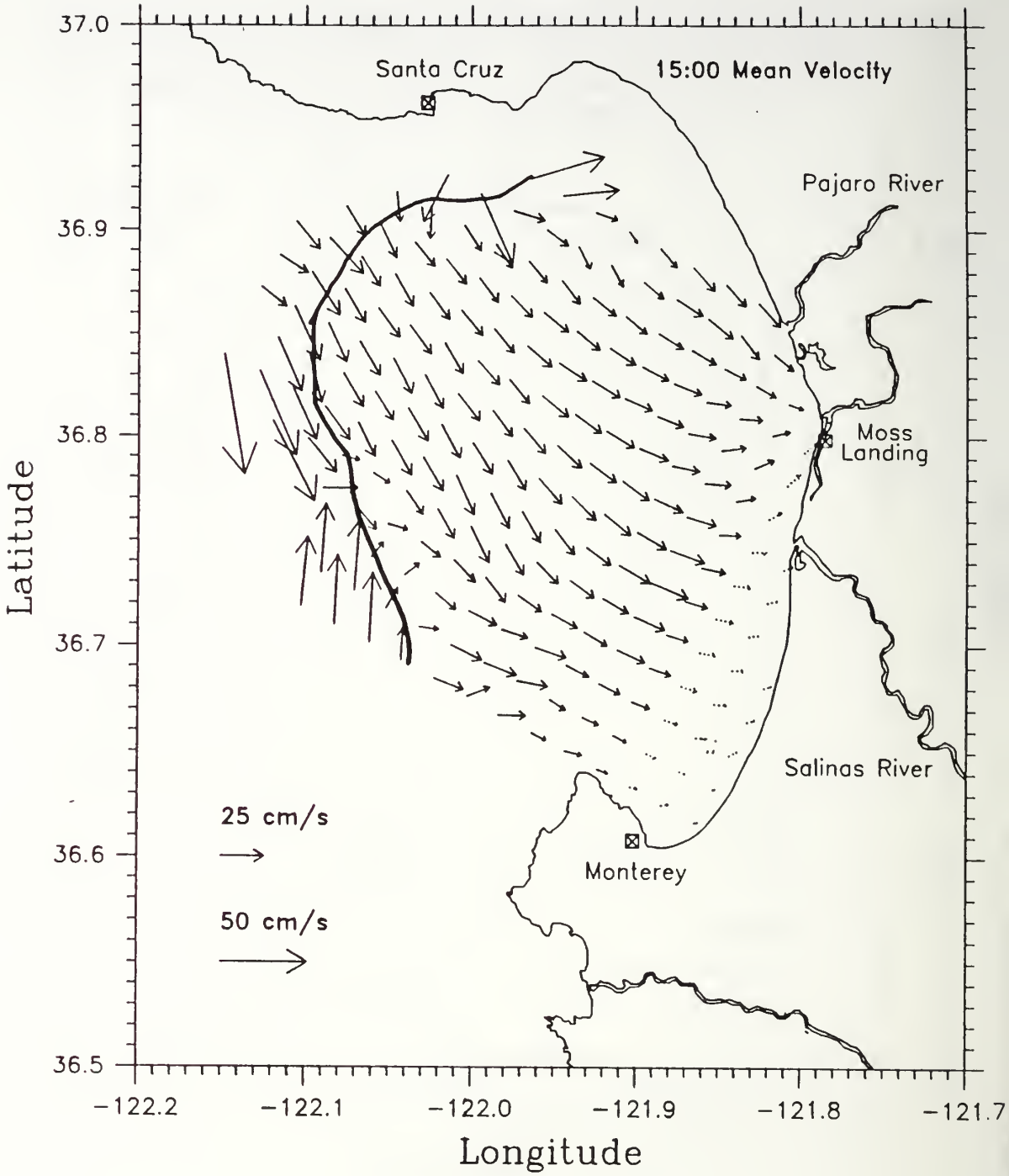

Figure 37. **15:00 PDT Canonical CODAR-derived Surface Currents:** The currents increase in speed and show a large convergence area near the baseline. The dark line represents the three-month mean 10% coverage line and is the limit of reasonable data. Dotted arrows represent current vectors made with the baseline assumption.

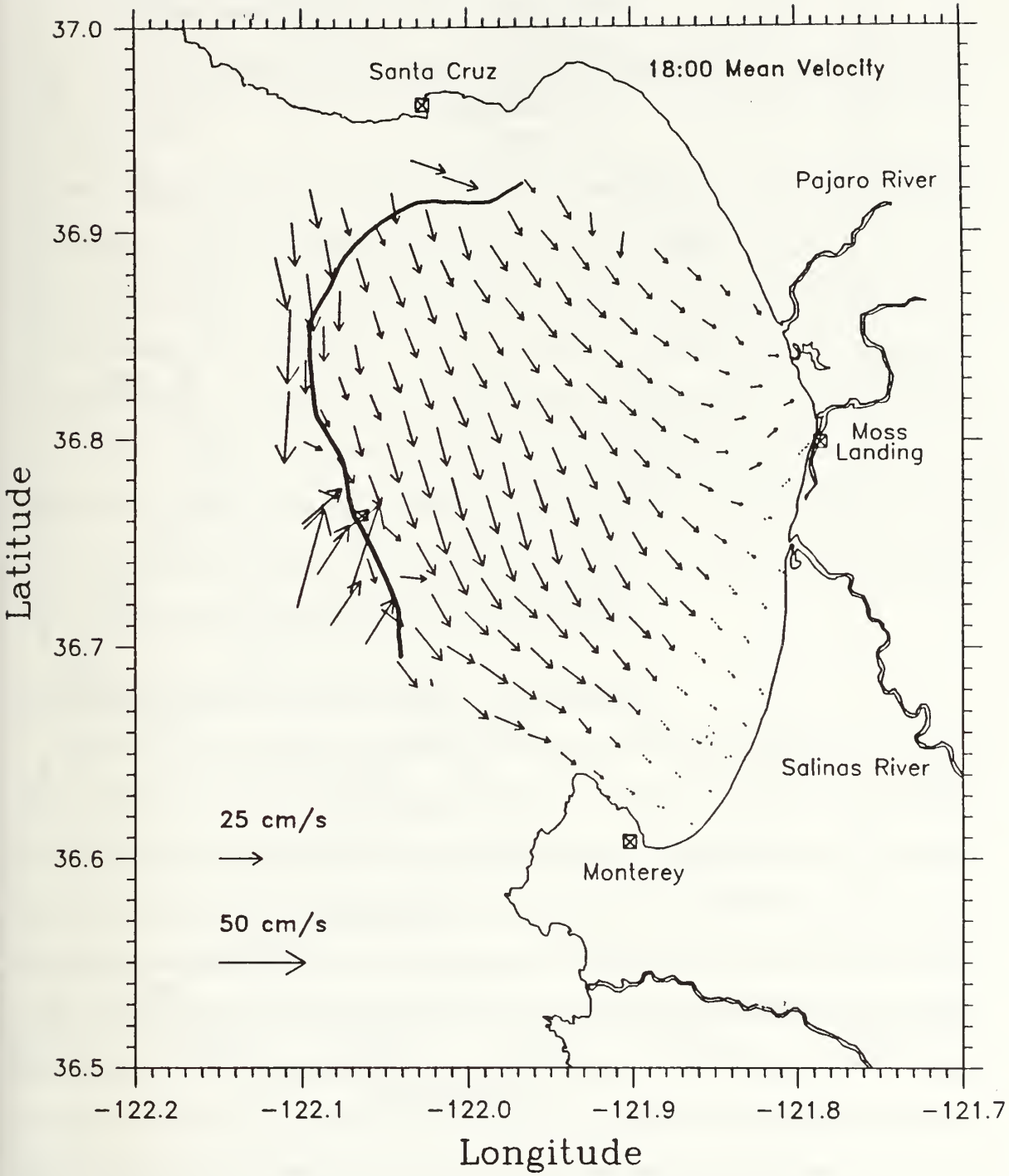

Figure 38. **18:00 PDT Canonical CODAR-derived Surface Currents:** The current pattern is similar to the 15:00 canonical currents. The dark line represents the three-month mean 10% coverage line and is the limit of reasonable data. Dotted arrows represent current vectors made with the baseline assumption.

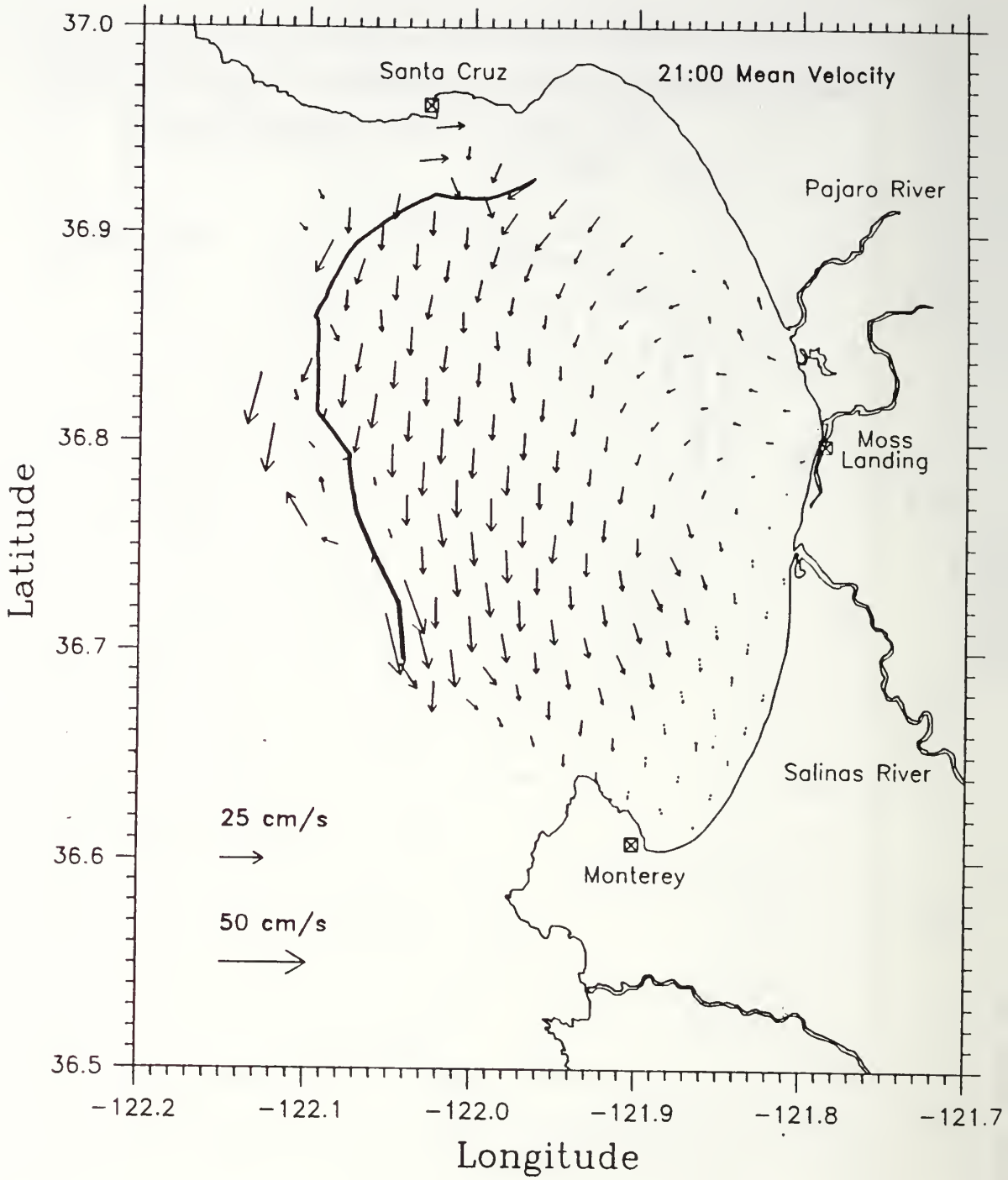

Figure 39. **21:00 PDT Canonical CODAR-derived Surface Currents:** The currents shift to the south in the outer bay and offshore currents are starting to develop north of Moss Landing. The dark line represents the three-month mean 10% coverage line and is the limit of reasonable data. Dotted arrows represent current vectors made with the baseline assumption.

IV. TIME SERIES ANALYSIS AND COMPARISON WITH IN SITU DATA

Individual CODAR gridpoints are compared to mooring data to verify and understand the CODAR results. CODAR-derived surface currents at gridpoints 13-10 and 14-06 were compared with the wind and ADCP current data measured at the MBARI mooring. These two points were chosen because 13-10 was closest to the mooring and 14-06 had 90% CODAR coverage. Gridpoint 13-10 is 1.5 km from the mooring and 14-06 is 7.0 km from the mooring. Comparisons of the U and V velocity components, speed and direction are made. Next, the time series are correlated with each other and the CODAR and ADCP time series are spectrally analyzed. These comparisons show the influence of the winds and tides and the relationships between the measurement types.

A. CODAR, ADCP AND WIND TIME SERIES

The raw U-V velocity components for CODAR-derived currents are shown in Figure 40 for the three-month period. The figure shows the three-hourly time series from both CODAR bins 13-10 (upper panel) and 14-06 (lower panel). In each case the V-component data has been offset in the vertical for clarity. The superior coverage at location 14-06 is immediately obvious. Only a few gaps greater than one day are present in that data during times when one or two of the radar units were not functioning. Conversely, the data from bin 13-10 has many gaps, particularly later in the time series. It is possible that this degradation with time is an indication of increasing corrosion at the Moss Landing radar site. In June, after the time period of this study, that radar's antenna was found to be severely corroded and was subsequently replaced.

The CODAR velocities at bins 13-10 and 14-06 show similar patterns overall. On a month-to-month time scale, the changes described earlier for the mean CODAR maps can be seen in the time series. During March, the flow is variable with significant periods of flow to the northwest, particularly at the more offshore bin 13-10. In April and May the flow is more typically toward the southeast. There is a lot of variability at high frequencies with periods of one day or less. There are also large oscillations on, approximately, two-week time scales, which will be more apparent in the low-passed time series and velocity spectra described below.

The raw U-V velocity components for ADCP currents and winds are shown in Figure 41 for the three-month period. The figure shows 15-minute data from ADCP bin 2 below the MBARI mooring (upper panel) and 10-minute data from the anemometer above the mooring (lower panel). The presentation highlights the gaps in the mooring data, particularly the ADCP data. Both data sets have a large gap in the beginning of the records. Near-continuous data does not begin until the 12th of March. The ADCP data has numerous other multi-day gaps related to problems with the remote data telemetry from the mooring to shore.

The patterns in the ADCP data reflect those in the CODAR time series. The flow is predominately southeastward superimposed with high-frequency variability and large events occurring on the two-week time scale. The month-to-month patterns in the wind data reflect those of the CODAR and ADCP time series. March is seen to be a transition period from northwestward to southeastward winds. There is a daily cycle in the wind records that is, presumably, related to the known sea breeze cycle over Monterey Bay in the spring and summer months. Analogs to the oceanic events on two-week time scales are harder to see in this presentation of the winds. They are present more as isolated bursts occurring every couple of weeks.

B. SPEED COMPARISONS

The mean velocity components, speeds and directions are given in Table 1 for the entire three-month period. The standard deviations are also shown. The mean speeds show that over the three-month period the wind speeds were 12 times the CODAR speeds and CODAR was 2.5 times the ADCP speed. To compare the instantaneous speeds, scatter plots of CODAR versus wind and CODAR versus ADCP speeds are drawn. Scatter plots are compiled from raw and concurrent data. The slope of a line fitted to the scatter plots determines the speed relationship.

Table 1. **MEAN AND STANDARD DEVIATION VALUES**

Statistic	WIND	CODAR 13-10	ADCP
U Mean Velocity (cm·s-1)	126.7	3.0	3.5
U Standard Dev. (cm·s-1)	161.7	10.7	4.3
V Mean Velocity (cm·s-1)	-59.8	-11.5	-3.7
V Standard Dev. (cm·s-1)	194.0	17.0	6.1
Mean Speed (cm·s-1)	249.0	19.9	7.9
Mean Direction (0° = true North)	115.3	165.6	136.3

Wind speeds were also determined to be twelve times the CODAR-derived surface current speeds as shown by the best-fit line in Figure 42. This speed difference is less than was reported in previous HF surface current radar studies (Essen et al., 1985, and Hammond et al., 1987). The linear model is poor for CODAR speeds less than 30 $cm \cdot sec^{-1}$ but improves with higher speeds. The overall correlation coefficient for speed is 0.55 (Table 2), which is higher than the correlation coefficients for either the U or V velocity components alone.

CODAR-derived surface current speeds are variable compared to the ADCP currents and are approximately five and a half times larger as shown by the scatter plot and best-fit

line in Figure 43. The correlation coefficient is 0.42 for speed but is actually larger for the U component (0.55) and the V component (0.48; Table 2).

The correspondence between wind and ADCP currents is poor for this "instantaneous" data. Table 2 shows the highest correlation coefficient is only 0.32 for the V component comparison.

Table 2. **WIND, CODAR AND ADCP CORRELATIONS**

Correlation	U Component	V Component	Speed
CODAR/Wind	0.35	0.48	0.55
CODAR/ADCP	0.55	0.48	0.42
Wind/ADCP	0.03	0.32	0.24

C. DIRECTION COMPARISONS

Table 1 shows that the mean wind direction points at 115°, CODAR direction at 165° and ADCP direction at 136° true. Figure 44 shows the direction histograms of the winds, CODAR-derived surface currents and ADCP currents. The histograms are calculated from raw data and the results were normalized by the total number of observations available for each data type. Each direction bin is 10° wide and directions are referenced to true north. The preferred direction for the wind was 104°, for CODAR it was 164° and for the ADCP currents it was 128° true. To compare the directional differences between CODAR and mooring data, the differences are computed from the raw and concurrent data. Figure 45 shows histograms of the directional differences between CODAR and the wind and CODAR and the ADCP currents. The directional differences of CODAR gridpoint 13-10 versus the wind show that CODAR peaks 53° to the right of the wind. The directional differences of CODAR gridpoint 13-10 versus ADCP show that CODAR peaks 21° to the right of ADCP but the distribution is bi-modal with a secondary peak at zero direction difference.

In comparing the wind and CODAR directions, the data shows that CODAR-derived surface currents were to the right of the winds following the Ekman spiral principle of steady state wind driven currents (Pond and Pickard, 1989). If the Ekman spiral principle holds true the ADCP currents are expected to be to the right of the CODAR-derived current. This is not observed in the directional histograms computed using "instantaneous" data. The ADCP currents at 10-18 m were 21° to the left of the CODAR currents. This is counter to the Ekman spiral principle where deeper currents are to the right of the overlying currents. The reason for this difference could be that the forces affecting the deeper currents are not entirely wind-driven. Another reason for the difference could be the response time required for the wind to effect the currents at the 12 to 20 m depth. All wind events may not necessarily penetrate to the depth measured by the ADCP. Ekman theory is a steady state model of wind-driven flow. Only for longer-period motions is it expected to hold.

D. LOW-PASS FILTERED VELOCITIES AND SST EVENTS

To provide a better view of the relationships between the various measurements, each time series was interpolated to fill gaps and low-pass-filtered using a 24-hour running-mean filter with a cut-off period of 50 hours. The filtered time series are shown in Figure 46. They highlight multi-day events and indicate, possibly, strong correlation between CODAR and ADCP. The observation times for the raw data are shown below the filtered time series so that periods of large gaps can be identified.

The most prominent feature in the low-passed data is a large oscillation in the north-south velocities with a time scale of about two weeks. Strong northward flow is observed around March 22nd giving way to strong southward flow around April 4th. This oscillation is present in both the CODAR-derived currents at bin 13-10 and the ADCP currents. The magnitudes of the ADCP currents are roughly half as large as the CODAR-

derived currents for these low-passed data. Features in the east-west velocity components are generally weaker than their alongshore counterparts and they show less correlation between CODAR-derived currents and ADCP currents. There are, however, events that show up in both data sets such as the relatively strong onshore flow during the first week of May.

The strong two-week oscillation in the alongshore currents is not mirrored in the wind data. It was, presumably, a purely oceanic event, or else it was driven by non-local wind forcing. There are, however, many events in the wind record lasting 3 to 5 days that are reflected in the current data, particularly the CODAR-derived currents. The best examples are on April 4th, April 21nd, April 30th, May 9th, and May 20th. Each of these strong wind events is associated with a burst of southward flow in the CODAR-derived currents and the ADCP currents. Interestingly, each of these events is also associated with a precipitous drop in sea surface temperature (SST). Figure 47 shows the raw time series of SST collected at the MBARI mooring together with a trace showing the observation times. SST decreased sharply by 1.5 °C to 3 °C in response to each of these wind events! The coincidence of strong southward current events at these times suggests that the SST may have responded to advection of colder water from the north rather than purely entrainment of cold water from the thermocline below.

E. LAGGED CROSS CORRELATIONS

The lagged cross correlations were calculated between measurement types to view any relationships that might occur at different time lags or leads. The cross correlations were derived from the interpolated and concurrent data sets. Both low-passed and unfiltered time series were used. The correlations were calculated at three hour time steps and for a lag range from -72 to +72 hours.

1. Using Low-passed Data

The cross correlations between low-passed CODAR gridpoint 13-10 and low-passed ADCP currents are shown in Figure 48 (this is the cross correlation of the time series in Figure 46). Maximum correlations are +0.68 for speed, +0.32 for the U velocity component and +0.73 for the V velocity component. The maximum correlation for speed is at the -15 hour time lag and the maximum correlations for U and V components are at the -12 hour time lag. This shows that the CODAR-derived surface currents lead the ADCP currents by 12 to 15 hours.

The cross correlations between low-passed CODAR gridpoint 13-10 and low-passed winds are shown in Figure 49. Maximum correlations are +0.57 for speed, +0.28 for the U velocity component and +0.64 for the V velocity component. The V velocity component maximum correlation is located at zero time lag and the speed maximum correlation suggests that CODAR-derived currents lead the wind by 3 hours. This unlikely lag is only one time step away from zero.

2. Using Unfiltered Data

The cross correlations between unfiltered CODAR gridpoint 14-06 and unfiltered ADCP currents are shown in Figure 50. These correlations were derived from five separate 120-hour segments corresponding to the largest continuous time series for the ADCP data. The results of the individual segments were then averaged together. Maximum coefficients are lower than in the low-passed case with +0.09 for the speed, +0.27 for the U velocity component and +0.21 for the V velocity component. The V velocity component correlations have the large values separated by 24 hours in lag showing a strong influence of diurnal motions. The U velocity component correlations show a different pattern. The largest correlations are at the zero time lag and other lags roughly 12 hours apart showing a strong influence of semi-diurnal motions. The speed correlations have the highest values

near +27 hour time lags and show a fairly random pattern of secondary peaks. Although the correlation magnitudes between the ADCP and the CODAR-derived currents at gridpoint 14-06 are not significant, these periodic patterns in the lagged correlations suggest tidal and diurnal wind forcing.

The lagged cross correlations between unfiltered CODAR gridpoint 14-06 and unfiltered winds are shown in Figure 51. Maximum coefficients are lower than in the low-passed case with +0.30 for the speed, +0.26 for the U velocity component and +0.31 for the V velocity component. The U and V velocity correlations have the largest values at the zero time lag and every ±24 hours showing strong diurnal influence. The speed correlations have the highest values at the -3 hour time lag and show the same pattern of higher correlations at ±24 hours as in the U and V velocity component cases.

3. Lagged Cross Correlation Summary

The lagged correlations reveal the relationship between and the influence of the diurnal winds and tides on the CODAR-derived and ADCP currents. The low-passed data shows that CODAR and ADCP have the highest correlations in speed and the alongshore (V) velocity component and CODAR-derived currents lead by 12 to 15 hours. The data also shows CODAR-derived currents and the winds have similar correlations in the speed and alongshore (V) velocity component. This suggests that for lower frequencies the CODAR-derived and ADCP currents are strongly influenced by the larger scale events in the winds. The lag of the ADCP currents can be explained by the slower response of the ADCP currents at the 12-20 m depth to the wind forcing. The weak correlation of the low-passed data for the onshore (U) velocity component is a result of the fact that the low-frequency events occur mostly in the alongshore direction. Conversely, the onshore currents are dominated by the daily wind cycle.

Although the magnitudes are low, the unfiltered lagged correlations reveal the higher frequency relationships between the winds, CODAR-derived and ADCP currents. CODAR and the ADCP have the highest correlations in the alongshore velocity component at 24 hour periods and for the onshore velocity component at 12 hour periods. CODAR and the winds have the highest correlation in speed, alongshore and onshore velocity components only at 24 hour periods. This suggests that CODAR-derived and ADCP currents are influenced by the semi-diurnal tides for the onshore velocity component and by the diurnal winds and tides for the alongshore velocity component.

F. ROTARY POWER SPECTRA

To view the energy levels contained in frequency bands the rotary power spectra were calculated for the CODAR and ADCP time series (Gonella, 1972). The rotary spectra combine the U and V component time series and separate the energy in clockwise and counterclockwise directional frequencies. Positive frequencies rotate in a counterclockwise direction and negative frequencies rotate clockwise.

Figure 52 shows the CODAR-derived surface current rotary power spectrum for gridpoint 14-06. The sampling rate is every three hours and results in a Nyquist period of six hours. The interpolated three month data period containing 762 points was broken into 32 day segments (256 points) and the rotary power spectra was calculated. The spectrum for gridpoint 13-06 is similar but higher frequencies are not accurately reflected due to the significant amount of interpolation required at that location and is not shown. At both gridpoints and directional frequencies, peaks in the spectra are at 17 day periods and 24, 12.5 and 12 hour periods. The 17 day period could correspond to the oceanic or weather cycle. The 24 hour period corresponds to the diurnal wind and tides. The 12.5 and 12 hour periods correspond to the semidiurnal tidal components M_2 and S_2, respectively. The clockwise (negative) frequencies contain more energy than the counterclockwise (positive)

frequencies. This clockwise rotation is apparent in the canonical day as current sweep (at the mooring location) from east-southeast at 12:00 (Figure 36) to the south at 21:00 (Figure 39).

Unfortunately the same rotary spectra cannot be calculated for the ADCP data due the number of gaps in the time series as shown in the U V plot (Figure 41). The longest time segments of continuous data are typically 120 hours. To attempt a comparison the rotary spectra is calculated from a collection of 120 hour segments from the ADCP data. Figure 53 shows the ADCP 120-hour rotary spectra. The peaks are at roughly diurnal and semidiurnal frequencies but are spread over wide bands associated with the shortness of the records from which the spectra were created. The negative frequencies contain more energy than the positive frequencies. The ADCP and the CODAR spectra show the same peaks at the semidiurnal and diurnal periods. These peaks reflect the effects of the diurnal winds and tides and the semidiurnal tides. Due to the width of the frequency bins of the 120 hour rotary spectra the difference between the M_2 and S_2 semidiurnal tidal components cannot be distinguished.

G. CROSS SPECTRA

The previous rotary spectra showed the predominance of energy at 24 and 12 hours in the CODAR-derived and ADCP currents. To further examine the relationships at these diurnal and semidiurnal periods, the rotary cross-spectra were calculated between the ADCP currents and all CODAR gridpoints at 24 and 12 hour periods in both frequency directions (Gonella, 1972). From the results, the cross spectra maps show the spatial correlation and phase differences of entire CODAR gridfield with the ADCP currents at the mooring. Coherence values greater than 0.5 are considered to be significant.

Figures 54 to 57 show the ADCP-CODAR coherence and phase at 12 hour periods for negative and positive frequencies. The CODAR and ADCP currents were coherent over a

moderate amount of area for both negative and positive frequencies. The phase maps show that the majority of CODAR gridpoints showing a high coherence were also in phase with the ADCP currents at the 12 hour period. Low coherence near the mooring is a result of the missing high frequency CODAR data (CODAR coverage was 30% at the mooring).

Figure 58 and 59 show the ADCP-CODAR coherence and phase at 24 hour periods for positive frequencies. The CODAR and ADCP currents were coherent over most of the area for positive frequencies. They were not coherent at any gridpoint for the negative frequencies. The phase map for the positive frequencies shows all CODAR gridpoints were in phase with the ADCP at the 24 hour period.

The maps show that at 12 hour periods the same tidal effects influence the CODAR-derived surface currents and the ADCP currents. The phase difference is relatively small showing the semidiurnal tides affect the entire area at nearly the same time. The 24 hour period maps show that only the positive directional frequencies (counterclockwise) are coherent. The phase difference is nearly the same over the entire gridfield. This shows that the combination of tides and winds affect the entire area at nearly the same time.

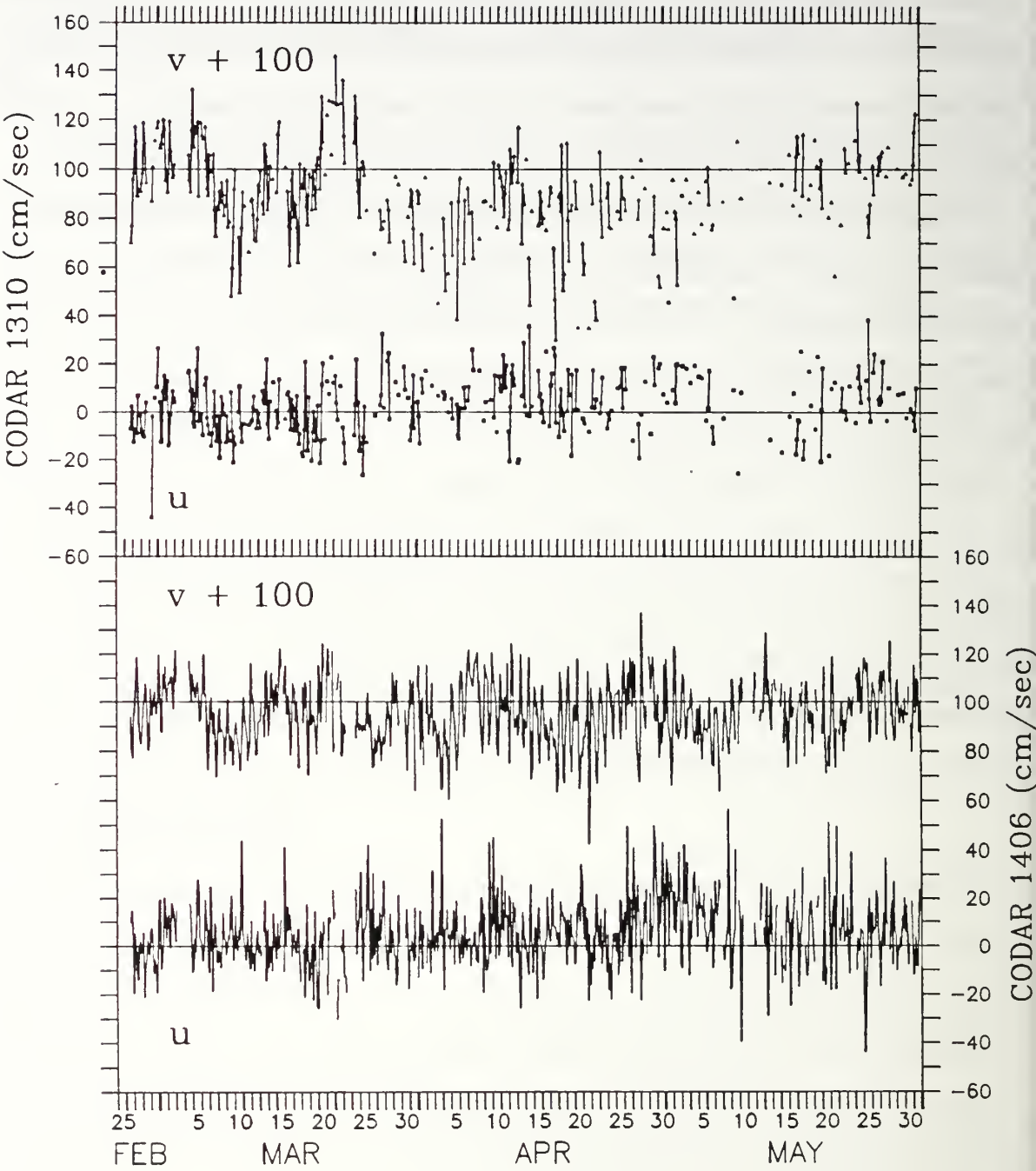

Figure 40. **CODAR-derived Surface Currents U-V Velocities:** The raw CODAR gridpoints 13-10 (upper panel) and 14-06 (lower panel) time series are shown above. The V component is offset +100 cm·sec^{-1} from zero and missing measurements in the time series are denoted by gaps.

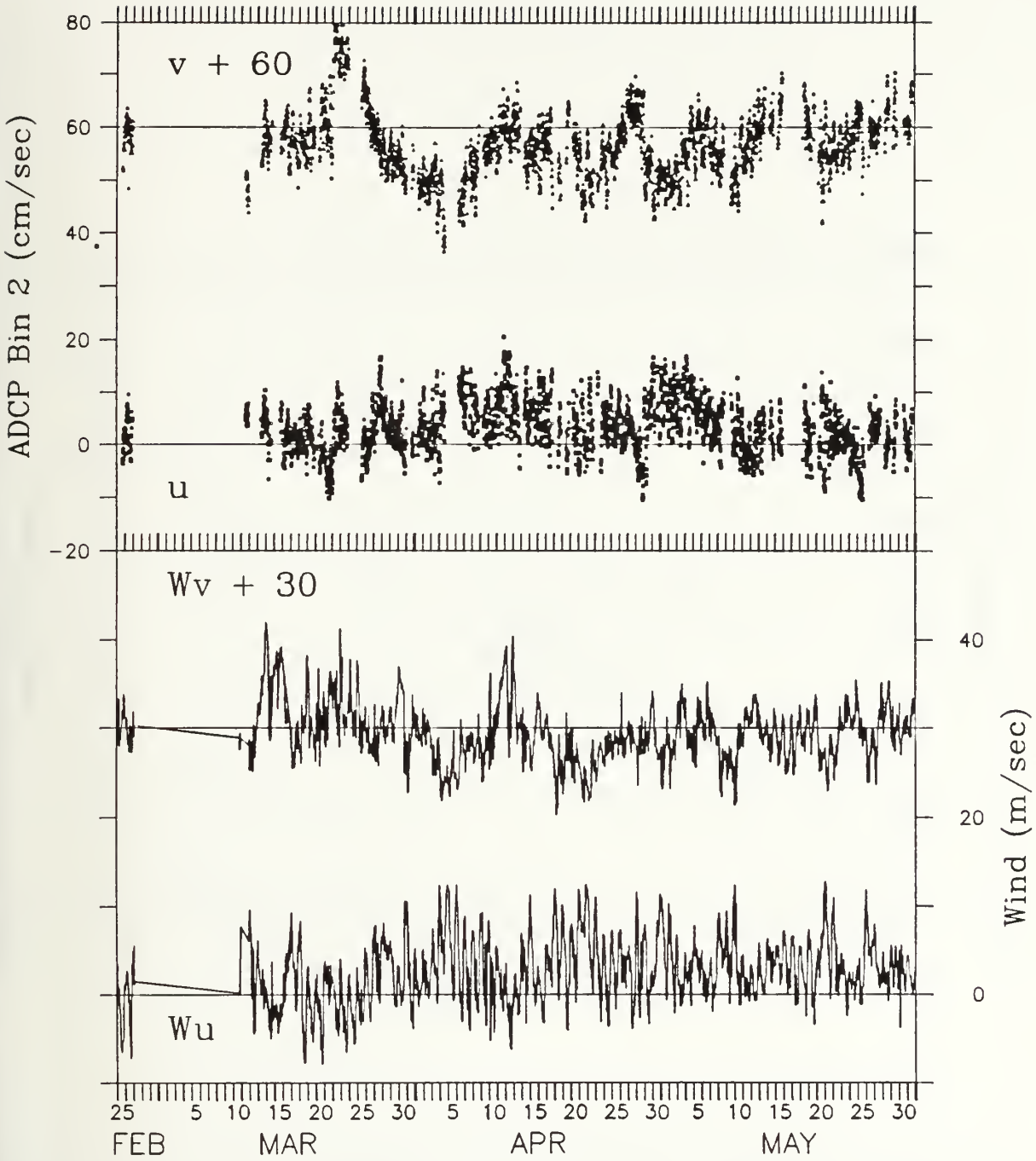

Figure 41. **ADCP Currents and Wind U-V Velocities from the MBARI Mooring:** The raw ADCP (upper panel) and Wind (lower panel) time series are shown above. The V component is offset +60 cm·sec^{-1} for ADCP and +30 m·sec^{-1} for the wind.

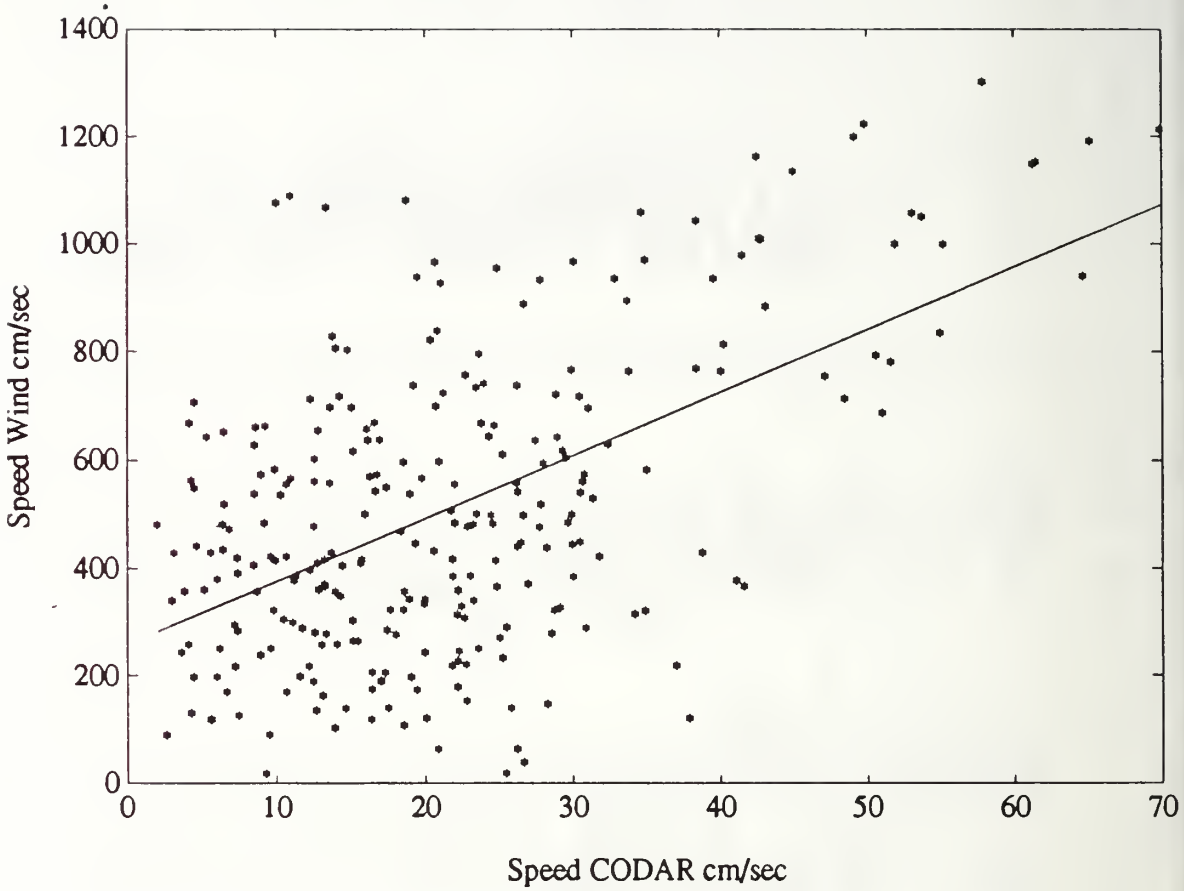

Figure 42. **Scatter Plots of CODAR and Wind Speeds:** This plot shows the raw and concurrent speed values. The slope of the line fitted to the data shows the winds to be twelve times greater the CODAR-derived current speeds.

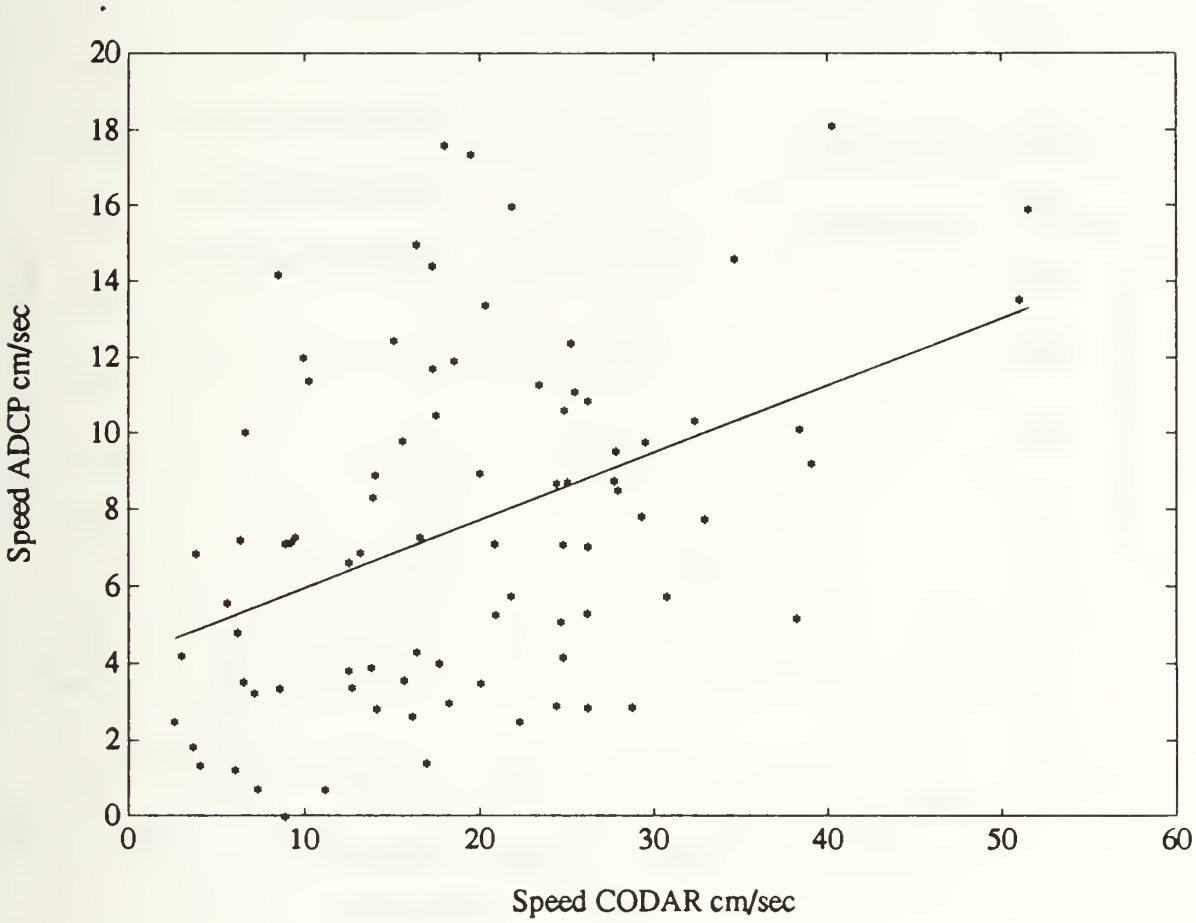

Figure 43. **Scatter Plots of CODAR and ADCP Speeds:** This plot shows the raw and concurrent speed values. The slope of the line fitted to the data shows the CODAR-derived current speeds to be five and a half times greater than the ADCP current speeds.

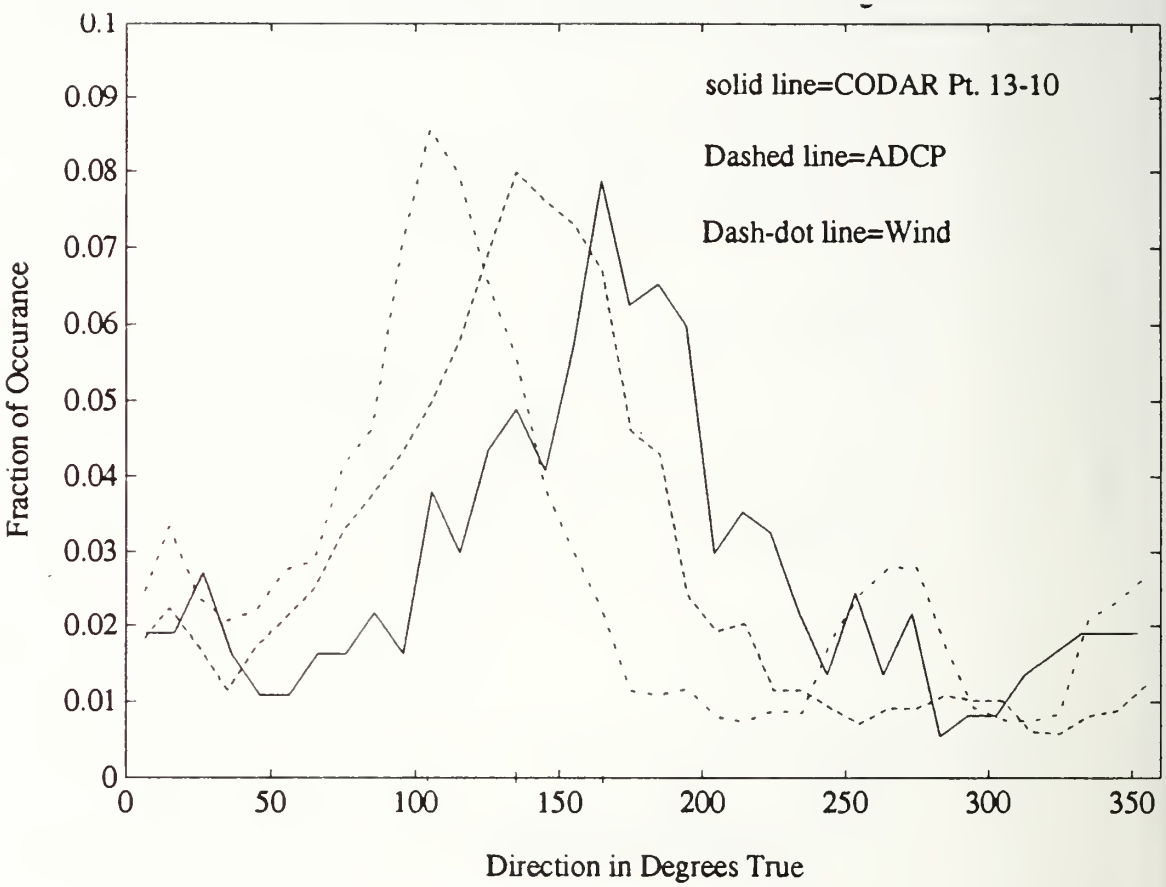

Figure 44. **Comparison of CODAR, Wind and ADCP Current Directions:** The lines represent the histograms of the directions of CODAR gridpoint 13-10 (solid line), ADCP (dashed line) and the wind (dash-dotted line). The histograms were calculated from the raw time series and the results normalized and plotted above. Directions are referenced to true North.

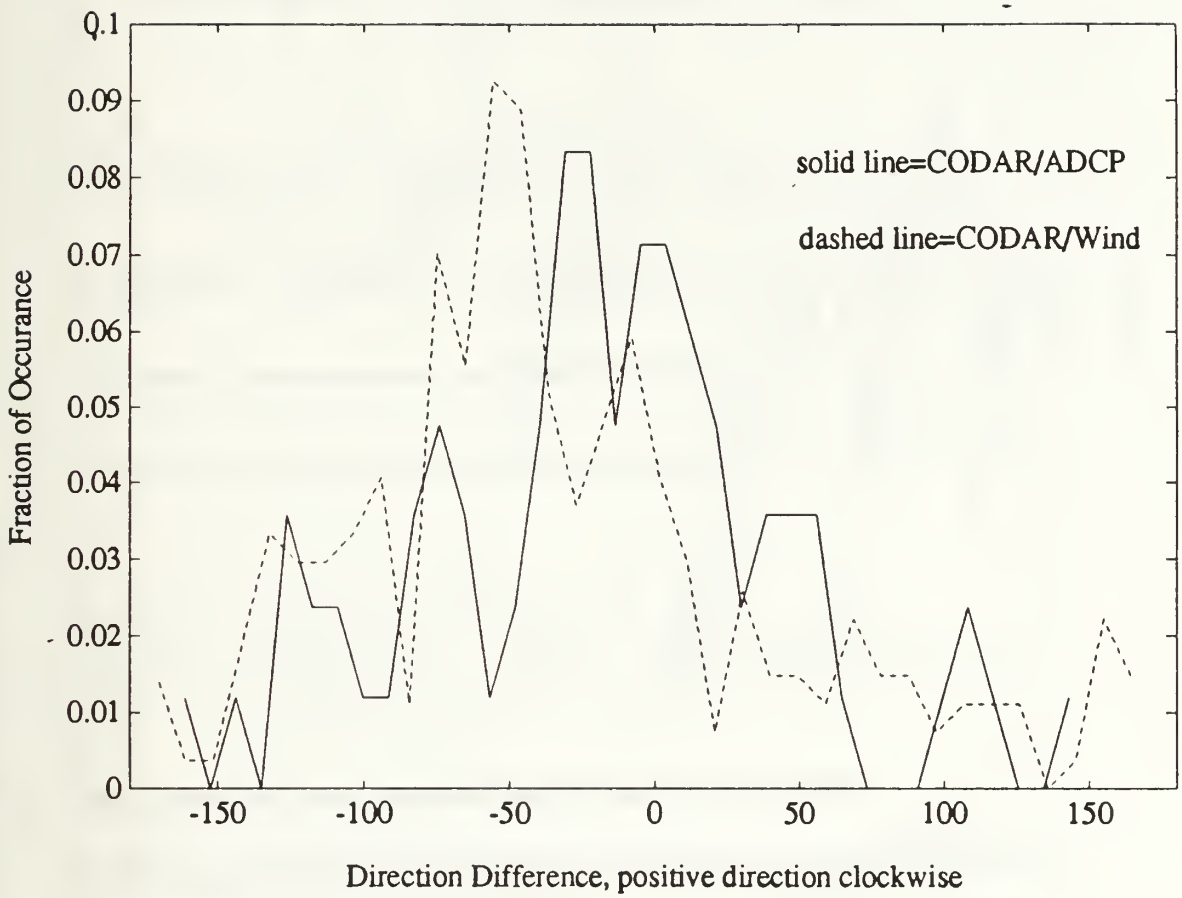

Figure 45. **Comparison of CODAR, Wind and ADCP Current Directional Differences:** The lines represent the histograms of the directional differences between CODAR gridpoint 13-10 and ADCP (solid line) and between CODAR gridpoint 13-10 and winds (dashed line). The direction differences were calculated from the raw and concurrent data. Histograms were calculated, the results normalized and are plotted above. Positive direction differences are clockwise and negative direction differences vice versa.

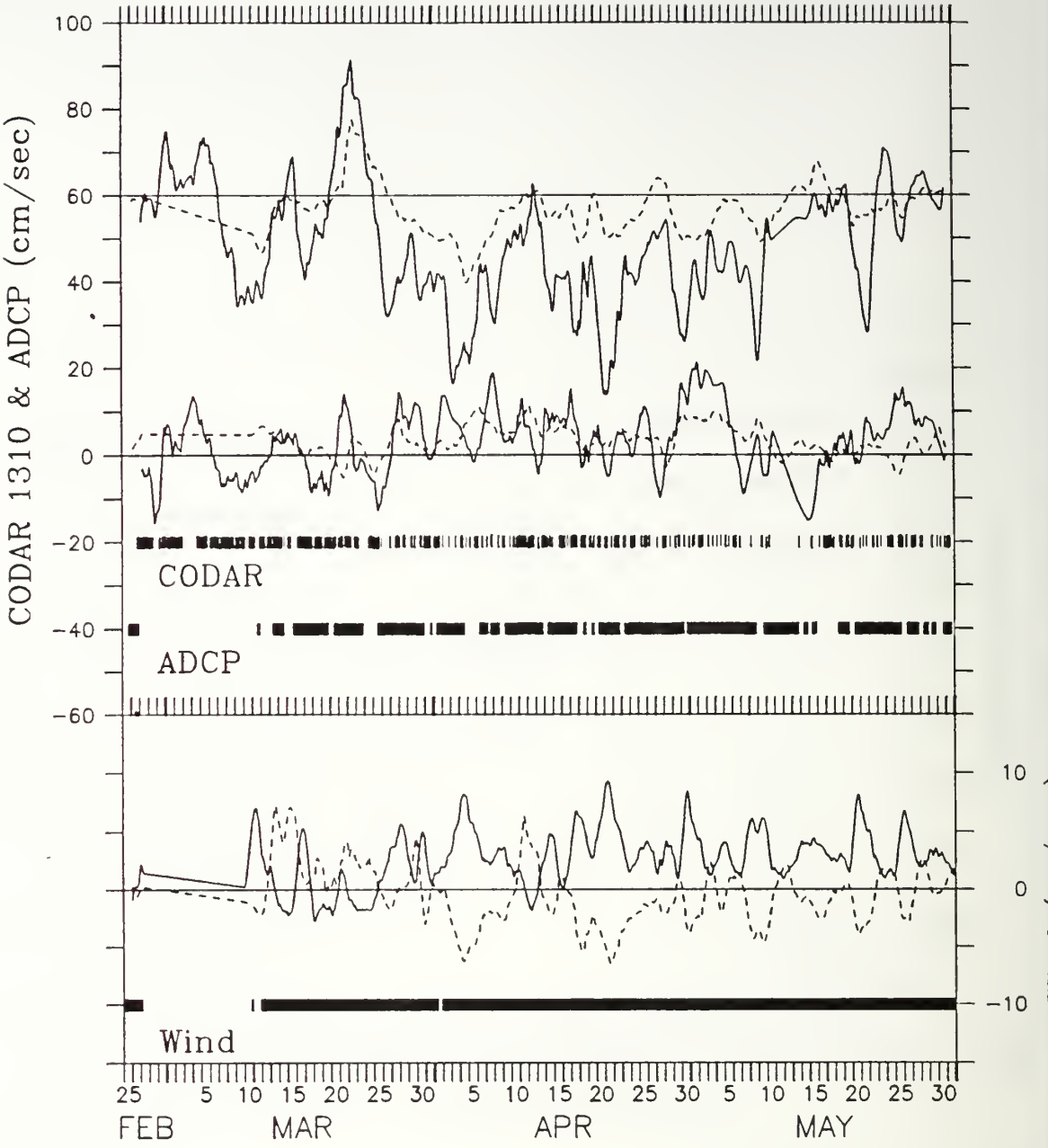

Figure 46. **Low-passed Filtered CODAR, Wind and ADCP Velocities:** The upper panel of the figure compares interpolated and low-passed CODAR-derived (solid lines) and ADCP (dashed lines) currents. The V component is offset +60 cm·sec^{-1} above the U component. The lower panel shows the interpolated and low-passed U (solid line) and V (dashed line) components of the winds. The times of the raw data for each measurement type are denoted by the dark bands. Gaps indicate missing records and highlight where interpolation played a significant role.

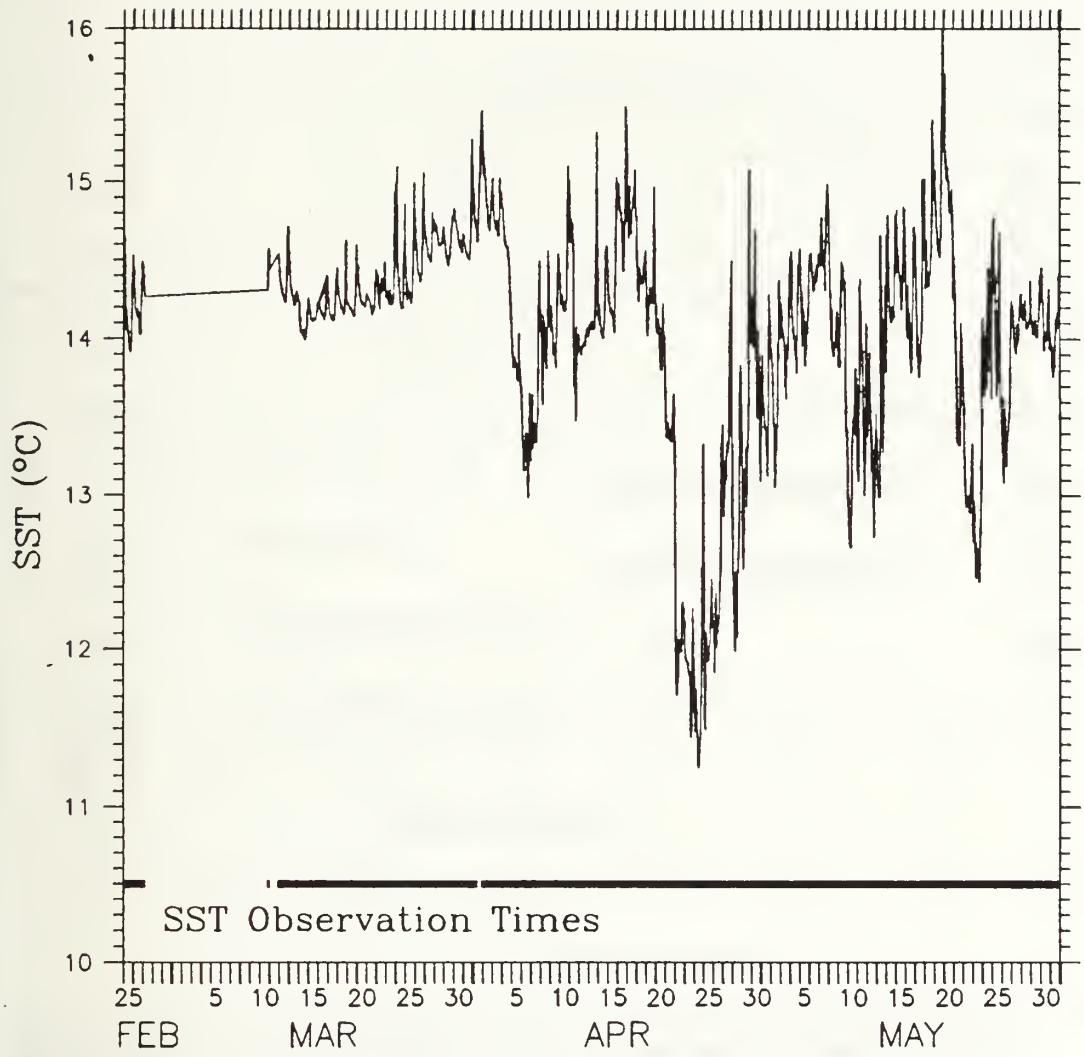

Figure 47. **Seas Surface Temperature Measured at the MBARI Mooring:** Note large drops in temperature that correspond with periods of large southward currents as seen in both CODAR and ADCP data (Figure 46).

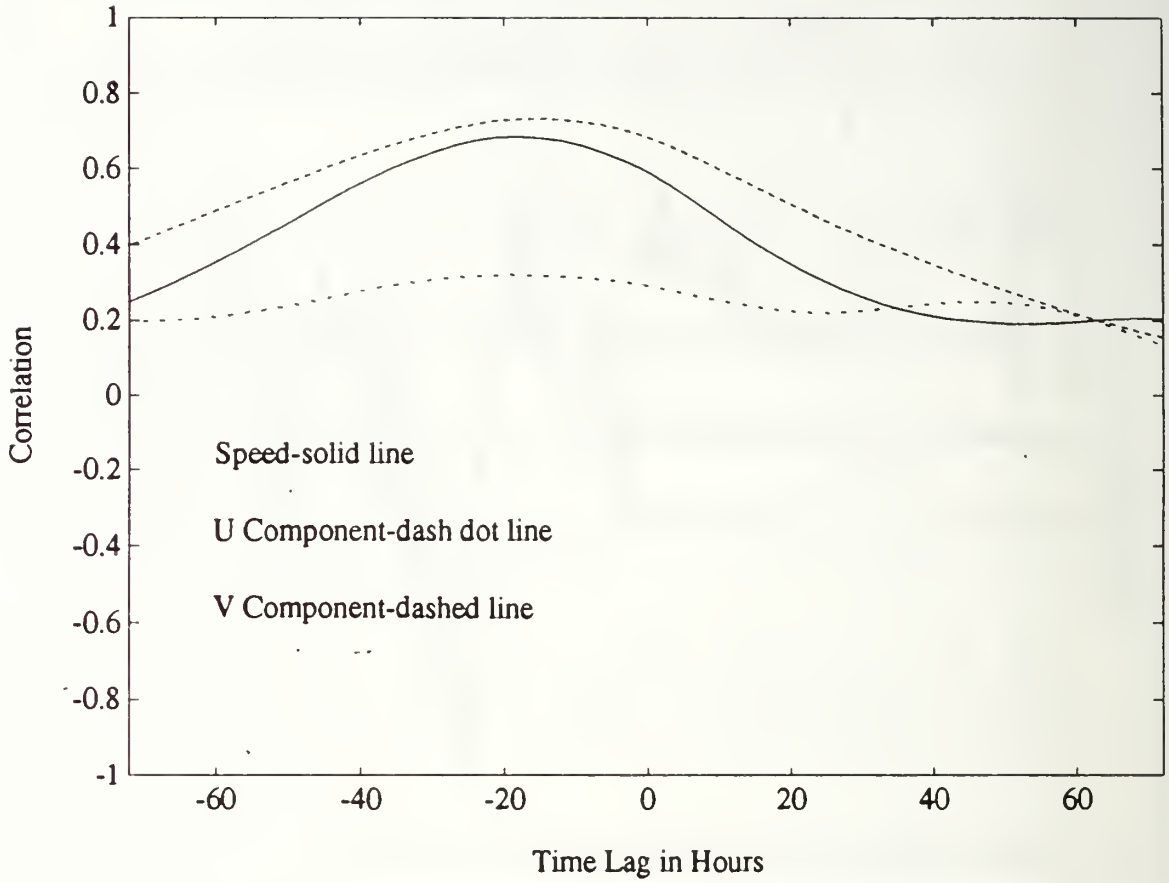

Figure 48. **Lagged Cross Correlation between CODAR PT. 13-10 and ADCP from Low-passed Time Series:** The correlations were calculated from the interpolated and low-passed time series. Overall correlations were the highest for speed and V component and were relatively uncorrelated for the U component. CODAR currents lead the ADCP currents by 15 hours.

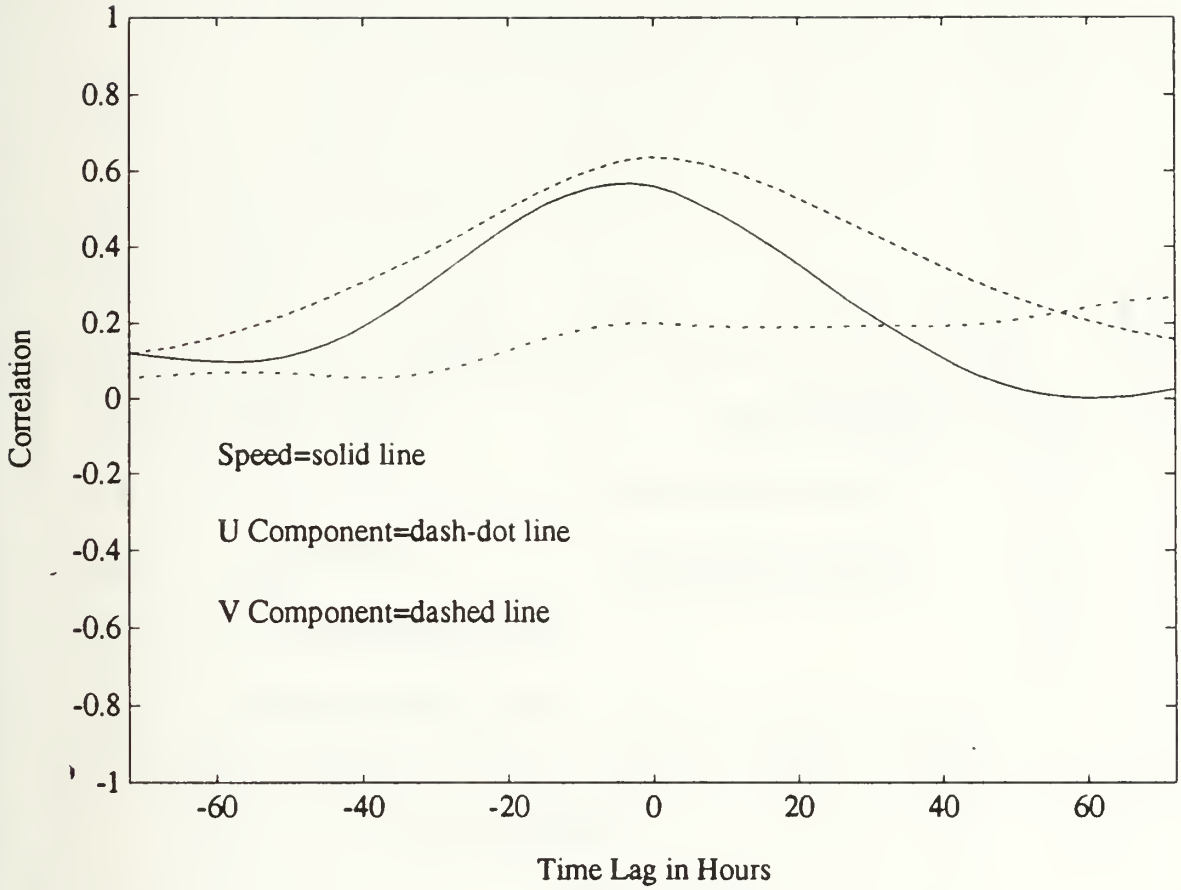

Figure 49. **Lagged Cross Correlation between CODAR PT. 13-10 and Wind from Low-passed Time Series:** The correlations were calculated from the interpolated and low-passed time series. Overall correlation coefficients are the highest for the speed and V component and are relatively uncorrelated for the U component .

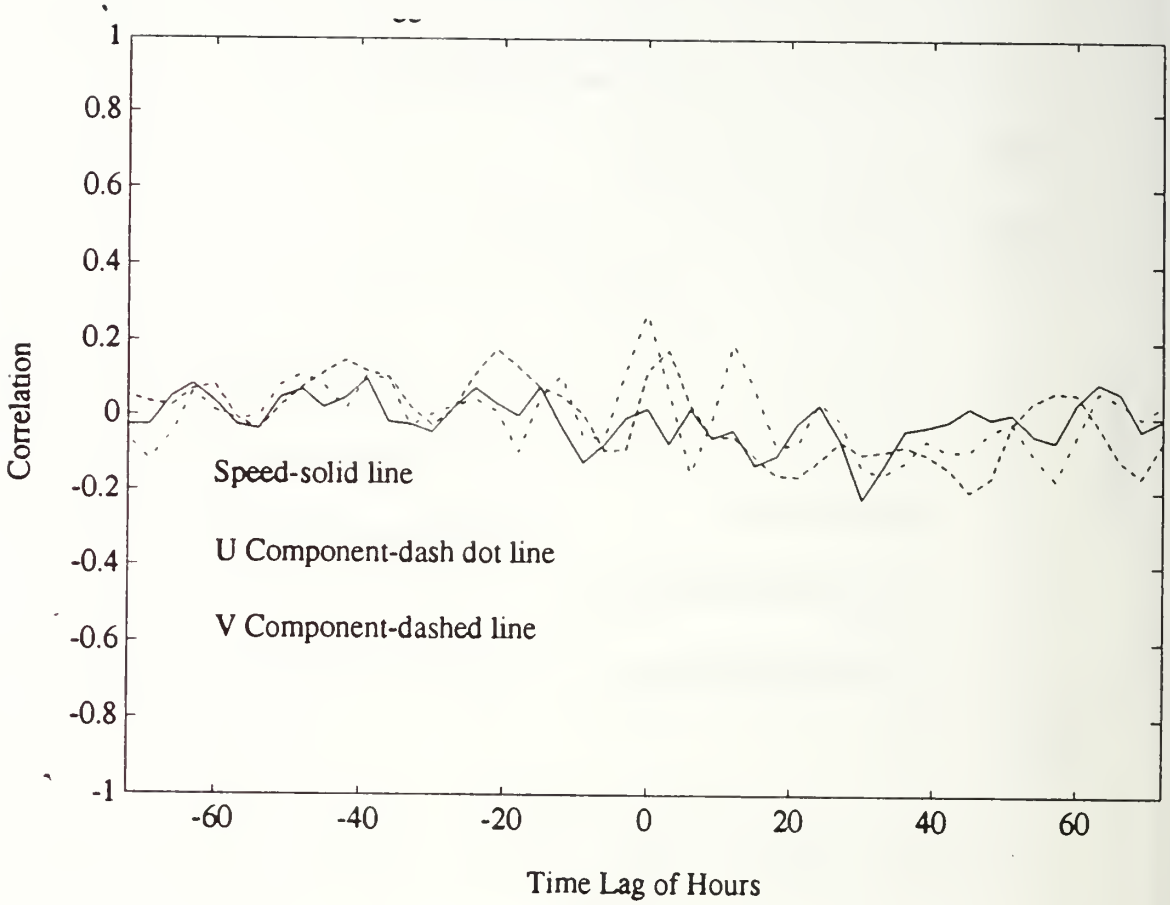

Figure 50. **Lagged Cross Correlation between CODAR PT. 14-06 and ADCP:** The correlations were calculated from averaging the correlations of 120-hour segments that correspond to the longest continuous ADCP records. Overall correlation values were low but show higher correlations at 24 hour periods for the V component and at 12 hour periods for the U component.

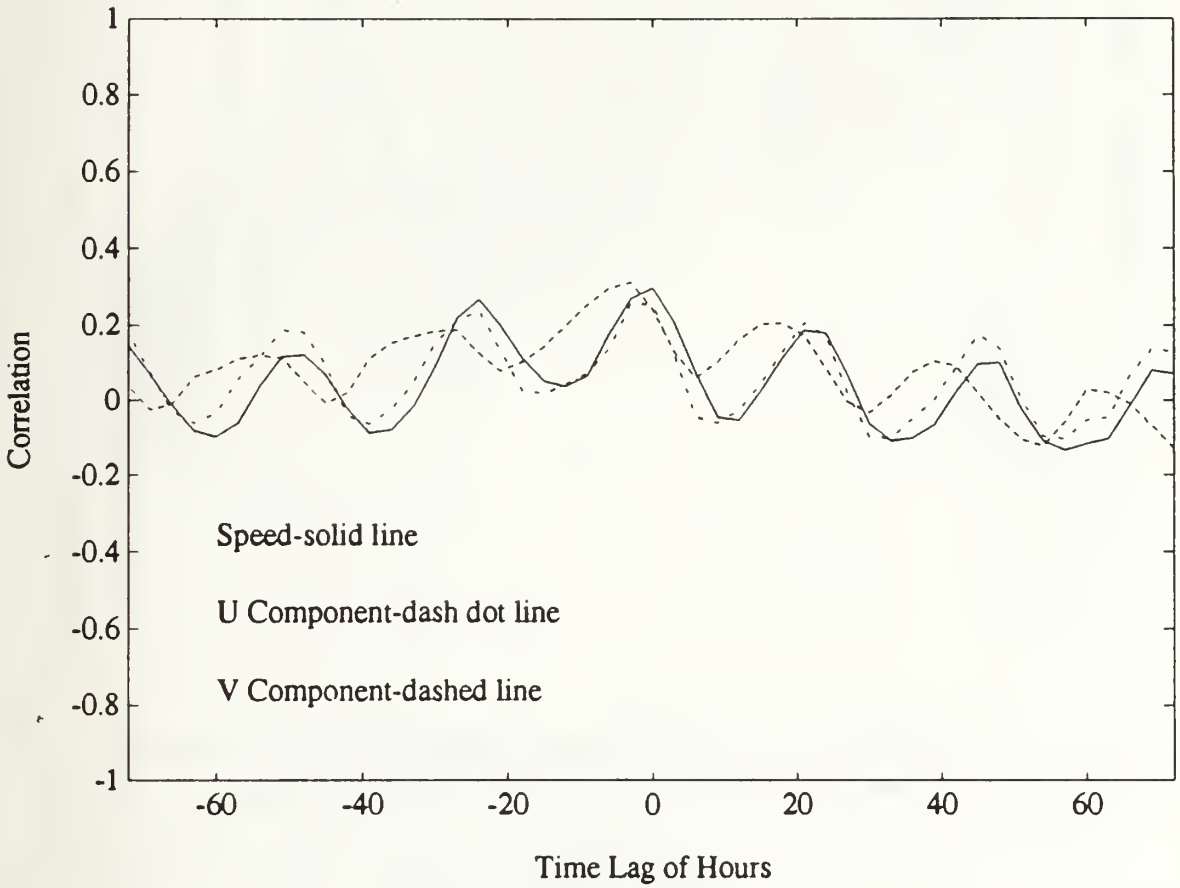

Figure 51. **Lagged Cross Correlation between CODAR PT. 14-06 and the Wind:** The correlations were calculated from the interpolated time series. Overall correlation coefficients are low but the speed U and V components have higher correlations at 24 hour periods.

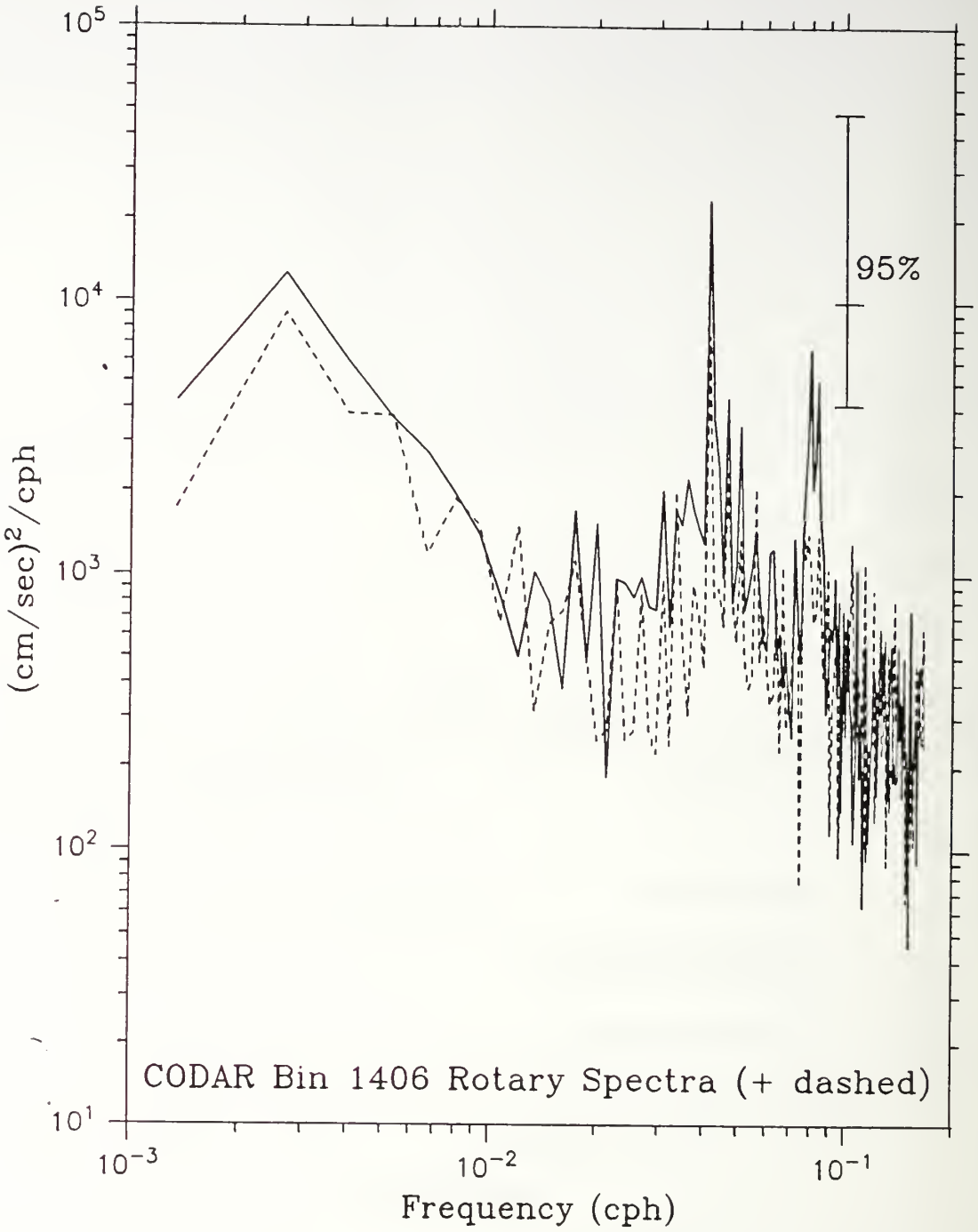

Figure 52. **Rotary Power Spectra of CODAR-derived Surface Currents, Gridpoint 14-06:** Peaks in the spectra correspond with 17 day and 24, 12.5 and 12 hour periods. The 24 hour peaks result from a combination of diurnal winds and tides. The 12.5 and 12 hour peaks result from the semidiurnal tides (M_2 and S_2 respectively). The solid and dashed lines represent the energy associated with counterclockwise (positive) and clockwise (negative) sweeping directions. The 95% confidence interval is denoted by the bar above the spectra

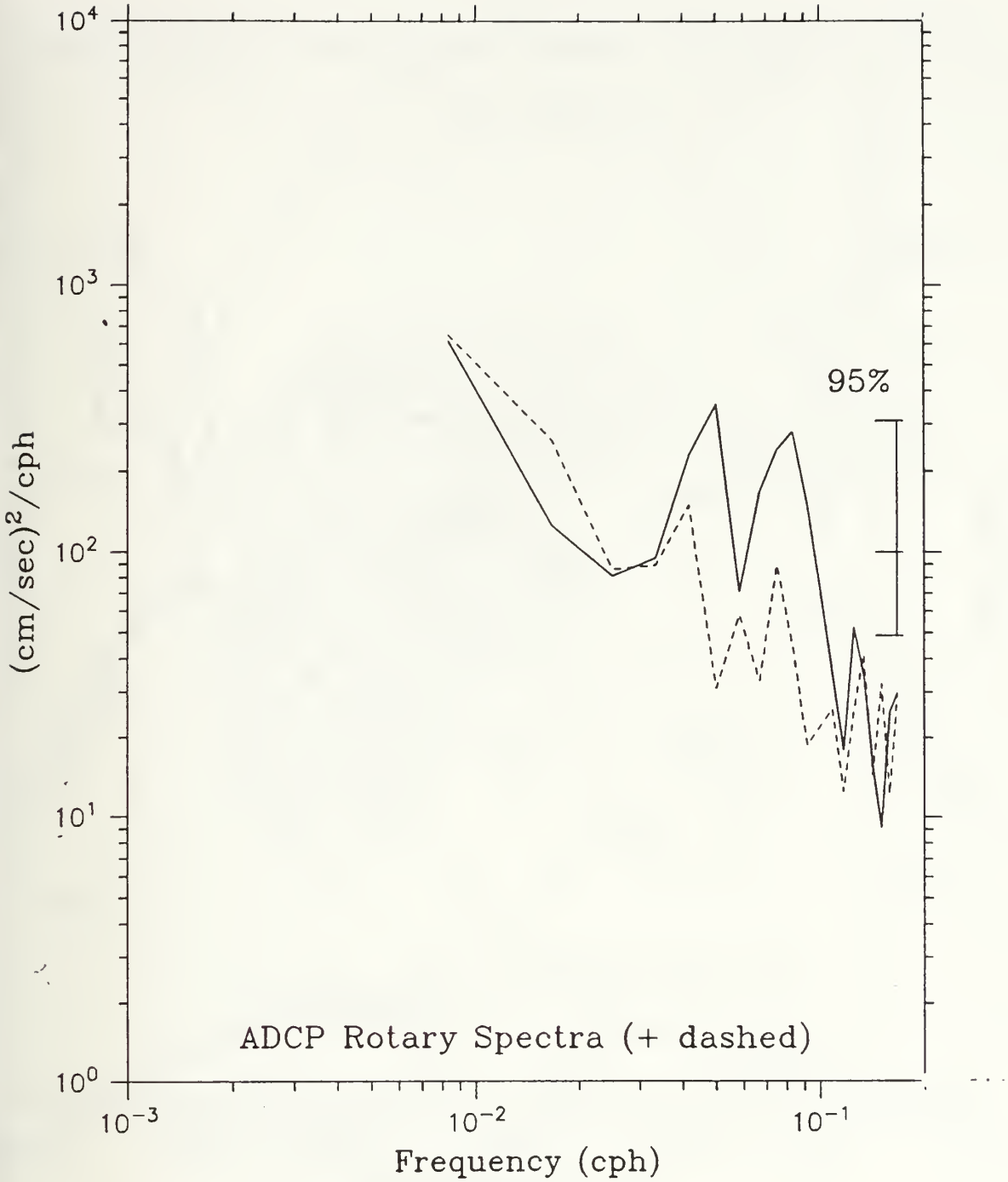

Figure 53. **ADCP 120-Hour Rotary Power Spectra:** Peaks in the spectra correspond with 24 and 12 hour periods. The peaks result from a combination of diurnal winds and tides at the 24 hour period and from the semidiurnal tides at the 12 hour period. The solid and dashed lines represent the energy associated with counterclockwise (positive) and clockwise (negative) sweeping directions. The 95% confidence interval is denoted by the bar above the spectra.

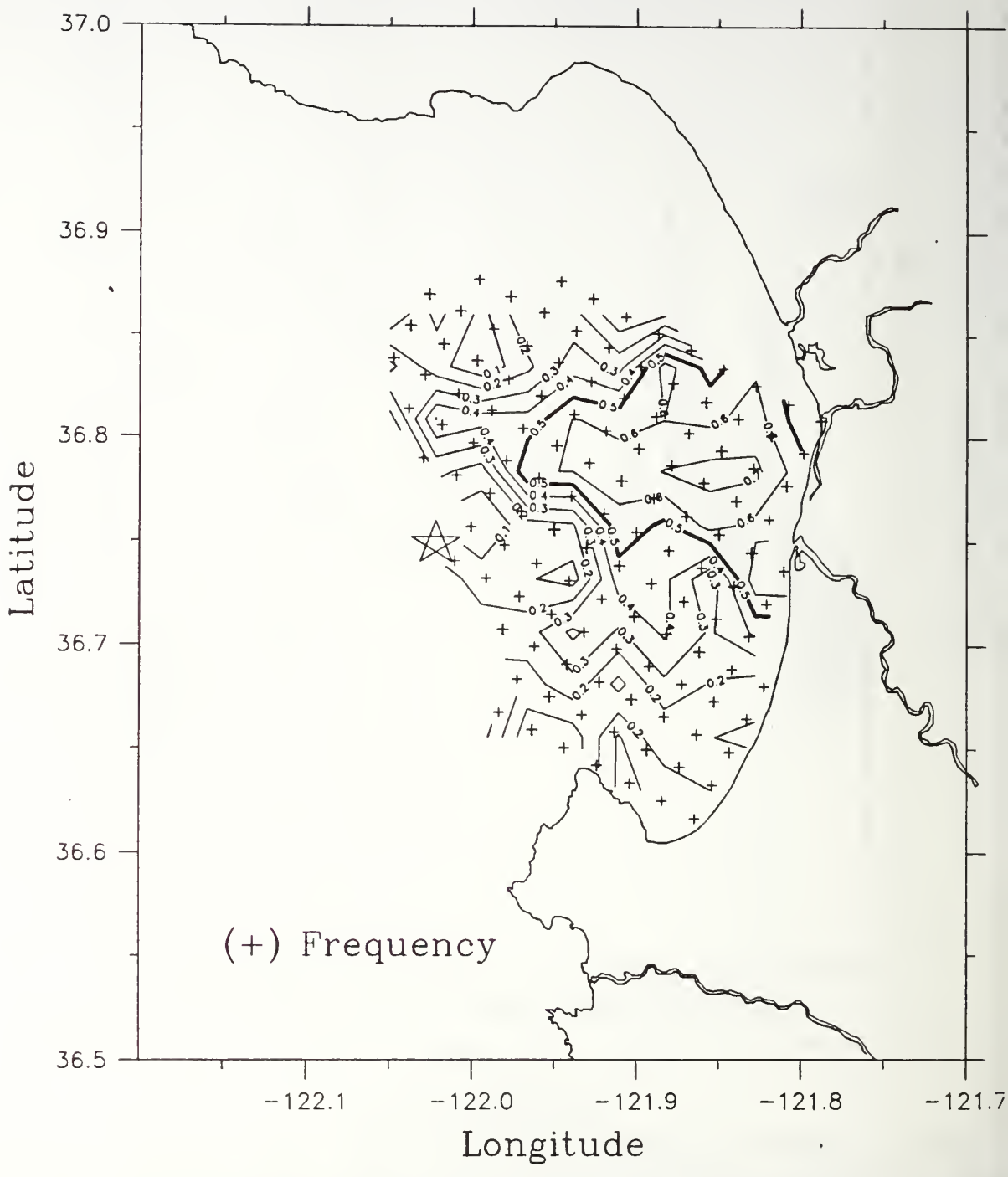

Figure 54. **ADCP-CODAR Coherence at 12 Hour Periods for Positive Frequencies:** Values greater than 0.5 are above the 95% significance level. Note the large area near the center that is coherent.

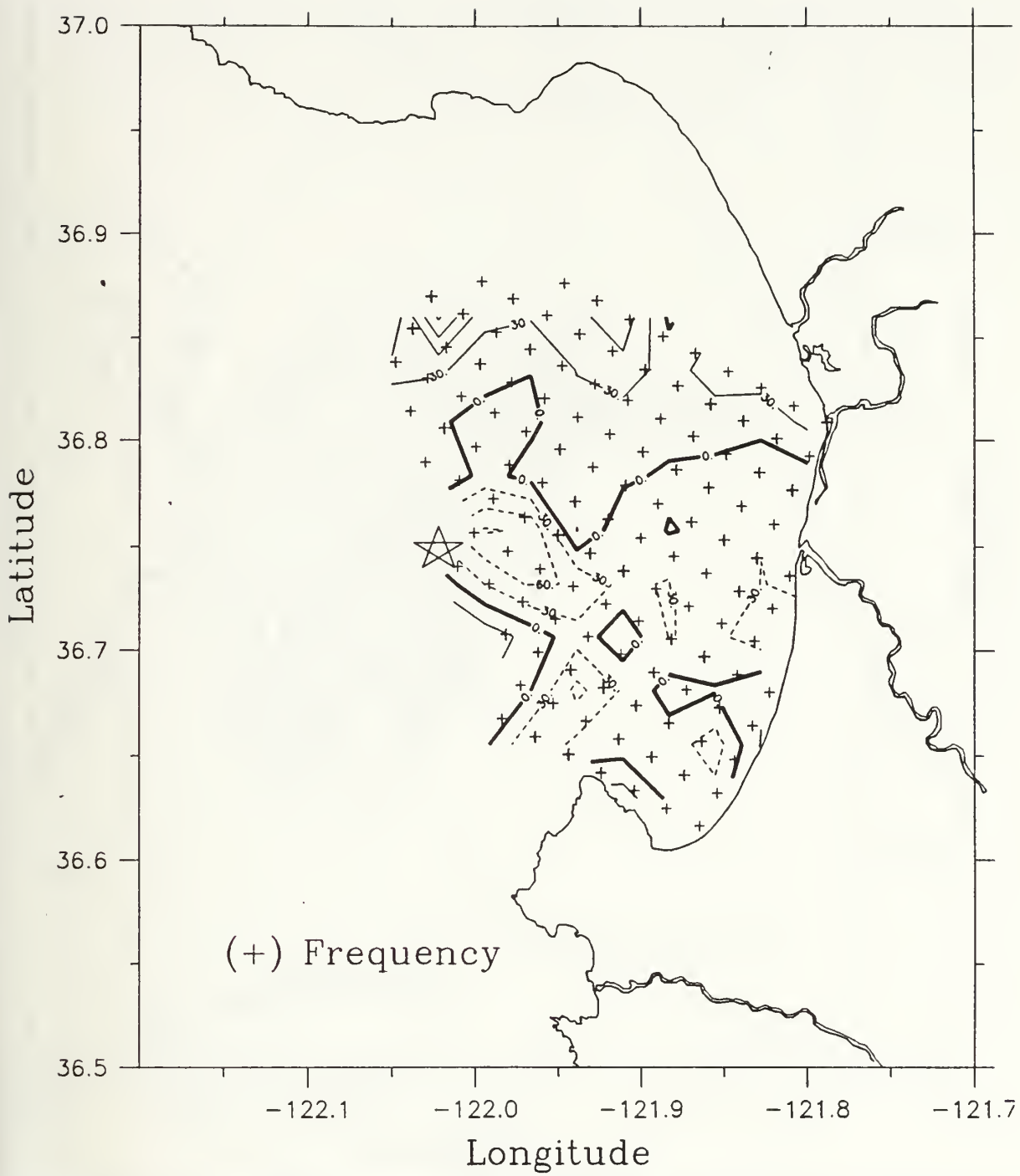

Figure 55. **ADCP-CODAR Phase at 12 Hour Periods for Positive Frequencies:** The majority of the area is less than 30° in phase at 12 hour periods.

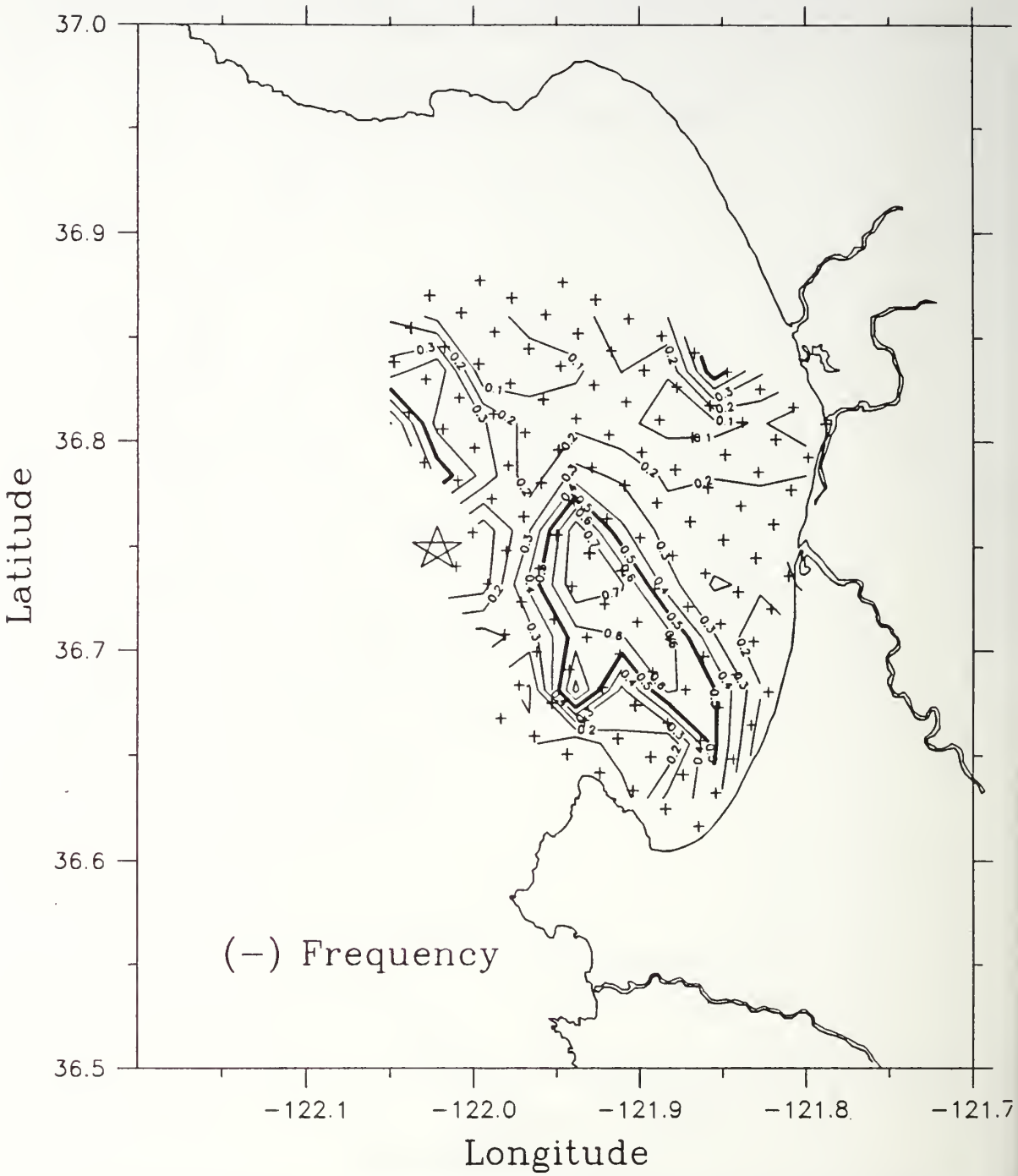

Figure 56. **ADCP-CODAR Coherence at 12 Hour Periods for Negative Frequencies:** Values greater than 0.5 are above the 95% significance level. Note the large area near the center that is coherent.

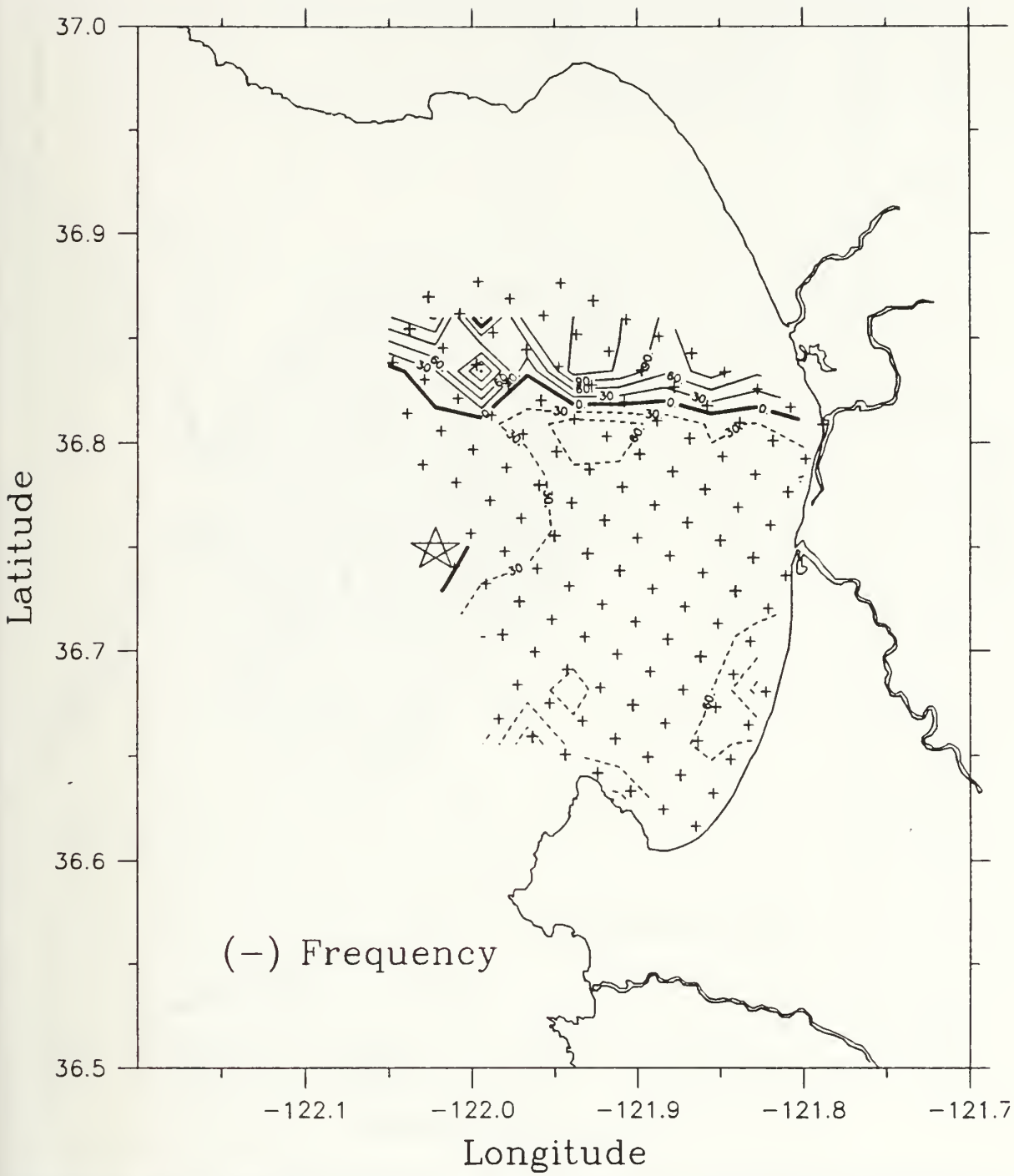

Figure 57. **ADCP-CODAR Phase at 12 Hour Periods for Negative Frequencies:** The majority of the area is less than 30° in phase at 12 hour periods.

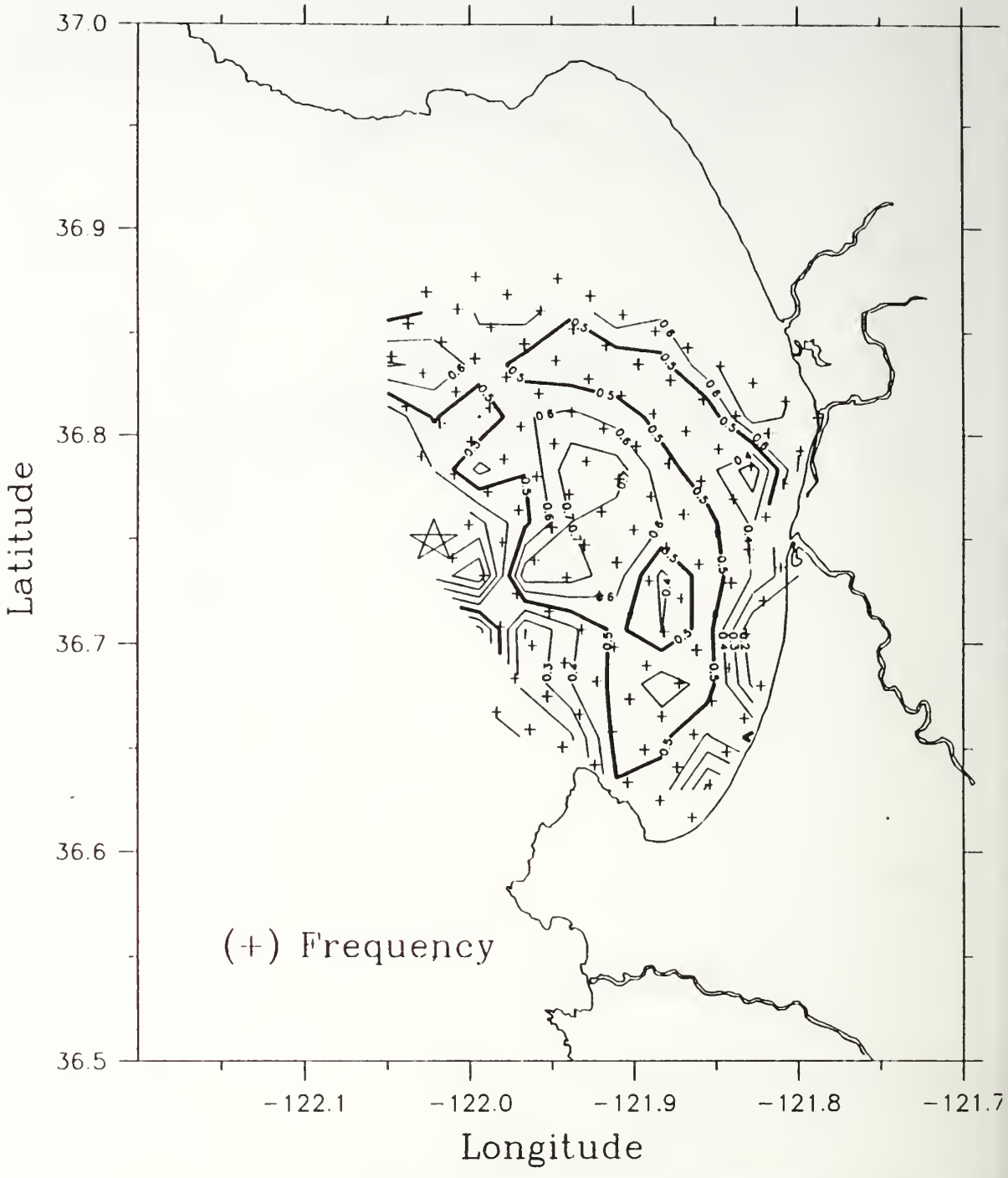

Figure 58. **ADCP-CODAR Coherence at 24 Hour Periods for Positive Frequencies:** Values greater than 0.5 are above the 95% significance level. Note the large area near the center that is coherent.

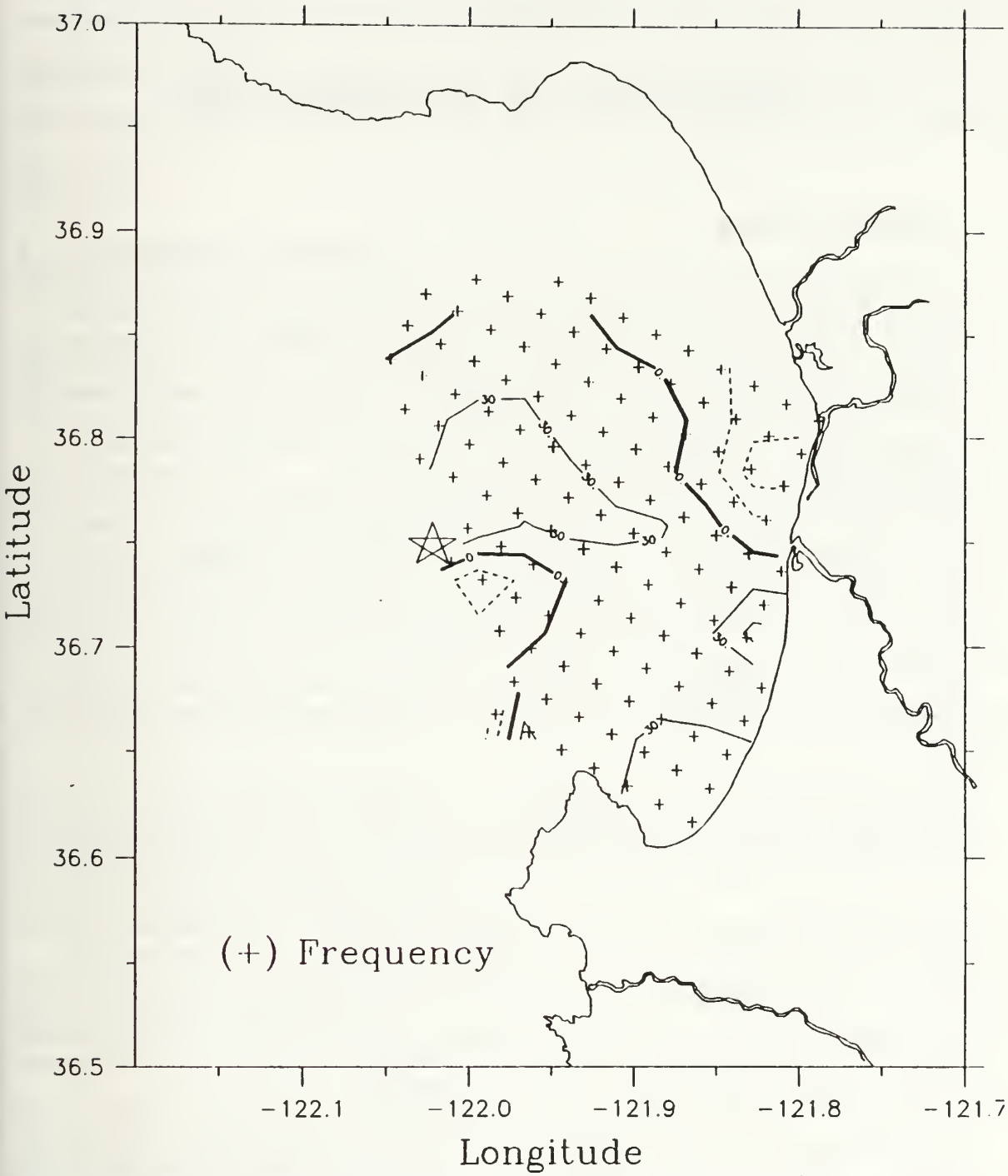

Figure 59. **ADCP-CODAR Phase at 24 Hour Periods for Positive Frequencies:** The majority of the area is less than 30° in phase at 12 hour periods.

V. CONCLUSIONS AND RECOMMENDATIONS

A. CONCLUSIONS

CODAR-derived surface currents are a useful tool in the study of Monterey Bay's circulation. CODAR remotely senses an area of ocean over 550 km2 with a finer spatial and temporal scale than other remote sensing systems. It provides a larger area of coverage than is possible with in situ measurement devices. The mean currents and the low-passed filtered time series provide insights into the lower frequency events (periods greater than one day) of the surface currents. The mean currents, however, are dominated by the daily patterns shown by the canonical currents. The effect of individual erratic, missing and improbable current vectors are minimized using these averaging techniques. The low-passed time series compare favorably with the in situ data measured from the MBARI buoy.

For the higher frequency events, CODAR does not exactly compare to either the winds or the ADCP data. Spectral analysis reveals the dominate forces that affect the CODAR-derived surface currents are a combination of the tides and winds. CODAR-derived surface currents are coherent with the winds at 24-hour periods and with the tides at 12, 12.5 and 24 hour periods. The differences between the measurement techniques may be explained by the spatial, depth and temporal variations of the sampling.

Real-time use of the CODAR-derived surface currents is hampered by the presence of erratic, missing and improbable current vectors. The MBARI buoy data compared in this study was incomplete. A more detailed and extensive comparison should be conducted to determine the relationship of CODAR-derived surface currents to other in situ

measurements. The failure to do this has lead the scientific community to be reluctant to use CODAR. Research on, and improvements of, the CODAR system should continue so that confident use of CODAR-derived surface currents can be made in real-time applications.

B. RECOMMENDATIONS

The first group of recommendations are related to the continued engineering improvement and careful systems testing of CODAR. This is necessary to prove the effectiveness and accuracy of CODAR in measuring the currents and allow its acceptance as an oceanographic tool. Improvements to the existing CODAR system should be implemented. A third CODAR operating site is planned for installation at Santa Cruz. This site should provide accurate measurement of the currents on the Monterey to Moss Landing baseline without the need for special assumptions. In July 1992, the interval between CODAR transmissions was decreased to two hours. The ultimate goal would have continuous CODAR transmissions allowing the currents to be mapped at intervals less than 30 minutes. This could be accomplished with the improved computer technology available. One dedicated computer could control the radar's operation and a separate computer would continuously process the returning signals.

The goal should be to verify or reject the real-time accuracy of the CODAR-derived surface currents. One possible test is to conduct concurrent CODAR, OSCR and in situ measurements for a three-month period. An extensive test and evaluation of the resulting data might prove the validity of HF surface current radar systems. If the results are favorable this would lead to the acceptance and use of HF surface current radar systems as a viable remote sensing system.

For future data sets, the CODAR-derived surface currents should be extensively compared to other in situ and remote measuring systems. In September 1992, ARGOS

surface drifters were deployed in Monterey Bay to compare their tracks to the CODAR-derived surface current vectors. The presence of strong daytime onshore flow was verified. This data brings into question the software implemented baseline assumption of no flow at the beach. This assumption should be eliminated.

The second group of recommendation focuses on the use of CODAR for oceanographic studies. The analysis of this three-month CODAR-derived surface current data set has only been started. Many interesting features and questions are unexplained. The radial current files need to be analyzed to determine if more data can be extracted to fill in the gaps of missing total current vectors or if the erratic vectors can be removed. An extensive comparison of CODAR to the winds using a complete wind time series should be conducted given the high correlation to the wind data. Comparing CODAR-derived surface current to SST measurements from the MBARI buoy and satellites could provide insight into the dynamics of cold water upwelling and advection into Monterey Bay. The data set could be used to conduct a more detailed study of the tidal effects similar to studies conducted with the OSCR-derived surface currents on Bristol Bay, UK (Hammond et al., 1987). There should be major efforts to extract the wind and tidal effects from the CODAR-derived surface currents and allow the episodic ocean current events to be studied.

LIST OF REFERENCES

Barrick, D. E., Headrick, J. M., Bogle, R. W.,and Crombie, D. D., "Sea Backscatter at HF: Interpretation and Utilization of the Echo", *Proceedings of IEEE*, 62, pp. 673-68, 1974.

Barrick, D. E., Evans, M. W., and Weber, B. L., "Ocean Surface Currents Mapped by Radar", *Science*, 198, pp. 138-144, 1977.

Barrick, D. E., Lipa, B. J., and Crissman. R. D., "Mapping Surface Currents with CODAR", *Sea Technology*, October, 1985.

Barrick, D. E., Lipa, B. J., and Lilleboe, P. M., "HF Radar Surface-Current Mapping: Recent U.S./Canadian Advances", paper sponsored by the Current Measurement Technology Committee of the Oceanic Engineering Society Institute of Electrical and Electronic Engineers, 1986.

Chavez, F. P., and others, "The MBARI Program for Obtaining Real-Time Measurements in Monterey Bay", *Oceans '91 Proceedings*, 1991.

CODAR Ocean Sensors, LTD, *NOAA CODAR Central-Site User's Guide*, 1992.

Crombie, D. D., "Doppler Spectrum of Sea Echo at 13.56 Mc/s", *Nature*, 175, pp. 681-682, 1955.

Crombie, D. D., "Resonant Backscatter from the Sea and its Application to Physical Oceanography", *Oceans '72' Conference Records*, IEEE Publishing number 72CHO660-1022, pp. 173-179, 1972.

Essen, H. H., Gurgel, K. W., and Schirmer, F., "Surface Currents in the Norwegian Channel measured by radar in March 1985", *Tellus*, 41A, pp. 162-174, 1989.

Gonella, J., "A rotary-component method for analysing meterological and oceanographic vector time series", Deep-Sea Research, 19, pp. 833-846, 1972.

Hammond. T. M., and others, "Ocean Surface Current Radar (OCSR) vector measurements on the inner continental shelf", *Continental Shelf Research*, 7, NO. 4, pp. 411- 431, 1987.

Janopaul, M. M.,and others, Comparison of measurements of sea currents by HF radar and by conventional means", *International Journal of Remote Sensing*, 3, NO. 4, pp. 409-422, 1982.

Lipa, B. J., and Barrick, D. E., "Least-Squares Method for the Extraction of Surface Currents from CODAR Crossed-Loop Data: Application at ARSLOE", *IEEE Journal of Oceanic Engineering*, v. OE-8, NO. 8, pp.226-253, 1983.

McLeish, W., and Maul, G. A., *CODAR in the Straits of Florida: Final Report*, NOAA Technical Report ERL 447-AOML 35, 1991.

Pond, S. and Pickard, G. L., *Introductory Dynamical Oceanography*, 2ed, pp. 106-111, Pergamon Press, 1989.

Prandle, D., "The Fine-Structure of Nearshore Tidal and Residual Circulations Revealed by H. F. Radar Surface Current Measurements", *Journal of Physical Oceanography*, 17, pp. 231-245, 1987.

Stewart, R. H., and Joy, J. W., "HF Radio Measurement of Surface Currents", *Deep Sea Research*, 21, pp. 1039-1049, 1974.

INITIAL DISTRIBUTION LIST

		No. Copies
1.	Attn: Library, Code 52 Naval Postgraduate School Monterey, CA 93940-5000	2
2.	Superintendent Attn: Chairman, Department of Oceanography (Code OCCo) Naval Postgraduate School Monterey, CA 93940-5000	1
3.	Superintendent Attn: Assistant Professor J. D. Paduan (Code OCPd) Naval Postgraduate School Monterey, CA 93940-5000	1
4.	Superintendent Attn: Assistant Professor J. A. Nystuen (Code OCNy) Naval Postgraduate School Monterey, CA 93940-5000	1
5.	NOAA/COAP Attn: Dr. Gary Sharp 2560 Garden Road, Suite 101 Monterey, CA 93940	1
6.	Monterey Bay Aquarium Research Institute Attn: Dr. Leslie K. Rosenfeld 160 Central Ave. Pacific Grove, CA 93950	1
7.	Minerals Management Service Attn: Mr. Walter Johnson 381 Elden Street Herndon, VA 22070	1
8.	Commanding Officer Naval Research Laboratory Stennis Space Center, MS 39529-5000	1
9.	Defense Technical Information Center Cameron Station Alexander, VA 22304-6145	2
10.	Scripps Institute of Oceanography Library Mailcode C-075 University of California, San Diego La Jolla, CA 92093	1